Characterization of cytokinesis and ventrolateral flange dynamics in *Giardia lamblia*

William Robert Hardin

A dissertation

submitted in partial fulfillment of the

requirements for the degree of

Doctor of Philosophy

University of Washington

2017

Reading Committee:

Alex Paredez, Chair

Jay Parrish

Linda Wordeman

Program Authorized to Offer Degree:

Biology

University of Washington

Abstract

Characterization of cytokinesis and ventrolateral flange dynamics in *Giardia lamblia*

William Robert Hardin

Chair of the Supervisory Committee:
Assistant Professor Alex Paredez
Biology

Giardia lamblia is recognized as one of the most common protozoan causes of diarrheal diseases worldwide. *Giardia* is an extracellular parasite that colonizes the intestine using its cytoskeleton to attach to the host intestine. The cytoskeleton is additionally involved in cell motility, membrane trafficking, mitosis, and cytokinesis. Although the actin-cytoskeleton is central for cell survival, *Giardia* does not have any canonical actin-binding proteins. Despite the number of processes the cytoskeleton contributes and having the most divergent actin-cytoskeleton of any eukaryote identified, very little is understood about the cellular and cytoskeletal dynamics during these events. The technical difficulties of performing live cell imaging in *Giardia* have hampered the understanding of these life-cycle events. This study developed live cell imaging and then used this tool to explore the cellular dynamics and molecular underpinnings of cytokinesis and the ventrolateral flange, a lamellipodia-like structure. Cytokinesis is completed in a myosin-independent manner that uses flagella to coordinate force generation and direct membrane trafficking. The ventrolateral flange is an enigmatic structure that reportedly aids in cell attachment. The first ventrolateral flange components were identified, actin, GlRac, and Flangin and found to be critical for its assembly. Taken together, live cell imaging was developed as a novel tool for giardial research that lead to new insights into cytokinesis and ventrolateral flange dynamics in the evolutionarily distant disease causing protist *Giardia*.

Table of Contents

Chapter 1

Introduction.

The intestinal parasite *Giardia lamblia* was first observed in the 1600's when Anton van Leeuwenhoek made an anecdotal linkage of *Giardia* in his stool to his ongoing bout of diarrhea [1]. Since this initial discovery, *Giardia* has become recognized as one of the most common protozoan causes of diarrheal diseases worldwide [2, 3]. It is estimated that over one billion people have the acute or chronic condition giardiasis [4, 5]. Giardiasis is especially problematic in children because it can lead to physical stunting and wasting, cognitive impairment and fine motor movement problems [2]. Current treatments for giardiasis are increasingly ineffective with 20% of cases drug resistant, indicating a need for new therapeutic strategies [6]. Despite *Giardia's* global importance many fundamental biological questions remain about in vivo infection dynamics, pathogenesis, and all of the life-cycle processes.

Giardia is an extracellular parasite and its parasitism depends on attachment in the small intestines. After the host ingests *Giardia* cysts through contaminated water or food they pass through the gastrointestinal tract, and are exposed to stomach acid and proteases causing them to "excyst" and become motile trophozoites [2, 7]. Using flagellar motility, trophozoites navigate the lumen of the small intestine until they encounter a suitable place for attachment to the intestinal microvilli [8]. Attachment is mediated by a suction cup-like cytoskeletal structure called the ventral disc, which allows the parasite to resist peristaltic flow [9]. Cells remain in the lumen and prefer the small intestine for colonization. *Giardia's* virulence relies upon its ability to survive in the small intestine of the host. Perhaps the greatest challenge facing *Giardia* in this

environment is peristalsis, the contraction of smooth muscles that propels intestinal contents forward. *Giardia* must be able to maneuver within the intestine to quickly attach to the epithelial cells to avoid being swept away. By factors not entirely defined, *Giardia* trophozoites are eventually induced to encyst and new infectious cysts exit the host via the feces. A wide range of zoonotic hosts then consumes the cysts and the life cycle is repeated [10].

It is clear the *Giardia* cytoskeleton is critical for parasite motility, host attachment, encystation, excystation, and the cell-cycle. Therefore it is appropriate to view the cytoskeleton central role for infection and as a potential virulence determinate in *Giardia* [11]. This is in contrast to numerous other intestinal pathogens attachment mediated by protein-protein interactions with the pathogen's protein determined virulence factor [12-14]. As such, disruption of the cytoskeleton will likely disrupt giardiasis and serve as a target for infection prevention [11]. Ideally therapeutic targets share minimal homology with the host. Perhaps due to *Giardia*'s evolutionary position the cytoskeleton is quite divergent. *Giardia* is a member of the Excavata supergroup, one of six evolutionarily and morphologically diverse supergroups. The Excavata is one of the primary lineages of protists, and is proposed to be one of the deepest branching groups, closest to the common ancestor of all eukaryotes [15-17]. The evolutionary diversity within the Excavata represents genetic distances perhaps as large as those between plants and animals and fungi. Protists reflect the majority of eukaryotic genetic and cytoskeletal diversity [18, 19]. While some functions of the cytoskeleton are conserved across eukaryotes in diverse supergroups (e.g. motility and mitosis), the molecular components and pathways underlying these mechanisms (particularly those involving actin cytoskeleton), have extensive variation in less well studied eukaryotic supergroups like the Excavata [20]. On the basis of their evolutionary distances and the complex composition of their diverse cytoskeletal structures,

excavate protists may represent an undiscovered reservoir of novel cytoskeletal genes and cytoskeletal mechanisms [21].

An example of *Giardia's* cytoskeletal evolutionary divergence is with its complex microtubule (MT) cytoskeleton (Figure 1). This elaborate MT cytoskeleton is essential for motility, attachment, intracellular transport, cell division, and encystation/excystation [7, 22]. The *Giardia* MT cytoskeleton is comprised of both unique structures (the *median body*, *ventral disc*, *funis* and *axoneme-associated elements*) and elements commonly found in flagellated protists (*flagella* and *mitotic spindle*). The MT cytoskeleton creates a stable scaffold for cell shape and cell polarization [22]. The ventral disk is critical to virulence as this unique and highly organized MT structure promotes giardial attachment to the intestinal microvilli, allowing parasites to colonize and resist peristalsis [23, 24]. The media body (MB) is another *Giardia* specific structure. This enigmatic structure is non-membrane-bound semi-organized MT array of unknown function [25]. It is absent in other diplomonads.

The MB varies in form and presence during the cell-cycle, disappearing after mitosis. It has been suggested that the MB is a reservoir of tubulin subunits for duplicating MT structures, such as daughter ventral discs [26, 27]. The presence of such a reservoir could allow rapid assembly of structures like the ventral disc, and minimize the removal of dividing trophozites by peristalsis. The funis is another MT structure only found in *Giardia* and has no known function. It has been suggested to have either a structural role in maintaining giardial cell shape and/or a potential role in the flexion of the entire posterior caudal region during detachment. It is composed of sheets of MTs associated with the caudal axonemes, and is thought to be nucleated in the area between the nuclei as bands of linked MTs than then laterally fan out at the point of emergence of the ventral axonemes [28]. The remaining MT structures (flagella and two mitotic

spindles) share similarities to other flagellated protists. As with all eukaryotes, excavate protists have lost or gained conserved cytoskeletal genes and have retained cytoskeletal genes lost in other eukaryotic lineages. Comparative genomic analyses support that the majority of well-studied MT-associated cytoskeletal proteins occur in the excavates, including the structural components of flagella [29], kinesin and dynein MT motor protein families [30, 31], and proteins involved in microtubule dynamics such as EB1, XMAP215, and katanin [32]. However, in general, a large proportion of *Giardia* cytoskeletal genes lack homology or are absent compared to other eukaryotic genes [21]. These cytoskeletal differences potentially represent a rich opportunity for giardiasis therapies.

Giardia contains the most divergent eukaryotic actin identified to date and is the first eukaryote known to lack all canonical actin-binding proteins. *Giardia* actin only shares 58% sequence identity to that of other eukaryotes [20]. Despite the lack of known actin binding proteins, actin still has a role in fundamental cellular processes in *Giardia* such as membrane trafficking, cytokinesis, polarity, and control of cellular morphology [20, 33, 34]. Actin also has an often-overlooked structural role in flagella, but has been observed in the flagella [20, 35]. *Giardia* has actin but lacks myosin and all known actin cytoskeletal components required for amoeboid motility [32]. A lack of conservation of such core cellular components could indicate a lack of constraints in the mechanisms of mitosis and cytokinesis is tolerable in *Giardia*. For example, mitosis and cytokinesis are uncoupled in *Giardia* as the spindle is dismantled before cytokinesis begins and no actin-mysoin ring forms during cytokinesis [21, 26]. As such, it is unclear how the division plane is specified, if division involves force generation for daughter cell separation, or if division occurs strictly through a membrane remodeling mechanism. The novel

mechanisms by which *Giardia*-specific actin-binding proteins regulate the cellular functions likely offer promising new targets for anti-giardial therapies.

The majority of work to understand *Giardia*'s life-cycle events has relied on fixed cell analysis. Examining fixed cells to interpret dynamic processes has slowed the understanding of these events and lead to confusion. For example, previous efforts to investigate the cell-cycle completely overlooked the presence of a mitotic spindle. Consequently, several alternative and incorrect mechanisms for cell division were proposed [36-40]. The first study to identify a spindle and *Giardia*'s mitotic stages reported that *Giardia* mitosis resembles that of plants and animals [26]. The spindle, however, is completely disassembled prior to cytokinesis and division occurs longitudinally between daughter cells, perpendicular to the axis of nuclear division [20, 26, 41]. Techniques for live imaging in *Giardia* are needed in order to advance our understanding of *Giardia* life stage events [42].

In addition to major life-cycle events, other concurrent cellular processes have been identified that only occur during a respective event. In particular, the median body is one of the most prominent MT structures and only appears in interphase cells. However, it is not present in nascent daughter cells just after the cell-cycle [26]. It's been suggested for over 30 years that the median body serves as a tubulin reservoir over the cell-cycle, but there is still no supporting live-imaging evidence [27]. Furthermore, the daughter cell ventral discs are made *de novo* and simultaneously only near the end of mitosis [41]. It is unclear whether the timing of daughter disc construction correlates with a possible role during cell division. There are also observations that four of the eight flagella are shorter only during mid to late mitosis [43]. It is unknown whether these short flagella serve a possible function during the cell-cycle. To date, all of these events have been observed by using DIC (differential interference contrast), electron

microscopy, and/or through fixed cell analysis [27, 41, 43]. Taken together, these data indicate numerous, possibly important, biological events remain poorly understood over the cell-cycle. More broadly, it is probable there are understudied and possibly undiscovered events that occur during the other major life-cycle events. The ability to perform fluorescent live-cell imaging is a critical step towards unlocking the role the cytoskeleton and cellular proteins play during dynamics events.

Live imaging is an essential tool to probing cellular kinetics and the movement of fine structures during dynamic cellular processes [22]. Currently, there are no robust standardized live cell imaging techniques for fluorescent or DIC imaging during *Giardia*'s life-cycle events. The majority of live-cell imaging is limited to interphase cells. Interphase cells are largely static and present no opportunity to uncover the kinetics/dynamics of any major life-cycle processes. There are several technical hurdles hampering fluorescent live-cell imaging: lack of effective cell synchronization, cell motility, oxygen sensitivity [44], 37C temperature requirement, a fluorescent protein with an appealing signal to noise ratio, and the lack of low florescence media that supports cell growth. The inability to overcome these obstacles limits the capacity to spatiotemporally probe the role of the cytoskeleton, cellular dynamics, and the functional role(s) of key proteins during each of *Giardia*'s critical life-cycle events. Effective live-cell imaging for the field of *Giardia* research will lead to a better understanding of all cell cycle regulated events.

References

1.   Wolfe, M.S., *Giardiasis.* Clin Microbiol Rev, 1992. **5**(1): p. 93-100.
2.   Savioli, L., H. Smith, and A. Thompson, *Giardia and Cryptosporidium join the 'Neglected Diseases Initiative'.* Trends Parasitol, 2006. **22**(5): p. 203-8.
3.   Muhsen, K. and M.M. Levine, *A systematic review and meta-analysis of the association between Giardia lamblia and endemic pediatric diarrhea in developing countries.* Clin Infect Dis, 2012. **55 Suppl 4**: p. S271-93.
4.   Ansell, B.R., et al., *Drug resistance in Giardia duodenalis.* Biotechnol Adv, 2015. **33**(6 Pt 1): p. 888-901.
5.   Upcroft, P. and J.A. Upcroft, *Drug targets and mechanisms of resistance in the anaerobic protozoa.* Clin Microbiol Rev, 2001. **14**(1): p. 150-64.
6.   Farthing, M.J., *Giardiasis.* Gastroenterol Clin North Am, 1996. **25**(3): p. 493-515.
7.   Adam, R.D., *Biology of Giardia lamblia.* Clin Microbiol Rev, 2001. **14**(3): p. 447-75.
8.   Ankarklev, J., et al., *Behind the smile: cell biology and disease mechanisms of Giardia species.* Nat Rev Microbiol, 2010. **8**(6): p. 413-22.
9.   Friend, D.S., *The fine structure of Giardia muris.* J Cell Biol, 1966. **29**(2): p. 317-32.
10.   Koehler, A.V., et al., *Giardia/giardiasis - a perspective on diagnostic and analytical tools.* Biotechnol Adv, 2014. **32**(2): p. 280-9.
11.   Nosala, C. and S.C. Dawson, *The Critical Role of the Cytoskeleton in the Pathogenesis of Giardia.* Curr Clin Microbiol Rep, 2015. **2**(4): p. 155-162.
12.   Li, M., et al., *Cryptosporidium parvum rhomboid1 has an activity in microneme protein CpGP900 cleavage.* Parasit Vectors, 2016. **9**(1): p. 438.
13.   Paluszynski, J., et al., *Biochemical and functional characterization of CpMuc4, a Cryptosporidium surface antigen that binds to host epithelial cells.* Mol Biochem Parasitol, 2014. **193**(2): p. 114-21.
14.   Hayman, J.R., T.R. Southern, and T.E. Nash, *Role of sulfated glycans in adherence of the microsporidian Encephalitozoon intestinalis to host cells in vitro.* Infect Immun, 2005. **73**(2): p. 841-8.
15.   Hampl, V., et al., *Phylogenomic analyses support the monophyly of Excavata and resolve relationships among eukaryotic "supergroups".* Proc Natl Acad Sci U S A, 2009. **106**(10): p. 3859-64.
16.   Baldauf, S.L., *The deep roots of eukaryotes.* Science, 2003. **300**(5626): p. 1703-6.
17.   Morrison, H.G., et al., *Genomic minimalism in the early diverging intestinal parasite Giardia lamblia.* Science, 2007. **317**(5846): p. 1921-6.
18.   Patterson, D.J., *The Diversity of Eukaryotes.* Am Nat, 1999. **154**(S4): p. S96-s124.
19.   Baldauf, S.L., et al., *A kingdom-level phylogeny of eukaryotes based on combined protein data.* Science, 2000. **290**(5493): p. 972-7.
20.   Paredez, A.R., et al., *An actin cytoskeleton with evolutionarily conserved functions in the absence of canonical actin-binding proteins.* Proc Natl Acad Sci U S A, 2011. **108**(15): p. 6151-6.
21.   Dawson, S.C. and A.R. Paredez, *Alternative cytoskeletal landscapes: cytoskeletal novelty and evolution in basal excavate protists.* Curr Opin Cell Biol, 2013. **25**(1): p. 134-41.
22.   Elmendorf, H.G., S.C. Dawson, and J.M. McCaffery, *The cytoskeleton of Giardia lamblia.* Int J Parasitol, 2003. **33**(1): p. 3-28.

23.   Holberton, D.V., *Mechanism of attachment of Giardia to the wall of the small intestine.* Trans R Soc Trop Med Hyg, 1973. **67**(1): p. 29-30.
24.   Holberton, D.V., *Fine structure of the ventral disk apparatus and the mechanism of attachment in the flagellate Giardia muris.* J Cell Sci, 1973. **13**(1): p. 11-41.
25.   Piva, B. and M. Benchimol, *The median body of Giardia lamblia: an ultrastructural study.* Biol Cell, 2004. **96**(9): p. 735-46.
26.   Sagolla, M.S., et al., *Three-dimensional analysis of mitosis and cytokinesis in the binucleate parasite Giardia intestinalis.* J Cell Sci, 2006. **119**(Pt 23): p. 4889-900.
27.   Brugerolle, G., *[Ultrastructure of the genus Enteromonas da Fonseca (Zoomastigophorea) and revision of the order of Diplomonadida Wenyon].* J Protozool, 1975. **22**(4): p. 468-75.
28.   Benchimol, M., et al., *Visualization of the funis of Giardia lamblia by high-resolution field emission scanning electron microscopy--new insights.* J Struct Biol, 2004. **147**(2): p. 102-15.
29.   Wickstead, B. and K. Gull, *The evolution of the cytoskeleton.* J Cell Biol, 2011. **194**(4): p. 513-25.
30.   Wickstead, B. and K. Gull, *Dyneins across eukaryotes: a comparative genomic analysis.* Traffic, 2007. **8**(12): p. 1708-21.
31.   Wickstead, B. and K. Gull, *A "holistic" kinesin phylogeny reveals new kinesin families and predicts protein functions.* Mol Biol Cell, 2006. **17**(4): p. 1734-43.
32.   Fritz-Laylin, L.K., et al., *The genome of Naegleria gruberi illuminates early eukaryotic versatility.* Cell, 2010. **140**(5): p. 631-42.
33.   Castillo-Romero, A., et al., *Participation of actin on Giardia lamblia growth and encystation.* PLoS One, 2009. **4**(9): p. e7156.
34.   Castillo-Romero, A., et al., *Rab11 and actin cytoskeleton participate in Giardia lamblia encystation, guiding the specific vesicles to the cyst wall.* PLoS Negl Trop Dis, 2010. **4**(6): p. e697.
35.   Kato-Minoura, T., M. Hirono, and R. Kamiya, *Chlamydomonas inner-arm dynein mutant, ida5, has a mutation in an actin-encoding gene.* J Cell Biol, 1997. **137**(3): p. 649-56.
36.   Kabnick, K.S. and D.A. Peattie, *In situ analyses reveal that the two nuclei of Giardia lamblia are equivalent.* J Cell Sci, 1990. **95 (Pt 3)**: p. 353-60.
37.   Ghosh, S., et al., *How Giardia swim and divide.* Infect Immun, 2001. **69**(12): p. 7866-72.
38.   Yu, L.Z., C.W. Birky, Jr., and R.D. Adam, *The two nuclei of Giardia each have complete copies of the genome and are partitioned equationally at cytokinesis.* Eukaryot Cell, 2002. **1**(2): p. 191-9.
39.   Solari, A.J., et al., *A unique mechanism of nuclear division in Giardia lamblia involves components of the ventral disk and the nuclear envelope.* Biocell, 2003. **27**(3): p. 329-46.
40.   Benchimol, M., *Mitosis in Giardia lamblia: multiple modes of cytokinesis.* Protist, 2004. **155**(1): p. 33-44.
41.   Tumova, P., J. Kulda, and E. Nohynkova, *Cell division of Giardia intestinalis: Assembly and disassembly of the adhesive disc, and the cytokinesis.* Cell Motility and the Cytoskeleton, 2007. **64**(4): p. 288-298.
42.   Elmendorf, H.G., et al., *Initiator and upstream elements in the alpha2-tubulin promoter of Giardia lamblia.* Mol Biochem Parasitol, 2001. **113**(1): p. 157-69.

43.   Nohynkova, E., P. Tumova, and J. Kulda, *Cell division of Giardia intestinalis: flagellar developmental cycle involves transformation and exchange of flagella between mastigonts of a diplomonad cell.* Eukaryot Cell, 2006. **5**(4): p. 753-61.

44.   Gut, J., et al., *An image-based assay for high throughput screening of Giardia lamblia.* J Microbiol Methods, 2011. **84**(3): p. 398-405.
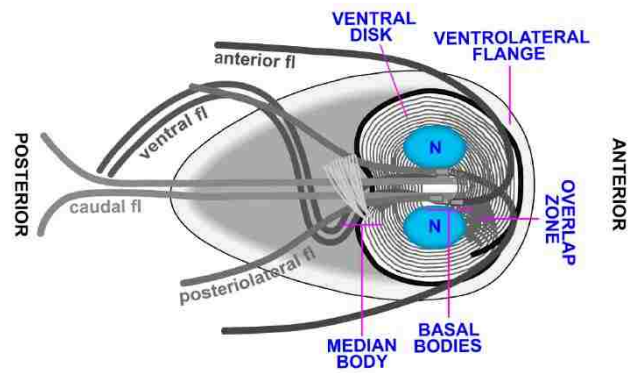
Figure 1

Figure 1. (A) Diagram of cellular features of an interphase trophozoite (N=nucleus; fl=flagellum).

Chapter 2

Myosin-independent cytokinesis in *Giardia* utilizes flagella to coordinate force generation and direct membrane trafficking

William R. Hardin[1], Renyu Li[1], Jason Xu[2], Andrew Shelton[1], Germain C. M. Alas[1], Vladimir N. Minin[1,2], Alexander R. Paredez[1*]

[1]Department of Biology, University of Washington, Seattle, United States; [2]Department of Statistics, University of Washington, Seattle, United States

Abstract: Devoid of all known canonical actin-binding proteins, the prevalent parasite, *Giardia lamblia,* uses an alternative mechanism for cytokinesis. Unique aspects of this mechanism can potentially be leveraged for therapeutic development. Here, live-cell imaging methods were developed for *Giardia* to establish division kinetics and the core division machinery. Surprisingly, *Giardia* cytokinesis occurred with a median time that is ~60 times faster than mammalian cells. In contrast to cells that utilize a contractile ring, actin was not concentrated in the furrow and was not directly required for furrow progression. Live-cell imaging and morpholino depletion of axonemal Paralyzed Flagella 16 (PF16) indicated that flagella-based forces initiated daughter cell separation and provided a source for membrane tension. Inhibition of membrane partitioning blocked furrow progression, indicating a requirement for membrane trafficking to support furrow advancement. Rab11 was found to load onto the intracytoplasmic axonemes late in mitosis and to accumulate near the ends of nascent axonemes. These developing axonemes were positioned to coordinate trafficking into the furrow and mark the center of the cell in lieu of a midbody/phragmoplast. We show that flagella motility, Rab11, and actin coordination are necessary for proper abscission. Organisms representing three of the five eukaryotic supergroups lack myosin II of the actomyosin contractile ring. These results support an emerging view that flagella play a central role in cell division amongst protists which lack

myosin II and additionally implicate the broad use of membrane tension as a mechanism to drive abscission.

Significance: Many protists, including *Giardia*, lack myosin II and thus are unlikely to use the canonical contractile mechanism of cell division. *Giardia* depends solely on its flagella for motility; here we show that flagella function is also required to drive daughter cells in opposite directions for cytokinesis. Additionally, just before cytokinesis, Rab11 accumulated in the forming furrow and the nascent intracytoplasmic axonemes were oriented to deliver Rab11. This mechanism constitutes a novel means to mark the center of the cell and guide trafficking to the furrow. These results support an emerging view that flagella play a central role in cell division amongst protists which lack myosin II.

Introduction:

Cell division is a fundamental process whereby cellular content is partitioned for proliferation. Drugs that target this process are immensely valuable as cancer therapeutics [1] and have promise for treating infectious disease [2-4]. *Giardia lamblia* (synonymous with *G. intestinalis and G. duodenalis*), is a common waterborne pathogen that infects 280 million people each year [5]. In addition to being a major parasite, *Giardia* belongs to possibly the earliest diverging eukaryotic lineage and could provide clues about early mechanisms of cell division [6, 7]. Despite the fundamental requirement for division in order to proliferate, the mechanisms underlying cytokinesis vary across the evolutionary tree [8]. Since *Giardia* has actin but lacks myosin and all known actin cytoskeletal components required for amoeboid motility and cytokinesis [9], it is not clear how the division plane is specified, if division involves force

generation for daughter cell separation, or if division occurs strictly through a membrane remodeling mechanism [8].

Our most complete mechanistic understanding of cytokinesis comes from studies of model organisms that are Unikonts, a group which is comprised of the supergroups Opisthokonta (*E.g.* yeast to man) and Amoebozoa (*E.g. Dictyostelium discoideum*) [10]. Animals use an actomyosin contractile ring to pinch the plasma membrane down onto the midbody microtubules [11]. Abscission at the midbody is subsequently completed by plus-end directed vesicle trafficking to the center of the midbody and ESCRT-III mediated scission [12]. Plants lack myosin II and the pinching down mechanism for scission; instead, extensive membrane trafficking is used to build a new cell wall, known as the cell plate, between daughter cells. After mitosis, interdigitated spindle microtubules maintain anti-parallel organization and transition to a cytokinetic apparatus known as the phragmoplast. Microtubules of the phragmoplast guide Golgi-derived vesicles to the center of the division plane using plus-end directed trafficking [13]. Intriguingly, proteomic analysis has revealed that the phragmoplast shares many molecular components with the mammalian midbody, suggesting that, despite appearances, plant cytokinesis employs a modified midbody mechanism [14].

Discovery of the diverse strategies that cells use to accomplish cell division will inform on the constraints of eukaryotic cell division. Although the myosin II-based actomyosin contractile ring has a central role in Unikont cytokinesis, cells can divide without myosin II under specific conditions [15-17]. *Dictyostelium* and mammalian cells with impaired myosin II function can complete cytokinesis using traction to pull daughter cells apart [15-17]. Hence, the use of myosin II may be implemented on top of a more ancient mechanism that is dependent on cortical tension and a Laplace-like pressure property of cells that serves to minimize the surface

area to volume ratio [18, 19]. Moreover, phylogenetic distribution of myosin II is limited to

Unikonts with one known exception that may be an example of horizontal gene transfer [20, 21];

thus, three of the five eukaryotic supergroups use an alternative to the canonical "purse-string"

mechanism of cytokinesis, as is the case in plants [22]. The number and types of alternative

mechanisms remain understudied [23], especially in cells that have been difficult to culture and

for which molecular and imaging methodologies are lacking.

The study of giardial mitosis and cytokinesis has been challenging due to a lack of

effective cell synchronization and live-cell imaging, which is complicated by *Giardia's* lethal

sensitivity to oxygen concentrations above 5% [24]. Initial studies completely missed the

presence of a mitotic spindle leading to the proposal of several incompatible mechanisms for cell

division [25-29]. Ultimately, *Giardia's* mitotic stages were found to begin similarly to that of

plants and animals [30]. The spindle, however, is completely disassembled prior to cytokinesis

and division occurs across the long rather than the short axis of the cell [30-32]. The mechanism

for coordinating membrane remodeling during cytokinesis and the timing of major events remain

unexplored. Here we combine the use of a hypoxic stage-top incubator, a newly developed low

fluorescence media formulation, and a bright fast-folding fluorescent protein tag [33] that, for the

first time, allow robust imaging of *Giardia* throughout the cell cycle. We use these technical

advances to uncover the core division machinery and establish a working model for *Giardia's*

mechanism of myosin-independent cytokinesis.

Results:

***Giardia* utilizes a tubulin reservoir to support rapid mitosis and ventral disc assembly**

The ability to follow fluorescent proteins in live cells has been one of the most powerful tools for

uncovering the mechanism of cytokinesis in model systems [34]. In order to study the dynamics

of individual proteins during the cell cycle, we developed a low fluorescence culture medium

that supports cell growth. Our newly formulated medium, SB5050, has a 92% reduction in

background fluorescence yet still maintains 35% as many mitotic events as standard media (Fig.

S1, Dataset S1). To follow tubulin dynamics, we tagged the N-terminus of β-tubulin with an 18

amino acid flexible linker and the fast folding bright fluorescent protein, mNeonGreen [33],

generating mNeonGreen-C18-β-tubulin (mNG-Tub). *Giardia* has a highly organized

microtubule cytoskeleton (Fig. 1A), including eight flagella, a ventral adhesive disc (formed

from an overlapping sheet of parallel microtubules that facilitates attachment to the host), and a

median body (a bundled microtubule structure thought to be a reservoir of tubulin and disc

components) [35]. Expression of mNG-Tub under its endogenous promoter permitted

visualization of microtubules in the ventral disc, median body, flagella, and mitotic spindles (Fig.

1; Movie S1).

Upon initiation of mitosis, the flagella and basal bodies rearranged and two independent

mitotic spindles nucleated in proximity to the basal bodies (Fig. 1B; T14). As the spindles grew

in size, the tubulin signal from the median body shrank proportionally (T13-19). During

telophase, the cage-shaped spindles collapsed into tight bundles of microtubules (compare T19

and T23). Daughter disc assembly was initiated at one end of each spindle in opposing

orientations (T23). As the ventral discs continued to grow in size, the spindle was disassembled

and nascent flagella grew in the region previously occupied by the spindle (T26). The observed

flux of tubulin from the median body to assembling microtubule structures is the first

experimental support for the previously proposed idea that the median body is utilized as a

reservoir of tubulin [36, 37]; however, our results indicate that, in addition to being a reservoir

for building the ventral discs (process requiring ~ 3 minutes), the median body supports

assembly of the spindle and nascent flagella. Meanwhile, during daughter ventral disc neogenesis, the parental disc disassembled from the interior causing the central microtubule bare area to grow as the disc thinned (T23-T26). Once the overlap zone of the disc disassembled, the disc microtubules straightened leading to the adoption of an open C-shaped conformation (T27). Furrow ingression coincided with transition to this open conformation. The timing of these events suggests that the parental disc physically impedes furrow progression and its disassembly is tightly coordinated with cytokinesis.

Giardia lacks the machinery for amoeboid motility and depends solely on flagella for locomotion [9, 38]. Notably, high speed imaging has revealed that Giardia's four flagella pairs have different modes of movement. The caudal flagella, which originate near the nuclei and have approximately 2/3 of their length running through the cell, are used to undulate the anterior of the cell so that this region acts like a flipper, while the anterior and posterolateral flagella generate canonical power strokes [39]. Corresponding with the parental disc opening, daughter cells moved in opposition to each other. We propose that caudal flagella flexion (sustained bending) is important for initiating daughter cell separation. As the intracytoplasmic axonemes of the caudal flagella are nucleated by basal bodies that are intimately associated with the nascent ventral discs [40], this arrangement could facilitate positioning the daughter ventral discs. Indeed, these intracytoplasmic axonemes were observed to flex in opposite directions during cytokinesis and as the daughter cells moved in opposite directions, the plasma membrane appeared to stretch around the two new discs and the furrow advanced between them (Fig. 1B, Movie S1, and Movie S2). Abscission occurred after daughter cells transitioned into a tail-to-tail orientation and swam in opposite directions, presumably driven by anterior flagella power strokes. After scission, daughter cells quickly attached to the cover glass, indicating that the

nascent ventral discs are functional upon cytokinesis despite the immaturity of the ventral flagella, which have been proposed to support attachment [41]. Notably, the ventral and posteriolateral flagella were observed to grow at different rates (Fig. 1B; Movie 1) suggesting that the mechanism of flagella-length control is more complex in *Giardia* than the constitutive regulatory mechanism of *Chlamydomonas reinhardtii* [42]. Also, there was no observed re-building of the median body during the time we observed the re-growth of the flagella supporting the idea that the median body is a microtubule reservoir.

Previous studies of fixed cells found that the start of mitosis is indicated by coordinated chromosome condensation, translocation of the two nuclei to the cell center, and re-positioning of basal bodies and their attached flagella to set up the mitotic spindles [30, 32, 43, 44]. A prior study using drugs to partially synchronize cells was able to follow a handful of cells through division using 40X phase optics and found that mitosis and cytokinesis took approximately 50 minutes [32]. Using long term 4D DIC imaging in the absence of any drugs we find that mitosis and cytokinesis occurred in ~7.5 minutes (Figure S2A, Movie S3), much faster than the original estimate made without temperature or atmospheric control [32]. The median time between mitosis to the initiation of cytokinesis was 6 minutes 28 seconds (Fig. S2B, n=93). Remarkably, the median time for cytokinesis was 50 seconds (Fig. S2C, n=130), with 89% of cells completing cytokinesis within 2 minutes. This time is 30 to 90 times faster than the rates reported for plants, fungi, and mammalian cells [23, 45-47]. Intriguingly, *Dictyostelium* myosin II mutants divide in approximately half the time of their wild type counterparts (6-8 minutes), suggesting that the myosin II based cytokinesis may have arisen for increased fidelity rather than speed [48]. The previously observed doubling time for the strain WBC6, used in this study, was ~8 hours; thus our timing is precisely in agreement with mitotic index of 1.3% observed in non-synchronized

cultures (6.5min/480min=0.013) [30, 49]. Cleavage furrow ingression measurements were averaged by randomly sampled LOESS curves; ingression is fastest after initiation then progresses at a steady rate and is followed by a slower final scission event (Fig. 1C, S2D, S2E). This non-uniform rate may indicate a requirement for the sequential action of multiple cell division components that cooperate together to achieve furrow ingression and abscission.

Flagella are required for cleavage furrow formation and abscission

Myosin II mutants of *Dictyostelium* were shown to use ameboid motility to crawl apart for cytokinesis [17]. Organisms that lack myosin II and depend on their flagella for motility, such as *T. brucei* and *Tetrahymena*, also require motility for abscission [50-52]. To address whether the flagella have a direct role in cytokinesis, we treated *Giardia* with small molecule inhibitors that have been shown to disrupt flagellar function in other systems [Ciliobrevin A, Ciliobrevin D, drug E, drug F, and drug P [53-55]]. However, these drugs did not visibly perturb *Giardia* flagella beating or length. We, therefore, tested the role of the flagella by knocking down Paralyzed Flagella 16 (PF16), a highly conserved key component of the axoneme central pair apparatus [56] required for stabilizing the orientation of the central pair microtubules in *C. reinhardtii* [57], mice [58], and T. *brucei* [52]. Misorientation of the central pair in *T. brucei* impairs cytokinesis [52]. Likewise, a previous study of PF16 in *Giardia*, aimed at testing the role of the flagella in parasite attachment, noted that PF16 knockdown reduced flagella motility and impaired cytokinesis [41]. The nature of this cytokinesis defect, however, was not reported.

To monitor the efficacy of the morpholino knockdown, we endogenously tagged PF16 with a C-terminal triple-hemagglutinin epitope tag (HA) [59]. As expected, PF16-HA localized to the flagella and quantitative western blotting revealed 69% depletion at the population level,

18

24 hours after morpholino treatment (Fig. 2A, S3A). With the exception of a single cell (1/885), fixed cell analysis revealed that the interphase PF16-depleted cells had typical polarity and cytoskeletal organization. However, 11.5% of the knockdown cells had 4 or more nuclei compared to only 1.2% in the control, suggesting impaired cytokinesis. These cells were categorized based on furrow progression, compared to the control we observed an increase in cells that did not initiate a furrow, or were in the process of cytokinesis or abscission. These data indicate a requirement of flagella function for *Giardia* cytokinesis (Fig 2A, B).

To explore the roles that PF16 and flagellar movement play in cytokinesis, we used DIC optics to film PF16-depleted cells between 16-28h after morpholino treatment. Significant differences were observed between control and PF16-HA knockdown cells in both time taken to and ability to divide; statistical significance was verified by Kaplan-Meier survival analysis (Fig. 2C, D and S4). To determine how PF16 impacts cleavage furrow ingression dynamics, we measured furrow progression from time-lapse movies of PF16-depleted cells. Due to varying levels of morpholino penetrance within the cell population, we examined the 11 slowest dividing cells to identify the point at which these cells slowed or stalled their furrow progression. Consistent with an increase in the number of cells that did not initiate a furrow in the fixed cell analysis, we found during live-cell analysis that upon the onset of cytokinesis, furrow progression halted and did not reach the abscission stage (Fig. 2E, S3B and Movie S4). In contrast, analysis of the 11 slowest control cells (lagging tail with division times >2 min) showed that the cleavage furrow rapidly proceeded to ~8µm, experienced a short delay, then completed division (Fig. 2E). These results indicate that the flagella are required to initiate cytokinesis. Given that the flagella are *Giardia's* only means for motility, it follows that the observed flexion of the intracytloplasmic axonemes of the caudal flagella initiate cell separation (Fig. 1, Movie 1,

2). As the daughter cells move apart, they become oriented such that beating of the extracellular flagella can propel the cells in opposite directions for scission. A mechanical role for the flagella, however, does not exclude the possibility that the flagella could have additional roles, such as serving as a scaffold for transport or polarity signaling [51, 60, 61].

Actin has two major roles for the progression of cytokinesis

We previously reported that actin depletion by morpholino knockdown results in the accumulation of aberrantly-nucleated cells, indicating a role for actin in cytokinesis [31]. However, our initial actin localization study reported actin localization in a cell that failed to complete cytokinesis and was not actively in the process of division [31]. We, therefore, re-examined actin localization throughout the cell cycle [31]. These studies were necessarily limited to fixed cells because attempts to fluorescently tag *Giardia* actin or to use common actin reporters have been unsuccessful in our hands. In agreement with our previous studies, actin was enriched around nuclei and forming spindles at the onset of mitosis and remained enriched around the spindles and the developing axonemes throughout mitosis (Fig. 3A) [31, 62]. The enrichment of actin around microtubule structures is consistent with actin's role in positioning them [31]. We did not observe any actin structure that marked the position of the furrow, which is in contrast to cells with a contractile ring where actin is enriched along the furrow. Actin levels were reduced in the first few microns of the cleavage furrow trajectory and an actin clearing was regularly observed just ahead of the furrow cortex (Fig. 3A, analysis in S5). The actin cytoskeleton accounts for most of the mechanical properties of the cell cortex [63], thus differential cortical reinforcement may indicate that selectively altering cortical mechanics is important for cleavage furrow ingression [18, 19].

To assess the role of actin during cytokinesis, we used time-lapse microscopy to image actin-depleted cells, 16 – 26 h after morpholino treatment (Fig. 3B). Actin depletion significantly impacted division timing (Fig. S4). Actin-depleted cells fell into two distinct phenotypic classes: stalled cells which took longer than two minutes to complete cytokinesis and blocked cells which never completed cytokinesis (Fig. 3B, C, and Movie 5, 6). Some cells that never completed cytokinesis appeared to have mis-positioned flagella that physically impeded cleavage furrow ingression (Fig. 3B and Movie 5). We previously reported that 40% of actin-depleted cells had mis-positioned flagella 24 hours after knockdown [31]; we now understand that this could block cytokinesis through misdirected force generation or physically impeding the furrow. To further examine effects of actin knockdown on cleavage furrow ingression, we measured furrow progression in cells that were stalled in cytokinesis; we focused on those that took 6-15 minutes to complete cytokinesis as this group was unique to the actin depleted population. Furrow progression began at rates similar to control cells, but after ~20 seconds, the rate of progression slowed (Fig. 3D, S3D). The cells were further delayed at the tail-to-tail stage revealing that actin has a specific role in supporting the abscission step of cytokinesis. Slower progression could result from defects in cortical mechanics that may normally work to direct furrowing between the daughter cells. Considering that *Giardia* actin has an established role in trafficking [31], the stalled phenotype could also indicate a role for actin in coordinating membrane trafficking during cytokinesis.

Membrane trafficking is essential for cleavage furrow progression

In animals, plants, and fungi, tethering complexes target Golgi-derived vesicles to the plasma membrane to support the increase in surface area required for cytokinesis [64-66]. In Figure 1 we pointed out the ventrolateral flange, a lamellipodia-like membrane protrusion that is consumed during cytokinesis; this structure may serve as a source of plasma membrane (also see Movie 2). The rapid speed at which *Giardia* divides, the presence of a potential plasma membrane reservoir, and the lack of both the exocyst and TRAPP-II tethering complexes [67], led us to question whether there is a requirement for new membrane delivery during cytokinesis. To address this, and generally disrupt endomembrane trafficking, we treated cells with Brefeldin A (BFA). BFA has been shown to disrupt ER to Golgi transport and change the distribution of membrane pools in model eukaryotes [68-70]. Although *Giardia* lacks a conventional Golgi, BFA has been shown to potently disrupt trafficking out of the ER as well as disrupt COP1 localization [70-73], similar to plants and animals. As expected, BFA treatment induced swelling of the perinuclear ER, as visualized by the ER marker PDI2 (Fig. S3E)[74]. BFA treatment similarly altered organization of the trafficking regulator Rab11 which has partially overlapping localization with PDI2 (Fig. S3E) and is required for cytokinesis in other eukaryotes (discussed below). Time-lapse microscopy and quantitative analyses revealed that BFA-treated cells either completed cytokinesis at statistically slower rates or arrested with partially ingressed cleavage furrows (Fig. 4A, B, and Movie 7). To determine the point at which the treatment impacted furrow progression, we measured the distance to scission in cells that never completed cytokinesis. At the onset of cytokinesis, furrows are ~14 μm long; BFA treatment stopped furrow progression shortly after cytokinesis began with ~8 μm of the furrow path remaining (Fig. 4C, S3F). This result

demonstrates that impaired membrane trafficking blocks cytokinesis and may indicate a requirement for additional membrane and associated regulator factors in supporting cytokinesis.

Rab11-GTPase localizes to the pre-furrow and is necessary for cytokinesis

Rab11 is essential for delivering membrane and cytoskeletal effector proteins to the cleavage furrow in plants, animals, and the protist *T. brucei* [75-78]. In animal cells, Rab11 is further used to support abscission via plus end trafficking on microtubules of the midbody [65, 76]. We used live-cell imaging to localize Rab11 throughout the cell cycle. In interphase cells, mNG-C18-Rab11 (mNG-Rab11) localized to the perinuclear ER and cell cortex (Fig. 5A). In late telophase, bright puncta and linear arrays of mNG-Rab11 were observed that corresponded to the position of intracytoplasmic axonemes (n=20 cells; Figure 5A Movie 8). Fixed cell analysis confirmed that the linear arrays are aligned with intracellular axonemes, implicating the flagella as highways for vesicle transport (Fig 5B). Ahead of anterior-to-posterior furrow ingression, Rab11 transiently delineated the cleavage furrow indicating a role in pre-furrowing. Pre-furrowing (formation of a dorsal-ventral invagination) could be observed in 4D DIC movies to occur 13.4 ± 5 seconds (n=50 cells), ahead of anterior-posterior furrow progression. As the anterior-posterior furrow advanced, mNG-Rab11 remained at the leading edge of the cleavage furrow, as well as along the length of the furrow (Fig. 5A, Movie 8). Remarkably, fixed cell analysis revealed that in addition to loading onto the intracytoplasmic axonemes of mature flagella, Rab11 was concentrated at the ends of the developing axonemes positioned to traffic Rab11 directly into the furrow (Fig. 5B, Movie S9). Similarly oriented to midbody microtubules, the plus ends of these axonemes terminate at the future site of the furrow; we propose that these developing axonemes have analogous function to the midbody/phragmoplast and are used to guide trafficking into the

23

furrow. Consistent with a role for actin in supporting vesicular trafficking, actin was observed to colocalize with Rab11 near the ends of the growing flagella tips (Fig 5B, S6A, Movie S9).

To verify a functional role for Rab11 in *Giardia* cytokinesis, we depleted Rab11 with morpholinos and validated the knockdown by generating an endogenously tagged morpholino sensitive [79] HA-Rab11 cell line. 24 hours after electroporation, Rab11 was depleted by ~70% versus the control (Fig. S6E). Rab11 depleted cells took longer to divide or failed to divide, in agreement with a critical contribution of membrane remodeling towards cleavage furrow progression and is consistent with the phenotype produced by of dominant negative and constitutively active Rab11 mutants (Figure 5C, D, S4, S6). The *Giardia* genome contains 6 Rab proteins. The more severe impairment of cytokinesis by BFA treatment may indicate that Rab11 only accounts for a subset of the membrane remodeling associated with cytokinesis. Yet, the overall importance of Rab11 for cytokinesis is likely under-reported by our timing data as many cells that completed division with normal kinetics had abnormal cleavage furrow placement or generated daughter cells with irregular morphology, reminiscent of the actin knockdown phenotype. Importantly, conservation of Rab11 function in *Giardia* implicates Rab11 as an ancient component of the cell division machinery.

Co-localization between Rab11 and actin as well as the abscission defect associated with depletion of either protein suggests these two systems act cooperatively. Thus, we examined whether Rab11 localization was impacted by actin knockdown. In addition to cells with abnormally positioned flagella, which could alter Rab11 trafficking, we observed that 55% of cells had abnormal morphology at the abscission site compared with 14% in the controls (Fig. 5E, 5F). This defect included missing regions of the cell body and/or Rab11 positive membrane accumulation at the abscission site. During DIC imaging of control cells similar membrane

accumulations were sometimes observed to form after abscission, particularly for cells initially connected by a cytoplasmic bridge. The excess membrane was eventually retracted and incorporated into the cell body, but actin depleted cells often had thicker than usual cytoplasmic bridges which could account for the excessive membrane found at the abscission site. The abnormal abscission site morphology and increased number of cells with Rab11 labeled membrane accumulations, is consistent with actin coordinating the final membrane remodeling steps required for abscission.

Discussion:

Here we set out to study how *Giardia*, a highly divergent eukaryote, lacking both the conserved contractile ring and amoeboid motility proteins, carries out cell division. Using newly developed live cell imaging methodologies, genetic disruption, and drug studies, we have established a role for membrane trafficking and the cytoskeleton in *Giardia* cytokinesis, as well as revealing several twists on extant mechanistic themes. Out of *Giardia's* eight-hour cell cycle, a relatively brief period is spent in mitosis and cytokinesis. For fixed cell studies of non-synchronized cells, our results indicate that only about 1.3% (6.5min/8hours) of the cells will be in mitosis and 0.17% (50 sec/8hours) of the cells will be in cytokinesis. These percentages are in agreement with the previously reported mitotic index [30]. However, in the past, challenges associated with finding and staging rarely observed dividing *Giardia* led to misunderstanding the normal progression of mitosis and cytokinesis. Cells in the process of cytokinesis should have daughter cells smaller than interphase trophozoites, lacking a median body, and possessing only four full-length flagella. The often shown heart-shaped cells with daughter cells equivalent in size to interphase trophozoites are abnormal cells that failed to complete cytokinesis. These are the

approximately 1% of cells that never completed cytokinesis in our controls (Fig S1C).

Remarkably, we observed heart shaped cells recover in the next round of division. We and others have mistakenly interpreted these configurations to be in the process of cytokinesis when they were not actively dividing [25, 30, 31, 80-82]. Therefore, the methodical advances and observations described here are of immense value for understanding the process of cytokinesis and enabling additional studies of living and dividing *Giardia*. Importantly, unique and divergent molecular machinery in *Giardia* has the potential to be leveraged for treating this major parasite. In particular, *Giardia* specific proteins that regulate cell polarity and coordinate the cytoskeletal dynamics and membrane remodeling described here could be important therapeutic targets for clearing infection [4].

The inside-out model for *Giardia* cytokinesis

Based on our analyses, we present a working model that can explain myosin-independent cytokinesis in *Giardia* (Fig. 6). Upon initiation of mitosis, the basal bodies and anterior flagellar exit sites are repositioned in a process that is, in part, actin dependent (Fig. 1, 3) [31]. The microtubules utilized to form the two spindles are derived from the median body (Fig. 1). At the end of mitosis, the two spindles transition from cage-like to bundled organization. The two daughter discs and four nascent flagella are assembled in opposing orientations near the spindle poles. As the daughter discs are further developed, the parental disc thins out; disassembly of the overlap zone of the disc coincides with the start of cytokinesis. The tips of the depolymerizing parental disc were sometimes observed to be coated with Rab11; thus, the disc may act as the initial guide for Rab11 enrichment between daughter cells. Force generated by the internal axonemes of the caudal flagella drive the daughter cells in opposite directions. This movement

causes the plasma membrane to stretch around the two daughter discs leading to membrane tension (Fig. 1, Movie S1-S3). Actin is cleared just ahead of the furrow cortex and may act to direct the progression of the cleavage furrow (Fig. S5). Additional membrane delivery is mediated by Rab11-vesicles that are trafficked along the intracytoplasmic axonemes and ultimately delivered by the growing posteriolateral and ventral flagella, whose plus ends point towards the furrow and act as the functional equivalent of a midbody/phragmoplast (Fig. 5). Just before scission, the force for daughter cell separation transitions from flexion of the intracytoplasmic caudal flagella axonemes, to propulsion by the beating external portions of the flagella, driving the cells in opposite directions (Movie S1-S3). The final swimming stage is reminiscent of traction-mediated cytokinesis observed in myosin II mutants of other eukaryotes; here swimming, rather than crawling, provides the force to pull the daughter cells apart.

An emerging view is that flagella may play a fundamental role in protozoan cytokinesis. In addition to a role in force generation, flagella act as scaffolds for signaling and polarity [51, 60, 61]. A requirement for motility in abscission has previously been reported for *T. brucei,* a protist that also lacks an actomyosin-based cytokinetic apparatus [51, 52, 83, 84], and *T. thermophila*, which uses ciliary driven cell motility during cytokinesis [50, 85, 86]. In *T. brucei*, more than 30 different motility mutants have been reported to have cell separation defects that correlate with the motility defect [2]. Remarkably, abscission defects can be rescued by mechanical agitation, illustrating the importance of membrane tension for abscission [52, 84]. Given the large number of protists that lack myosin II [20, 21], a role for flagella in cytokinesis could be more common in nature than what is presumed from studies of model eukaryotes, which only represent a small proportion of the eukaryotic tree.

Instead of taking the lead, actin plays a supporting role in furrowing

Given actin's central role in cell division of model eukaryotes, it is not surprising that actin has a role in *Giardia's* cytokinesis; yet the implementation is different. Distinct from that observed in model eukaryotes, *Giardia* actin is notably found at high levels along the cell edges where the ventral disc presses against the plasma membrane, but is cleared just ahead of the advancing furrow (Fig. S5). We propose that *Giardia* actin has a role in guiding cleavage furrow ingression. Cortical tension and membrane fluidity are important factors in regulating cytokinesis in model systems [18, 87]. Abnormal furrow placement and delayed abscission resulting from actin depletion are consistent with this proposed role (Fig 5E, 5F). Yet, we propose that actin's most critical role is in positioning the tubulin cytoskeleton so that the flagella can direct trafficking and force generation along the furrow. The mechanism used to activate actin polymerization for organelle positioning and differential cortical organization remain to be determined, although it is likely that *Giardia's* sole Rho family GTPase, GlRac has some role in coordinating actin polymerization and membrane remodeling during cytokinesis [31, 79].

In otherwise normal-looking cells, we observed many actin-depleted and Rab11-depleted cells that were stuck at the tail-to-tail stage of cytokinesis. This indicates a role for these proteins in the final membrane remodeling events required for abscission. A subset of Rab11 vesicles co-localize with actin in interphase cells, and in dividing cells actin and Rab11 were observed to co-localize near the ends of the nascent flagella. This is consistent with actin having some role in directing Rab11 traffic. In other systems, Rab11 has been found to utilize dynein, kinesins, and myosins for transport where long distance trafficking is supported by the microtubule cytoskeleton and actin is utilized for short range transport. *Giardia* lacks all myosin homologs and the FIP proteins that normally connect Rab11 to molecular motors [88]. Given localization

of Rab11 to the flagella and tips of depolymerizing discs, it seems likely that dynein and kinesin

motors are employed to support Rab11 trafficking. The specific molecules that link Rab11 to the

actin and tubulin cytoskeleton and whether GlRab11 delivers cytoskeletal effectors to the furrow

as in animal cells (Reviewed in [65], remains to be determined.

Materials and methods

Parasite strain and growth conditions

G. *lamblia* strain WB Clone 6 (ATCC 50803) was cultured as in [30].

Morpholino knockdown

Knockdown experiments were performed as described in [89] with morpholinos sourced from

Gene Tools. See Dataset S2 for sequences.

Vector Construction

All constructs used in this study were made using standard techniques, see Dataset S2 for

sequences and workflow. Note that N-terminal fusions result in morpholino resistant constructs

[62], therefore we included the first 27bp of the coding sequence to restore morpholino

sensitivity [79] to the 3HA-Rab11^{MS} construct.

Live imaging

In an effort to increase the mitotic index, cells were treated with 0.25µM Albendazole ~4hrs

before being imaged. Cells were chilled with ice for 20 minutes to detach from the culture tube

and then placed into an Attofluor cell chamber (Molecular Probes) and incubated in a GasPak EZ

anaerobic pouch (BD) for 1-2 hrs at 37° C. Cells were then washed four times with SB5050

(0.1% K2HP04, 0.06% KH2P04, 1% glucose, 0.2% NaCl, 0.2% cysteine-HCI monohydrate,

0.02% ascorbic acid, 0.0228% ferric ammonium citrate, 0.05% bovine bile and 5% bovine serum,

pH 7.1; see Dataset S1 for variants tested). Drug-free cells were overlaid with a mixture of 0.7-1% ultra-low gelling agarose (Sigma A2576) melted in HBS (137mM NaCl, 5mM KCl, 0.91mM Na_2HpO_4-heptahydrate, 5.55mM Glucose, 20mM HEPES, and pH7) and diluted into SB5050, left at room temperature for 10 min to solidify the agarose. Imaging was performed under 2.5% O_2, 5% CO_2, and 37° C (Oko Lab Boldline CO_2/O_2). Time-lapse imaging was performed on a DeltaVision Elite microscope (GE, Issaquah, WA) equipped with DIC optics, using a 100x1.4 NA or 60x1.42 NA objective, and sCMOS 5.4 PCle Air-cooled camera (PCO-TECH Inc).

Long-term imaging with DIC

Cells were imaged as above; however, cells were not exposed to albendezole and the washes and overlay utilized standard TYDK instead of SB50505.

Cleavage furrow measurements

Measurements were made along the length of the cleavage furrow, anterior to posterior starting upon the onset of cytokinesis through the completion of the process utilizing SoftWorx (API, Issaquah, WA).

Cell division rate assay

Confluent cultures were diluted by 60%. The cells were incubated in 50ng/mL Albendazole at 37° C for 5.5 hrs. Cells were detached and collected by centrifugation. The cell pellet was resuspended in 6mL drug-free media, 1mL of cell culture was mixed with paraformaldehyde, and then counted on a hemocytometer. The remaining 5mL cell culture was placed at 37° C for 1 hr then fixed with paraformaldehyde and counted on a hemocytometer.

Immunofluorescence microscopy

Fixed imaging was performed as in [79] using starve and release (3.5 hours) to increase mitotic index [30].

Western blotting

Blotting was performed as in [89].

Brefeldin A treatment

The long-term imaging with DIC as above, except cells were exposed to 25µM BFA in 0.035% DMSO three hours before and during imaging.

Statistical analysis

Highly statistically significant differences between times until cytokinesis are obtained using the Kaplan-Meier estimator, a nonparametric method (does not require distributional assumptions) from survival analysis [90]. We set a conservative censoring rule for cells that do not complete cytokinesis at 900 seconds without completion, a lower bound on widely varying total imaging times. To create curves and confidence bands cleavage furrow measurements obtained at each frame of imaging data were interpolated using local polynomial (LOESS) regression, producing a smooth curve corresponding to each representative cell [90]. Resampling this set of curves with replacement to generate 5000 bootstrap replicate datasets, we obtain nonparametric estimates of the median curve and 95% confidence intervals [91]. These results are displayed using standard pointwise confidence bands as well as using functional boxplots for completeness, which generalize notions such as outliers to entire curves rather than points; see [92] for details. In this case, the two visualization methods are not noticeably different, and provide more detailed support for results of formal hypothesis tests of significance based on Kaplan-Meier estimates of time until cytokinesis. Plots were generated using R (www.R-project.org).

References

1. Vermeulen, K., D.R. Van Bockstaele, and Z.N. Berneman, *The cell cycle: a review of regulation, deregulation and therapeutic targets in cancer.* Cell Proliferation, 2003. **36**(3): p. 131-149.
2. Ralston, K.S. and K.L. Hill, *The flagellum of Trypanosoma brucei: new tricks from an old dog.* Int J Parasitol, 2008. **38**(8-9): p. 869-84.
3. Lock, R.L. and E.J. Harry, *Cell-division inhibitors: new insights for future antibiotics.* Nature Reviews Drug Discovery, 2008. **7**(4): p. 324-338.
4. Hennessey, K.M., et al., *Identification and Validation of Small-Gatekeeper Kinases as Drug Targets in Giardia lamblia.* PLoS Negl Trop Dis, 2016. **10**(11): p. e0005107.
5. Lane, S. and D. Lloyd, *Current trends in research into the waterborne parasite Giardia.* Crit Rev Microbiol, 2002. **28**(2): p. 123-47.
6. Baldauf, S.L., *The deep roots of eukaryotes.* Science, 2003. **300**(5626): p. 1703-6.
7. He, D., et al., *An alternative root for the eukaryote tree of life.* Curr Biol, 2014. **24**(4): p. 465-70.
8. Dawson, S.C. and A.R. Paredez, *Alternative cytoskeletal landscapes: cytoskeletal novelty and evolution in basal excavate protists.* Curr Opin Cell Biol, 2013. **25**(1): p. 134-41.
9. Fritz-Laylin, L.K., et al., *The genome of Naegleria gruberi illuminates early eukaryotic versatility.* Cell, 2010. **140**(5): p. 631-42.
10. Hampl, V., et al., *Phylogenomic analyses support the monophyly of Excavata and resolve relationships among eukaryotic "supergroups".* Proc Natl Acad Sci U S A, 2009. **106**(10): p. 3859-64.
11. D'Avino, P.P., M.G. Giansanti, and M. Petronczki, *Cytokinesis in animal cells.* Cold Spring Harb Perspect Biol, 2015. **7**(4): p. a015834.
12. Guizetti, J. and D.W. Gerlich, *ESCRT-III polymers in membrane neck constriction.* Trends Cell Biol, 2012. **22**(3): p. 133-40.
13. Müller, S. and G. Jürgens, *Plant cytokinesis—No ring, no constriction but centrifugal construction of the partitioning membrane.* Seminars in Cell & Developmental Biology, 2016. **53**: p. 10-18.
14. Baluska, F., D. Menzel, and P.W. Barlow, *Cytokinesis in plant and animal cells: endosomes 'shut the door'.* Dev Biol, 2006. **294**(1): p. 1-10.
15. Kanada, M., A. Nagasaki, and T.Q.P. Uyeda, *Adhesion-dependent and contractile ring-independent equatorial furrowing during cytokinesis in mammalian cells.* Molecular Biology of the Cell, 2005. **16**(8): p. 3865-3872.
16. Uyeda, T.Q.P., C. Kitayama, and S. Yumura, *Myosin II-independent cytokinesis in Dictyostelium: its mechanism and implications.* Cell Structure and Function, 2000. **25**(1): p. 1-10.
17. Neujahr, R., C. Heizer, and G. Gerisch, *Myosin II-independent processes in mitotic cells of Dictyostelium discoideum: redistribution of the nuclei, re-arrangement of the actin system and formation of the cleavage furrow.* J Cell Sci, 1997. **110 (Pt 2)**: p. 123-37.
18. Poirier, C.C., et al., *Deconvolution of the Cellular Force-Generating Subsystems that Govern Cytokinesis Furrow Ingression.* Plos Computational Biology, 2012. **8**(4).
19. Zhang, W. and D.N. Robinson, *Balance of actively generated contractile and resistive forces controls cytokinesis dynamics.* Proc Natl Acad Sci U S A, 2005. **102**(20): p. 7186-91.

20.   Foth, B.J., M.C. Goedecke, and D. Soldati, *New insights into myosin evolution and classification.* Proc Natl Acad Sci U S A, 2006. **103**(10): p. 3681-6.

21.   Sebe-Pedros, A., et al., *Evolution and classification of myosins, a paneukaryotic whole-genome approach.* Genome Biol Evol, 2014. **6**(2): p. 290-305.

22.   Eggert, U.S., T.J. Mitchison, and C.M. Field, *Animal cytokinesis: from parts list to mechanisms.* Annu Rev Biochem, 2006. **75**: p. 543-66.

23.   Pollard, T.D. and J.Q. Wu, *Understanding cytokinesis: lessons from fission yeast.* Nat Rev Mol Cell Biol, 2010. **11**(2): p. 149-55.

24.   Gut, J., et al., *An image-based assay for high throuput screening of Giardia lamblia.* J Microbiol Methods, 2011. **84**(3): p. 398-405.

25.   Benchimol, M., *Mitosis in Giardia lamblia: Multiple modes of cytokinesis.* Protist, 2004. **155**(1): p. 33-44.

26.   Ghosh, S., et al., *How Giardia swim and divide.* Infect Immun, 2001. **69**(12): p. 7866-72.

27.   Kabnick, K.S. and D.A. Peattie, *In situ analyses reveal that the two nuclei of Giardia lamblia are equivalent.* J Cell Sci, 1990. **95 (Pt 3)**: p. 353-60.

28.   Solari, A.J., et al., *A unique mechanism of nuclear division in Giardia lamblia involves components of the ventral disk and the nuclear envelope.* Biocell, 2003. **27**(3): p. 329-46.

29.   Yu, L.Z., C.W. Birky, Jr., and R.D. Adam, *The two nuclei of Giardia each have complete copies of the genome and are partitioned equationally at cytokinesis.* Eukaryot Cell, 2002. **1**(2): p. 191-9.

30.   Sagolla, M.S., et al., *Three-dimensional analysis of mitosis and cytokinesis in the binucleate parasite Giardia intestinalis.* J Cell Sci, 2006. **119**(Pt 23): p. 4889-900.

31.   Paredez, A.R., et al., *An actin cytoskeleton with evolutionarily conserved functions in the absence of canonical actin-binding proteins.* Proc Natl Acad Sci U S A, 2011. **108**(15): p. 6151-6.

32.   Tumova, P., J. Kulda, and E. Nohynkova, *Cell division of Giardia intestinalis: Assembly and disassembly of the adhesive disc, and the cytokinesis.* Cell Motility and the Cytoskeleton, 2007. **64**(4): p. 288-298.

33.   Shaner, N.C., et al., *A bright monomeric green fluorescent protein derived from Branchiostoma lanceolatum.* Nat Methods, 2013. **10**(5): p. 407-9.

34.   Cheffings, T.H., N.J. Burroughs, and M.K. Balasubramanian, *Actomyosin Ring Formation and Tension Generation in Eukaryotic Cytokinesis.* Current Biology, 2016. **26**(15): p. R719-R737.

35.   Dawson, S.C. and S.A. House, *Imaging and analysis of the microtubule cytoskeleton in giardia.* Methods Cell Biol, 2010. **97**: p. 307-39.

36.   Crossley, R., et al., *Immunocytochemical differentiation of microtubules in the cytoskeleton of Giardia lamblia using monoclonal antibodies to alpha-tubulin and polyclonal antibodies to associated low molecular weight proteins.* Journal of Cell Science, 1986. **80**(1): p. 233-252.

37.   Feely, D.E.E.D.V., *The Biology of Giardia*, in *Giardiasis*, E.A. Mayer, Editor. 1990, Elsevier: Amsterdam and New York. p. 11-49.

38.   Morrison, H.G., et al., *Genomic minimalism in the early diverging intestinal parasite Giardia lamblia.* Science, 2007. **317**(5846): p. 1921-6.

39.   Lenaghan, S.C., et al., *High-speed microscopic imaging of flagella motility and swimming in Giardia lamblia trophozoites.* Proc Natl Acad Sci U S A, 2011. **108**(34): p. E550-8.

40.   McInally, S.G. and S.C. Dawson, *Eight unique basal bodies in the multi-flagellated diplomonad Giardia lamblia.* Cilia, 2016. **5**: p. 21.

41.   House, S.A., et al., *Giardia flagellar motility is not directly required to maintain attachment to surfaces.* PLoS Pathog, 2011. **7**(8): p. e1002167.

42.   Ludington, W.B., et al., *Organelle size equalization by a constitutive process.* Curr Biol, 2012. **22**(22): p. 2173-9.

43.   Nohynkova, E., P. Tumova, and J. Kulda, *Cell division of Giardia intestinalis: flagellar developmental cycle involves transformation and exchange of flagella between mastigonts of a diplomonad cell.* Eukaryot Cell, 2006. **5**(4): p. 753-61.

44.   Vicente, J.J. and W.Z. Cande, *Mad2, Bub3, and Mps1 regulate chromosome segregation and mitotic synchrony in Giardia intestinalis, a binucleate protist lacking an anaphase-promoting complex.* Molecular Biology of the Cell, 2014. **25**(18): p. 2774-87.

45.   Azimzadeh, J., J. Traas, and M. Pastuglia, *Molecular aspects of microtubule dynamics in plants.* Curr Opin Plant Biol, 2001. **4**(6): p. 513-9.

46.   Kumagai, F., et al., *Fate of nascent microtubules organized at the M/G1 interface, as visualized by synchronized tobacco BY-2 cells stably expressing GFP-tubulin: time-sequence observations of the reorganization of cortical microtubules in living plant cells.* Plant Cell Physiol, 2001. **42**(7): p. 723-32.

47.   Mullins, J.M. and J.J. Biesele, *Terminal phase of cytokinesis in D-98s cells.* J Cell Biol, 1977. **73**(3): p. 672-84.

48.   Nagasaki, A., E.L. de Hostos, and T.Q. Uyeda, *Genetic and morphological evidence for two parallel pathways of cell-cycle-coupled cytokinesis in Dictyostelium.* J Cell Sci, 2002. **115**(Pt 10): p. 2241-51.

49.   Hahn, J., et al., *High Sensitivity of Giardia duodenalis to Tetrahydrolipstatin (Orlistat) In Vitro.* Plos One, 2013. **8**(8).

50.   Brown, J.M., C. Hardin, and J. Gaertig, *Rotokinesis, a novel phenomenon of cell locomotion-assisted cytokinesis in the ciliate Tetrahymena thermophila.* Cell Biol Int, 1999. **23**(12): p. 841-8.

51.   Langousis, G. and K.L. Hill, *Motility and more: the flagellum of Trypanosoma brucei.* Nat Rev Microbiol, 2014. **12**(7): p. 505-18.

52.   Ralston, K.S., et al., *Flagellar motility contributes to cytokinesis in Trypanosoma brucei and is modulated by an evolutionarily conserved dynein regulatory system.* Eukaryotic Cell, 2006. **5**(4): p. 696-711.

53.   Engel, B.D., et al., *A cell-based screen for inhibitors of flagella-driven motility in Chlamydomonas reveals a novel modulator of ciliary length and retrograde actin flow.* Cytoskeleton (Hoboken), 2011. **68**(3): p. 188-203.

54.   Firestone, A.J., et al., *Small-molecule inhibitors of the AAA+ ATPase motor cytoplasmic dynein.* Nature, 2012. **484**(7392): p. 125-9.

55.   Wada, Y., S.A. Baba, and S. Kamimura, *Effects of the dynein inhibitor ciliobrevin on the flagellar motility of sea urchin spermatozoa.* Cytoskeleton (Hoboken), 2015. **72**(4): p. 182-92.

56.   Smith, E.F. and P.A. Lefebvre, *PF16 encodes a protein with armadillo repeats and localizes to a single microtubule of the central apparatus in Chlamydomonas flagella.* J Cell Biol, 1996. **132**(3): p. 359-70.

57.   Dutcher, S.K., B. Huang, and D.J. Luck, *Genetic dissection of the central pair microtubules of the flagella of Chlamydomonas reinhardtii.* J Cell Biol, 1984. **98**(1): p. 229-36.

58.   Sapiro, R., et al., *Male infertility, impaired sperm motility, and hydrocephalus in mice deficient in sperm-associated antigen 6.* Mol Cell Biol, 2002. **22**(17): p. 6298-305.

59.   Gourguechon, S. and W.Z. Cande, *Rapid tagging and integration of genes in Giardia intestinalis.* Eukaryot Cell, 2011. **10**(1): p. 142-5.

60.   de Graffenried, C.L., H.H. Ho, and G. Warren, *Polo-like kinase is required for Golgi and bilobe biogenesis in Trypanosoma brucei.* J Cell Biol, 2008. **181**(3): p. 431-8.

61.   Li, Z., T. Umeyama, and C.C. Wang, *Polo-like kinase guides cytokinesis in Trypanosoma brucei through an indirect means.* Eukaryot Cell, 2010. **9**(5): p. 705-16.

62.   Paredez, A.R., et al., *Identification of obscure yet conserved actin associated proteins in Giardia lamblia.* Eukaryot Cell, 2014. **13**(6): p. 776-84.

63.   Girard, K.D., et al., *Dynacortin contributes to cortical viscoelasticity and helps define the shape changes of cytokinesis.* EMBO J, 2004. **23**(7): p. 1536-46.

64.   Rybak, K., et al., *Plant cytokinesis is orchestrated by the sequential action of the TRAPPII and exocyst tethering complexes.* Dev Cell, 2014. **29**(5): p. 607-20.

65.   Schiel, J.A., C. Childs, and R. Prekeris, *Endocytic transport and cytokinesis: from regulation of the cytoskeleton to midbody inheritance.* Trends in Cell Biology, 2013. **23**(7): p. 319-327.

66.   Wang, N., et al., *Roles of the TRAPP-II Complex and the Exocyst in Membrane Deposition during Fission Yeast Cytokinesis.* PLoS Biol, 2016. **14**(4): p. e1002437.

67.   Koumandou, V.L., et al., *Control systems for membrane fusion in the ancestral eukaryote; evolution of tethering complexes and SM proteins.* BMC Evol Biol, 2007. **7**: p. 29.

68.   Donaldson, J.G., D. Finazzi, and R.D. Klausner, *BREFELDIN-A INHIBITS GOLGI MEMBRANE-CATALYZED EXCHANGE OF GUANINE-NUCLEOTIDE ONTO ARF PROTEIN.* Nature, 1992. **360**(6402): p. 350-352.

69.   Helms, J.B. and J.E. Rothman, *INHIBITION BY BREFELDIN-A OF A GOLGI MEMBRANE ENZYME THAT CATALYZES EXCHANGE OF GUANINE-NUCLEOTIDE BOUND TO ARF.* Nature, 1992. **360**(6402): p. 352-354.

70.   Ritzenthaler, C., et al., *Reevaluation of the effects of brefeldin A on plant cells using tobacco Bright Yellow 2 cells expressing Golgi-targeted green fluorescent protein and COPI antisera.* Plant Cell, 2002. **14**(1): p. 237-61.

71.   Stefanic, S., et al., *Neogenesis and maturation of transient Golgi-like cisternae in a simple eukaryote.* Journal of Cell Science, 2009. **122**(16): p. 2846-2856.

72.   Lujan, H.D., et al., *DEVELOPMENTAL INDUCTION OF GOLGI STRUCTURE AND FUNCTION IN THE PRIMITIVE EUKARYOTE GIARDIA-LAMBLIA.* Journal of Biological Chemistry, 1995. **270**(9): p. 4612-4618.

73.   Touz, M.C., L. Kulakova, and T.E. Nash, *Adaptor Protein Complex 1 Mediates the Transport of Lysosomal Proteins from a Golgi-like Organelle to Peripheral Vacuoles in the Primitive Eukaryote Giardia lamblia.* Mol. Biol. Cell, 2004. **15**(7): p. 3053-3060.

74.   Abodeely, M., et al., *A Contiguous Compartment Functions as Endoplasmic Reticulum and Endosome/Lysosome in Giardia lamblia.* Eukaryotic Cell, 2009. **8**(11): p. 1665-1676.

75.   Fielding, A.B., et al., *Rab11-FIP3 and FIP4 interact with Arf6 and the exocyst to control membrane traffic in cytokinesis.* Embo j, 2005. **24**(19): p. 3389-99.

76.   Wilson, G.M., et al., *The FIP3-Rab11 protein complex regulates recycling endosome targeting to the cleavage furrow during late cytokinesis.* Mol Biol Cell, 2005. **16**(2): p. 849-60.

77.   Chow, C.M., et al., *Rab-A2 and Rab-A3 GTPases define a trans-golgi endosomal membrane domain in Arabidopsis that contributes substantially to the cell plate.* Plant Cell, 2008. **20**(1): p. 101-23.

78.   Gabernet-Castello, C., et al., *Rab11 Function in Trypanosoma brucei: Identification of Conserved and Novel Interaction Partners.* Eukaryotic Cell, 2011. **10**(8): p. 1082-1094.

79.   Krtkova, J., et al., *Rac Regulates Giardia lamblia Encystation by Coordinating Cyst Wall Protein Trafficking and Secretion.* MBio, 2016. **7**(4).

80.   Dunn, L.A., et al., *The activity of protease inhibitors against Giardia duodenalis and metronidazole-resistant Trichomonas vaginalis.* Int J Antimicrob Agents, 2007. **29**(1): p. 98-102.

81.   Benchimol, M., *Participation of the adhesive disc during karyokinesis in Giardia lamblia.* Biol Cell, 2004. **96**(4): p. 291-301.

82.   Piva, B. and M. Benchimol, *The median body of Giardia lamblia: an ultrastructural study.* Biol Cell, 2004. **96**(9): p. 735-46.

83.   Garcia-Salcedo, J.A., et al., *A differential role for actin during the life cycle of Trypanosoma brucei.* EMBO J, 2004. **23**(4): p. 780-9.

84.   Branche, C., et al., *Conserved and specific functions of axoneme components in trypanosome motility.* J Cell Sci, 2006. **119**(Pt 16): p. 3443-55.

85.   Brown, J.M., et al., *Kinesin-II is preferentially targeted to assembling cilia and is required for ciliogenesis and normal cytokinesis in Tetrahymena.* Molecular Biology of the Cell, 1999. **10**(10): p. 3081-3096.

86.   Xia, L., et al., *Polyglycylation of tubulin is essential and affects cell motility and division in Tetrahymena thermophila.* Journal of Cell Biology, 2000. **149**(5): p. 1097-1106.

87.   Diz-Munoz, A., D.A. Fletcher, and O.D. Weiner, *Use the force: membrane tension as an organizer of cell shape and motility.* Trends in Cell Biology, 2013. **23**(2): p. 47-53.

88.   Welz, T., J. Wellbourne-Wood, and E. Kerkhoff, *Orchestration of cell surface proteins by Rab11.* Trends Cell Biol, 2014. **24**(7): p. 407-15.

89.   Krtkova, J. and A.R. Paredez, *Use of Translation Blocking Morpholinos for Gene Knockdown in Giardia lamblia.* Methods Mol Biol, 2017. **1565**: p. 123-140.

90.   Kaplan, E.L. and P. Meier, *Nonparametric estimation from incomplete observations.* Journal of the American statistical association, 1958. **53**(282): p. 457-481.

91.   Efron, B. and R.J. Tibshirani, *An introduction to the bootstrap*. 1994: CRC press.

92.   Sun, Y. and M.G. Genton, *Functional boxplots.* Journal of Computational and Graphical Statistics, 2012.
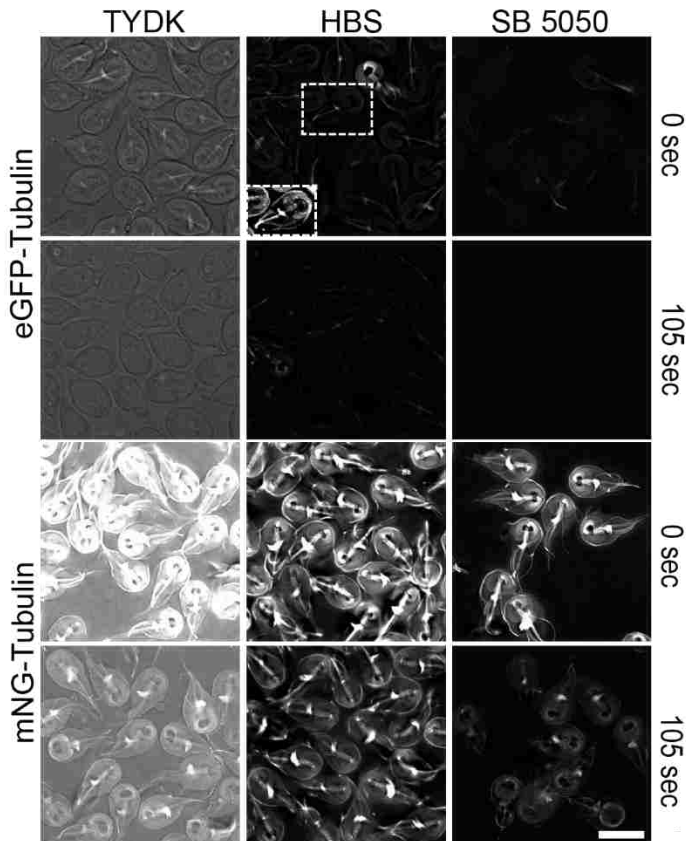
A
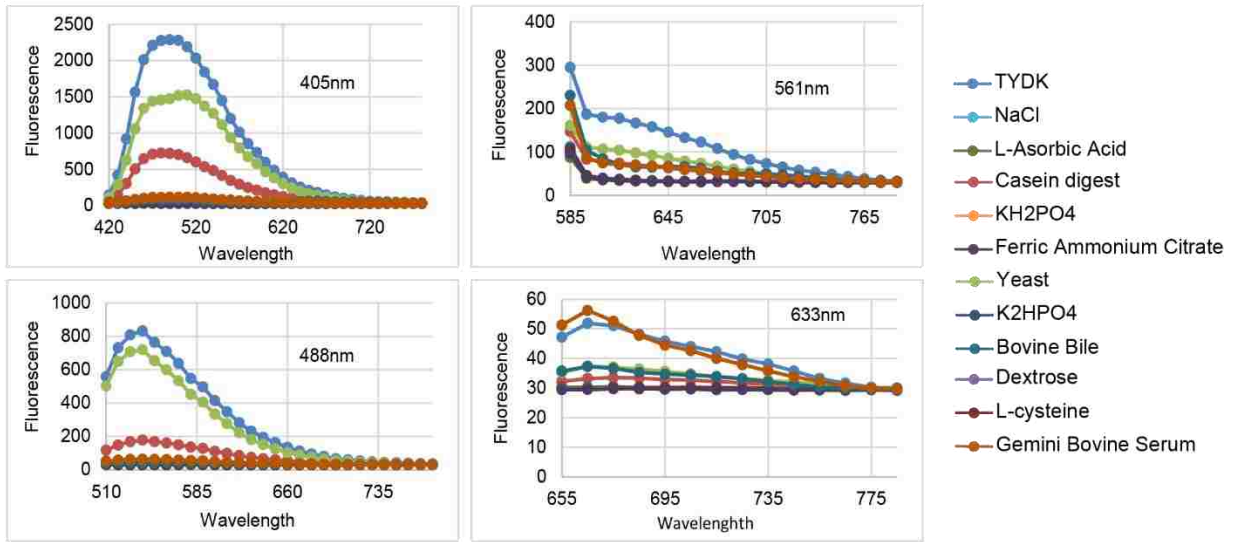
	TYDK	HBS	SB 5050
FL background	100%	4.7%	7.8%
Percent divided after release	17%	*2.5%	6%

B

C

Fig. S1. Development of low fluorescence SB5050. (**A**) Spectral scan of TYDK components. The fluorescence from each TYDK component was analyzed over the typical spectra used in fluorescence microscopes. Note that autofluorescence decreases at higher wavelengths. Approximately 90% of the TYDK autofluorescence comes from N-Z Case and Yeast Extract. See Dataset S1 for tested formulations. (**B**) The table indicates fluorescence (FL) background normalized to TYDK (EX 475/28 nm, EM 523/36 nm), the percent of cells dividing within 1 hr of being released from the microtubule inhibitor albendazole used to partially synchronize the cell cycle. *All division in HBS occurred within 5 minutes of cells being transferred from TYDK+albendazole, which precludes the use of agarose overlay to inhibit cell motility. Measurements are from three independent experiments. (**C**) SB5050 medium reduces autofluorescence and aids in time-lapse imaging. All images were acquired and scaled identically except for inset. TYDK background fluorescence is problematic, eGFP is unusable and signal-to-noise quickly becomes an impediment as imaging bleaches out mNeonGreen. mNeonGreen is a superior fluorescent protein for imaging in *Giardia* due to fast fold times (less than 5 minutes) and higher intrinsic brightness. Inset shows eGFP-Tubulin scaled for optimal viewing to demonstrate that eGFP was given sufficient time to fold (40 minutes). Scale bar=10 µm.

Media	Fluorescence	% growth	Yeast Extract	NZ-Case plus	Cysteine	Bile	Serum
TYDK	9373	100.0%	100%	100%	100%	100%	100%
1X HBS	197	0.0%	0%	0%	0%	0%	0%
50% TYDK / 50% 1X HBS	N/A	99%	50%	50%	50%	50%	50%
25% TYDK / 75% 1X HBS	N/A	93%	25%	25%	25%	25%	25%
* HBS 1X variant	N/A	0.0%	0%	0%	100%	100%	100%
Medium 199 1X(Gibco by Life Technologies)	N/A	0.0%	0%	0%	0%	0%	0%
* Medium 199 1X variant	N/A	N/A	0%	0%	100%	100%	100%
* Live Cell Imaging Solution 1X(Molecular Probes by Life Technologies)	N/A	N/A	0%	0%	100%	100%	100%
^ 1X Vitamine Casamino acids variant(Becton Dickinson)	N/A	0.0%	0%	0%	100%	100%	100%
~1X Vitamine Casamino acids variant	N/A	0.9%	0%	0%	100%	100%	100%
< 1X Vitamine Casamino acids variant	N/A	2.4%	100%	0%	100%	100%	100%
> 1X Yeast Nitrogen base variant	N/A	0.3%	0%	100%	100%	100%	100%
# 1X Vitamine Casamino acids variant	N/A	4.8%	0%	0%	100%	100%	100%
! 1X Vitamine Casamino acids variant	N/A	4.9%	0%	0%	100%	100%	100%
+ 50% N-Z-Case Plus/50% Yeast Extract	2271	103.0%	50%	50%	100%	100%	100%
- 25% N-Z-Case Plus/25% Yeast Extract	1272	85%	25%	25%	100%	100%	100%
= 100% 1X Yeast Nitrogen Base(Becton Dickinson)	N/A	13.4%	0%	100%	100%	100%	100%
= 50% 1X Yeast Nitrogen Base	N/A	31.8%	0%	100%	100%	100%	100%
= 25% 1X Yeast Nitrogen Base	N/A	41.3%	0%	100%	100%	100%	100%
= 35% 1X Yeast Nitrogen Base	N/A	0.1%	0%	100%	100%	100%	100%
= 12.5% 1X Yeast Nitrogen Base	N/A	29.3%	0%	100%	100%	100%	100%
= 0% 1X Yeast Nitrogen Base	N/A	28.6%	0%	100%	100%	100%	100%
` 75% N-Z-Case Plus variant	1058	84%	0%	75%	100%	100%	100%
` 50% N-Z-Case Plus variant	724	71%	0%	50%	100%	100%	100%
` 25% N-Z-Case Plus variant	N/A	50%	0%	25%	100%	100%	100%
` 0% N-Z-Case Plus variant	N/A	30.4%	0%	0%	100%	100%	100%
(*) 0% 1X Yeast Nitrogen Base variant	315	N/A	0%	0%	100%	100%	100%
(*) 12.5% 1X Yeast Nitrogen Base variant	355	N/A	0%	0%	100%	100%	100%
1X YC complete variant/1X Casamino acids	N/A	8.6%	0%	0%	100%	100%	100%
(+) 1X YC complete variant/1X Casamino acids	N/A	13.8%	0%	0%	100%	100%	100%
(=) 1X Vitamine Casamino acids	N/A	13.1%	0%	0%	100%	100%	100%
(=) 1X Vitamine Casamino acids	N/A	10.8%	0%	0%	100%	100%	100%
(=) 1X Vitamine Casamino acids	N/A	6.8%	0%	0%	100%	100%	100%
(^) TYDK variant	482	69.0%	0%	0%	100%	100%	100%
(^) TYDK variant	457	0.7%	0%	0%	0%	100%	100%
(#) TYDK base	526	20.0%	0%	0%	33%	100%	100%
(#) TYDK base	517	23.0%	0%	0%	66%	100%	100%
(#) TYDK base	500	68.0%	0%	0%	50%	100%	100%
(#) TYDK base	205	1.8%	0%	0%	50%	0%	0%
(#) TYDK base	417	15.0%	0%	0%	50%	0%	100%
(#) TYDK base	521	31.0%	0%	0%	50%	50%	100%
(#) SB5050	365	15.0%	0%	0%	50%	50%	50%
(#) TYDK base	278	5.0%	0%	0%	50%	50%	0%
(#) TYDK base	261	7.0%	0%	0%	50%	25%	25%
(#) TYDK base	288	6.7%	0%	0%	50%	25%	50%
(#) TYDK base	294	5.4%	0%	0%	50%	50%	25%
(#) TYDK base	227	5.0%	0%	0%	50%	10%	10%

N/A not avilable

* L-Asorbic acid and Ferric Ammonium Citrate

^ Yeast nitrogen base, Tyrosine, Tryptophan, Asparagine, Glutamine, dextrose, NaCl, KH2PO4, K2HPO4,L-Asorbic Acid, and Ferric Ammonium Citrate

~ Yeast Nitrogen base, dextrose, NaCl, KH2PO4, K2HPO4,L-Asorbic Acid, and Ferric Ammonium Citrate

< Dextrose, NaCl, KH2PO4, K2HPO4, L-cysteine, L-Asorbic Acid, Ferric Ammonium Citrate

> Casein digest, dextrose, NaCl, KH2PO4, K2HPO4, L-Asorbic Acid, and Ferric Ammonium Citrate

Yeast Nitrogen base, dextrose, NaCl, KH2PO4, K2HPO4, L-Asparagine, L-Glutamine, L-Tryptophan, DL-Tyrosine, L-Asorbic Acid, and Ferric Ammonium Citrate

! Yeast Nitrogen base, dextrose, NaCl, KH2PO4, K2HPO4, L-Asparagine, L-Glutamine, L-Tryptophan, L-Asorbic Acid, and Ferric Ammonium Citrate

+ and - Dextrose, NaCl, KH2PO4, K2HPO4, L-Asorbic Acid, and Ferric Ammonium Citrate

= dextrose, NaCl, KH2PO4, K2HPO4, L-Asorbic Acid, and Ferric Ammonium Citrate

` 12.5% 1X Yeast Nitrogen Base, dextrose, NaCl, KH2PO4, K2HPO4, L-Asorbic Acid, and Ferric Ammonium Citrate

(*) Dextrose, NaCl, KH2PO4, K2HPO4, L-Asorbic Acid, and Ferric Ammonium Citrate

(+) Dextrose, NaCl, KH2PO4, K2HPO4, L-Asorbic Acid, and Ferric Ammonium Citrate

(=) 12.5% 1X Yeast Nitrogen Base, dextrose, NaCl, KH2PO4, K2HPO4, L-Asorbic Acid, and Ferric Ammonium Citrate

(^) Dextrose, NaCl, KH2PO4, K2HPO4, L-Asorbic Acid, and Ferric Ammonium Citrate

(#) Dextrose, NaCl, KH2PO4, K2HPO4, L-Asorbic Acid, and Ferric Ammonium Citrate

Dataset S1. Alternative media formulations. Over 40 different medium formulations were tested for their ability to support growth and reduce autofluorescence as compared to TYDK media. Cell counts and fluorescence levels for experimental media formulations are reported as mean values from three technical replicates.
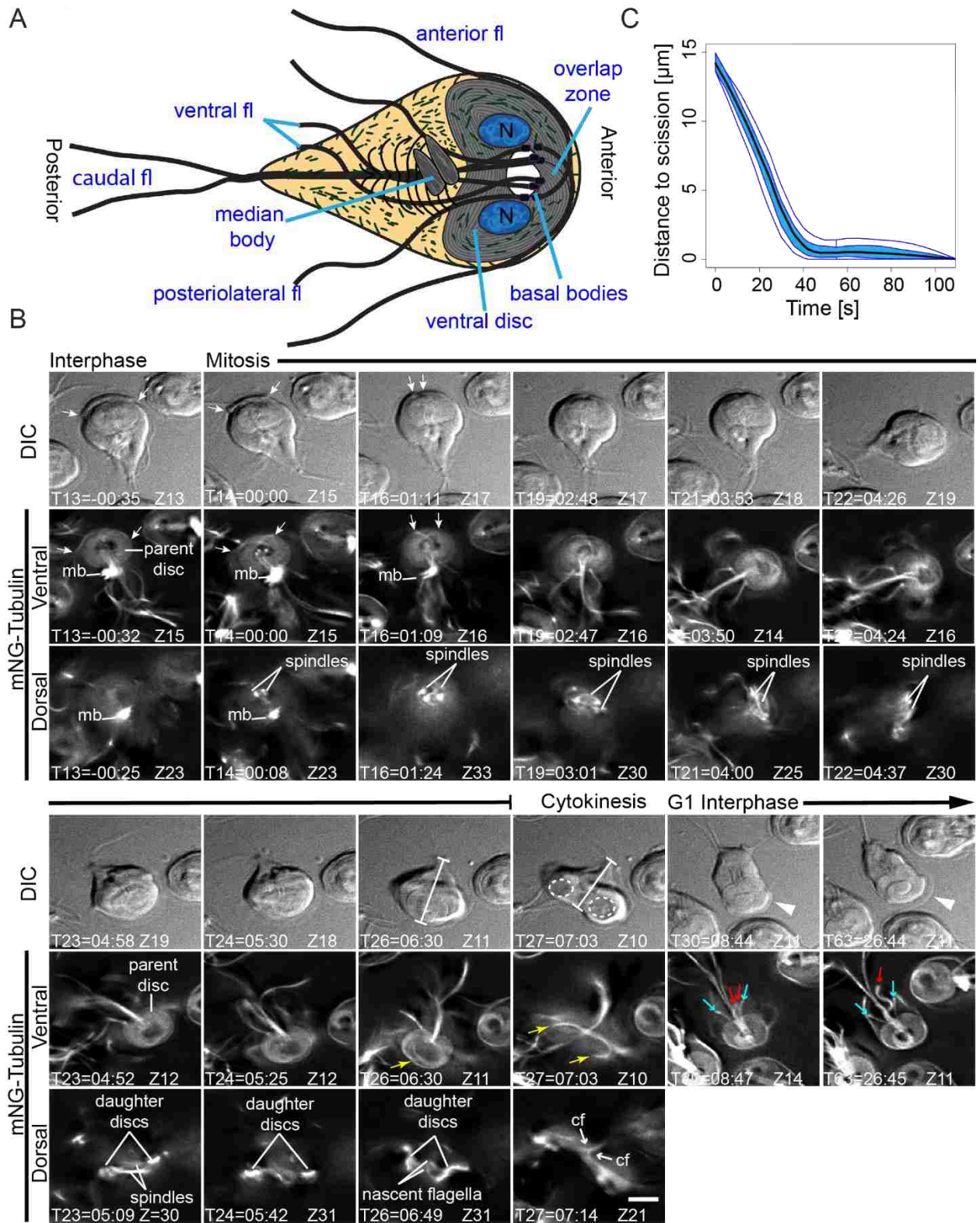
A

anterior fl

ventral fl

caudal fl

Posterior

median body

posteriolateral fl

ventral disc

basal bodies

overlap zone

N

N

Anterior

C

B

Interphase | Mitosis

DIC

T13=-00:35 Z13 | T14=00:00 Z15 | T16=01:11 Z17 | T19=02:48 Z17 | T21=03:53 Z18 | T22=04:26 Z19

mNG-Tubulin — Ventral

parent disc

mb

T13=-00:32 Z15 | T14=00:00 Z15 | T16=01:09 Z16 | T19=02:47 Z16 | =03:50 Z14 | T22=04:24 Z16

Dorsal

mb

spindles | spindles | spindles | spindles | spindles

T13=-00:25 Z23 | T14=00:08 Z23 | T16=01:24 Z33 | T19=03:01 Z30 | T21=04:00 Z25 | T22=04:37 Z30

Cytokinesis | G1 Interphase

DIC

T23=04:58 Z19 | T24=05:30 Z18 | T26=06:30 Z11 | T27=07:03 Z10 | T30=08:44 Z11 | T63=26:44 Z11

mNG-Tubulin — Ventral

parent disc

T23=04:52 Z12 | T24=05:25 Z12 | T26=06:30 Z11 | T27=07:03 Z10 | T30=08:47 Z14 | T63=26:45 Z11

Dorsal

daughter discs | daughter discs | daughter discs | cf
spindles | | nascent flagella | cf

T23=05:09 Z30 | T24=05:42 Z31 | T26=06:49 Z31 | T27=07:14 Z21

Figure 1

Fig. 1. Characterization of mNG-Tub dynamics over the cell cycle. (**A**) Diagram of cellular features of an interphase trophozoite (N=nucleus; fl=flagella). (**B**) A trophozoite captured from interphase through cytokinesis (T, time in min:sec; Z= optical slice). DIC images show orientation and correspond to fluorescent images (ventral and dorsal plane). The onset of mitosis was signified by re-arrangement of anterior flagella exit points (white arrows, magnified view in Figure S2) and nucleation of the spindle (both begin at T14). Concomitant with spindle assembly (dorsal row), the median body (mb) microtubules were depleted (ventral row, T14-T19). The spindles transitioned from basket-shaped to collapsed MT bundles (T21 -T23). Construction of daughter ventral discs initiated (T23). The center of the parental disc was depleted of mNG-Tub as daughter discs grew (T26, Z11, yellow arrow indicate overlap zone). Cytokinesis begins at T27 and is completed at T28 (Dashed ellipses, position of the daughter discs; dimension bars mark the trajectory of the furrow, yellow arrows, ends of the now open parental ventral disc). Note the flexion of the caudal flagella (cf) in opposite directions (T27 Z21). Daughter cells attach to the substrate at T30 (one shown in ventral view). The DIC image shows that the daughter initially lacks a ventrolateral flange indicating that this structure was consumed during cytokinesis (T30 and more fully formed at T63, white arrowhead). Additionally, posterolateral (blue arrows) and ventral flagella pairs (red arrows) lengthened after division with different growth rates. Scale bar=5 µm. Similar observations were made for at least ten other mNG-Tub expressing cells. (**C**) Functional box plot of bootstrapped LOESS curves derived from cleavage furrow measurements (dimension bars in DIC row T26 and T27, also see Figure S2). Distance to scission is the distance that the furrow has to travel for daughter cell separation, average cells begin with a ~14 µm path length. Data are from 25 randomly selected cells completing cytokinesis within 2 minutes. Central black line is the mean of the bootstrapped LOESS curves; the blue band indicates the 50% confidence interval bound by 95% confidence bands of bootstrapped distances.
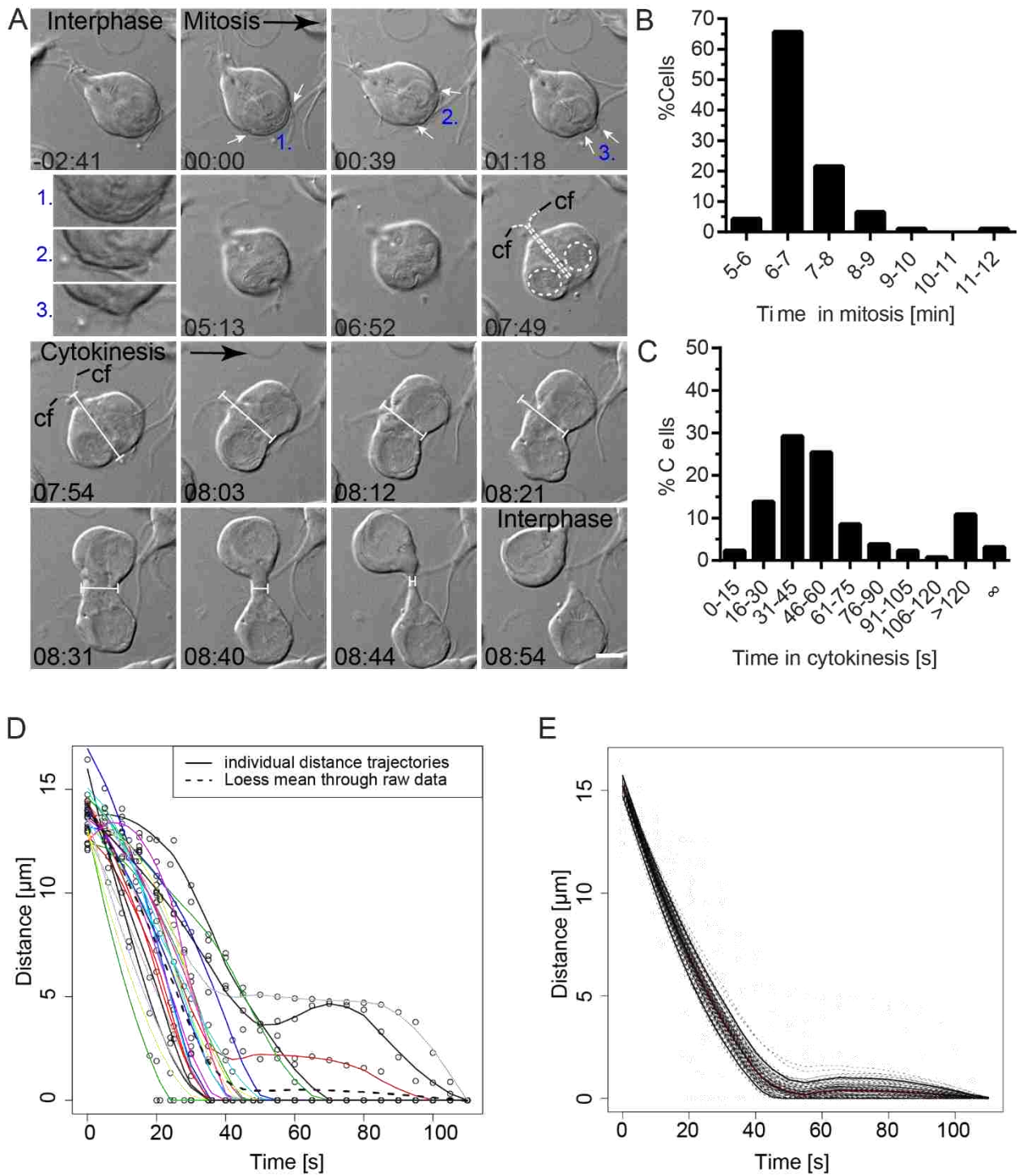
Figure S2

Fig. S2. Timing of mitosis and cytokinesis in live *Giardia*. (**A**) A representative division event as captured with 4D DIC time-lapse microscopy. Mitosis starts at 00:00, signified by re-arrangement of anterior flagella exit points (white arrows). Blue numbers correspond to magnified views. At 07:49, daughter cell ventral discs are nearly fully formed, marked by dashed ellipses. The path of the cleavage furrow was predicted by the position of the internal axonemes of the caudal flagella (cf, dashed lines). At 07:54 the cleavage furrow began to ingress between the two daughter discs and between the intracytoplasmic axonemes of the caudal flagella, white dimension line denotes path and distance to scission. Cytokinesis was completed by 8:54. Time in mm:ss. Scale bar=5 μm. (**B**) Histogram describes the time cells (n=93) spent in mitosis, median=6 min 28±52 sec. Dataset collected from more than three independent movies. (**C**) Histogram describes time cells (n=130) spent in cytokinesis, median time 50 sec, ∞ indicates cells did not complete cytokinesis during the recording (imaged at least 15 minutes). Note that 89% of cells completed cytokinesis within 2 minutes. (**D**) Cleavage furrow measurements for individual cells with smoothed LOESS trajectories. (**E**) Bootstrapped LOESS curves within the 95% confidence interval.

Morpholinos

Target	Anti-sense translation blocking morpholino sequences
Control	5' CCTCTTACCTCAGTTACAATTTATA 3'.
PF16 (GL50803_16202)	5' TACGACGAAGCGATTAGTTGCCATG 3'
Actin (GL50803_40817)	5' GCAGGGTTGTCGTCTGTCATTTTAC 3'
Rab11 (GL50803_1695)	5' CGCGTCAGTCATCCGATTTTTTGAT 3'

Vector Construction

Plasmid	Sequence
mNeonGreen_C18_Beta-Tubulin	
pjet1.2-mNeonGreen_C18	F-5' atggtgagcaagggcgagga 3'
	R-5' GCTTCCGCTTCCGCCGGATGCGCTGCCTCCACCGCTGCCAGATCTGAGTCCGGActtgtacagctcgtccatgcc 3'
Tubulin Promoter (GL50803_101291)	OL97-Fw tggagctccaccgcggtggcggccgcTGCAAGTACGATGGTCAAAT
	OL98-Rv tcctcgcccttgctcaccatggTTTTAAATTTTGGCAGTCC
mNeonGreen C18	OL99-Fw TGGACTGCCAAAATTTAAAAccatggtgagcaagggcgag
	OL100-Rv ATGTGGACGATCTCACGCATGCTTCCGCTTCCGCCGGATG
Beta-Tubulin gene (GL50803_101291)	OL101-Fw CATCCGGCGGAAGCGGAAGCATGCGTGAGATCGTCCACAT
	OL102-Rv aaagGTCGACGGAAAgaattcTCAAGCGTACTCGTCGCCGA
	mNeonGreen C18 Beta-Tubulin was linearized for homologous recombination into Giardia Genome using BamHI
PF16 pKS-3HA-NEO	F- 5' tttgcggccgcATGGCAACTAATCGCTTCGTC 3'
	R- 5' CAGAGAATATGCTCGATCTGATCAAGgcacttaagcca 3'
	The vector was linearized for homologous recombination into the *Giardia* genome using BsrGl.
pKS3HA-Rab11_PAC	
Rab11 promoter	F-5' cgcggtggcggccgctctagaCTGGAGAGTGC-ATCCGAGG 3'
	R-5' acgtcataaggatat-tccatCCGATTTTTTGATCGAACTTTATTGACC 3'
Rab11 coding sequence	F-5' taccagattacgctggatccATGACTGACGCGTAC- GACC 3'
	R-5' aacgatgatgcaaaggaattcTCAGCAACGCTTCTTTTGCTTAG 3'
3XHA epitope	F-5' atggaatatccttatgacgtccca 3'
	R-5' ggatccagcgtaatctggtac 3'
pKS3HA-Rab11^{MS}_PAC	
Rab11 Promoter	OL494-F ccaccgcggtggcggccgctctagaCTGGAGAGTGCATCCGAGGA
	OL495-R acgtcataaggatattccatATAAAGATGGTCGTACGCGTCA
3HA-Rab11	OL496-F taccagattacgctggatccATGACTGACGCGTACGACC
	OL497-R aacgatgatgcaaaggaattcTCAGCAACGCTTCTTTTGCT
	The vector was linearized for homologous recombination into the Giardia genome using NcoI.
pTet_3HA_Rab11_PAC	F-5' agattacgctggatccttcgaaATGACTGACGCGTACGACCA 3'
	R-5' AGCAAAAGAAGCGTTGC-TGAgcggccgcagtgaattctttcc 3'
pTet_3HA-Rab11^{CA} (Rab11Q71L)	F 5'-agcggtagcgctcgaggccggcagtgtc-3'
	R5'-gacactgccggcctcgagcgctaccgct-3'
pTet::3HA-Rab11^{DN} (Rab11S22N)	F 5'-gaacctcgagaggatgtt- gtttttaccgactgcagagtccccaata-3'
	R 5'-tattggggactctgcagtcggta-aaaacaacatcctctcgaggttc-3'

Notes

First pjet1.2-mNeonGreen_C18 was created using CloneJet PCR cloning Kit (Thermo) using PCR product amplified from mNeonGreen template (Allele Biotechnology) using primers

In-fusion (Clontech) was used to ligate the fragments found below into pKS-3HA_PAC prepared with NotI and EcoRI

amplified from WBC6 genomic DNA

amplified from pjet1.2_mNeonGreen_C18

amplified from WBC6 genomic DNA

PF16 was amplified from WBC6 genomic DNA and inserted into the the pKS-3HA-NEO vector using Gibson assembly.

The restriction enzymes XbaI and EcoRI were used to linearize the pKS-3HA_PAC vector. In-fusion was used to insert the PCR amplified promoter, HA tag, Rab11, and linearized pKS_PAC vector.

The promoter plus 27bp of coding sequence was amplified from genomic DNA along with the 3HA-Rab11 coding sequence from PKS 3HA-Rab11 and then the two fragments were ligated using In-Fusion into pKS 3HA_Pac that had been prepared with Xba1 and EcoR1.

Genomic DNA used as template
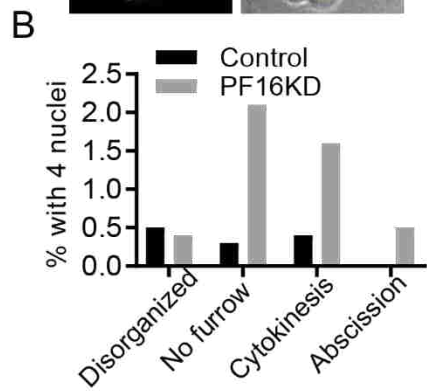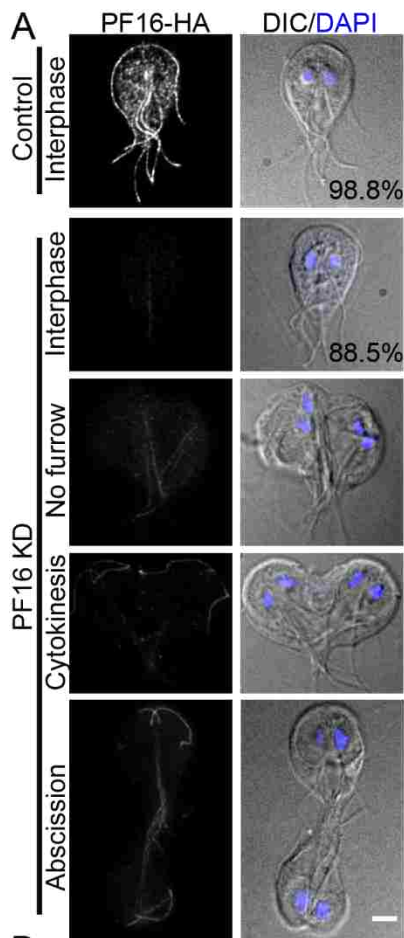
pKS3HA-Rab11_PAC used as template

pKSHA-Rab11_PAC was used as a template for these primers. Then pTet_3HA_PAC was linearized using BamHI and NotI, and the construct was assembled using Gibson.

Derived from pTet_3HA_Rab11_PAC using QuickChange Lighting (Agilent)

Derived from pTet_3HA_Rab11_PAC using QuickChange Lighting (Agilent)

Dataset S2. Oligo Sequences
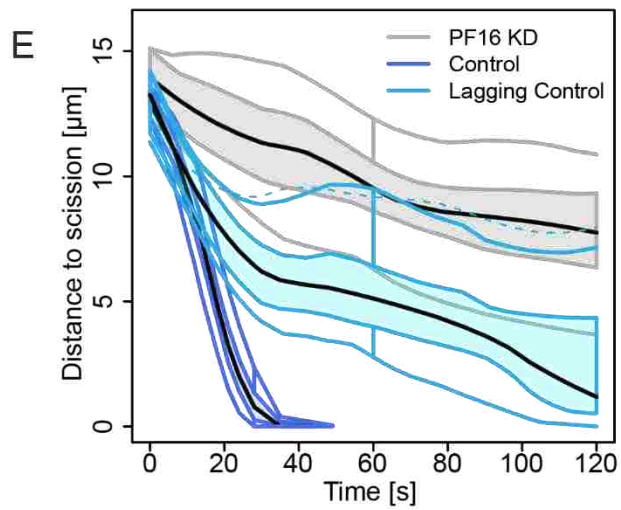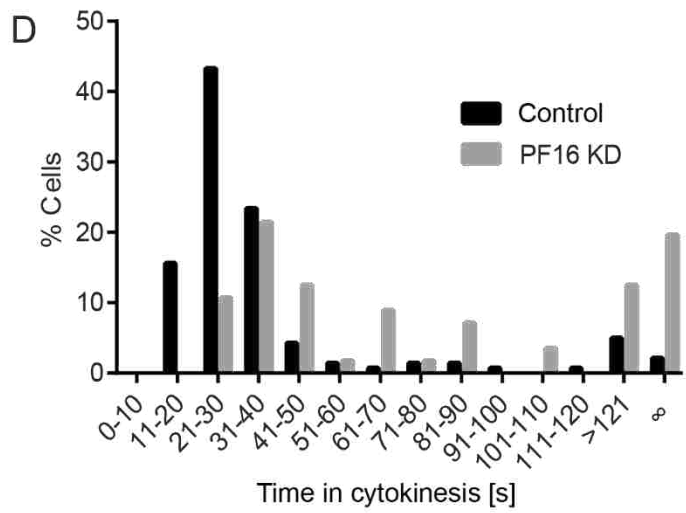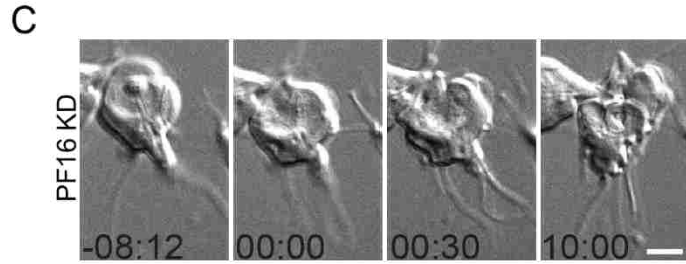
Fig. 2. Flagella function is required for furrowing progression and abscission. (**A**) PF16 localization in control and PF16 knockdown cells (KD) with equal exposure and scaling. Note that 98.8% of control and 88.5% of PF16 KD cells are normally organized interphase cells. (**B**) Categorization of the 1.2% of control and 11.5% of PF16 KD cells with 4 nuclei. With the exception of disorganized cells which lacked normal polarity and could not be scored, images representing the categories are shown above. (**C**) Still images from a timelapse movie of a PF16 KD cell that failed to complete cytokinesis. (**D**) Histogram of division times for PF16 KD cells (n=56) and morpholino control cells (n=141). Data acquired from at least three independent replicates. (**E**) Functional box plot of furrow trajectories for the first two minutes of 11 PF16 knockdown cells that never completed cytokinesis (grey), compared with 20 randomly sampled control cells (blue) and the 11 slowest control cells (light blue). Central black line is the mean of the bootstrapped LOESS curves; the colored band indicates the 50% confidence interval bound by 95% confidence bands of bootstrapped distances.
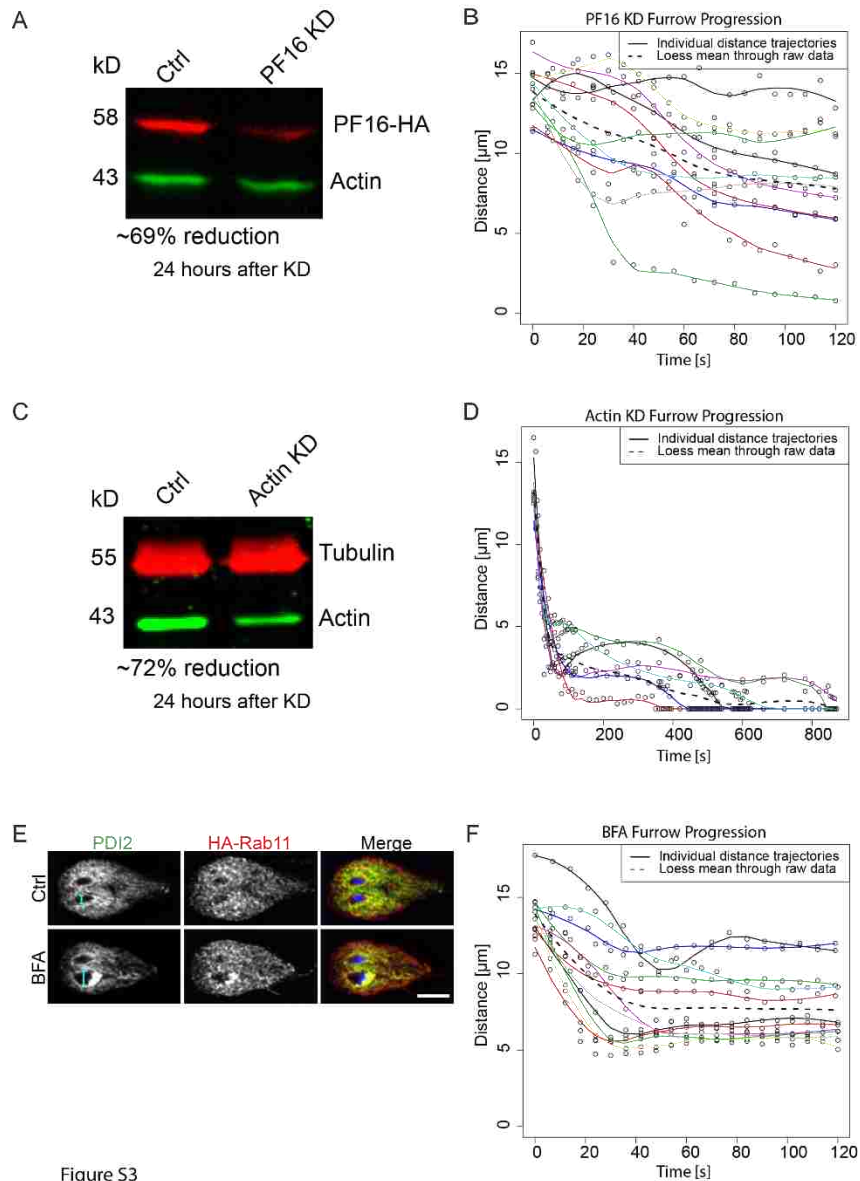
Figure S3

Fig. S3. Individual trajectories from PF16 KD, Actin KD, and BFA treatment. (**A**) Western blot showing ~69% reduction in PF16 24 hours after morpholino treatment. (**B**) Individual trajectories of PF16 knockdown cells. (**C**) Western blot showing ~72% reduction of actin 24 hours after morpholino treatment. (**D**) Individual trajectories of actin knockdown cells. (**E**) PDI2 and HA-Rab11 localization 60 minutes after DMSO and BFA treatment. Scale bar=5 μm. Note cyan dimension bars showing swelling after BFA treatment. (**F**) Individual trajectories of Brefeldin A treated cells. Cells for analysis were selected from three independent experiments.
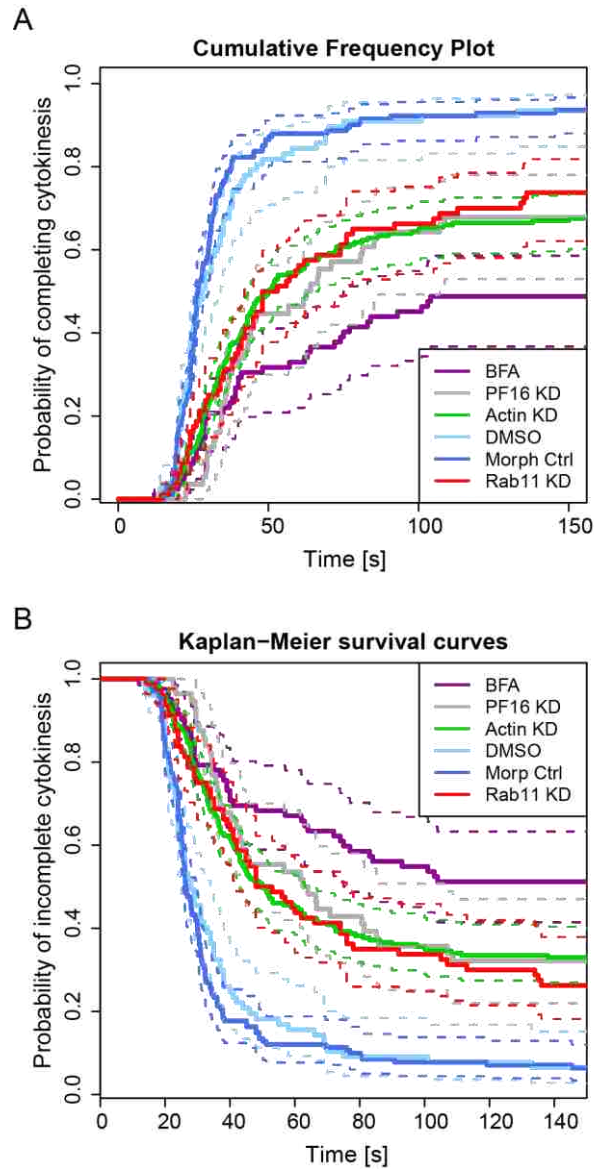
Fig. S4. Statistical analysis of experimental manipulations. (A) Frequency plots showing % of cells dividing over time. (B) Kaplan-Meier survival analysis. Experimental treatments resulted in reduced probability of completing cytokinesis as compared with control treatments. PF16 KD: p=3.17e-11, n_{PF16}=56, n_{ctrl}=141; Actin KD: p≈0, n_{actin}=191 n_{ctrl}=141; Rab11 KD: p= 3.07e-09 n_{Rab11}=80, n_{ctrl}=141; BFA p≈0, n_{BFA}=83, n_{DMSO}=106. All data was acquired from at least three independent experiments except for the DMSO control and Rab11 which came from two independent experiments.
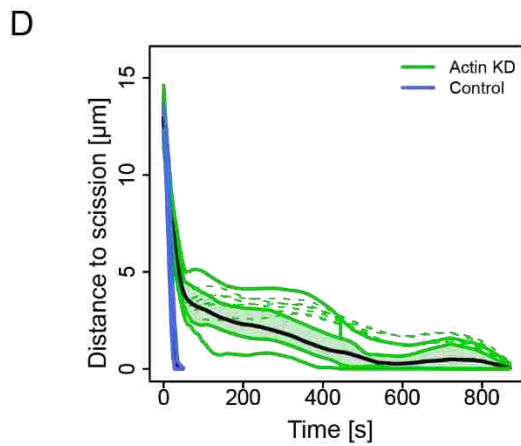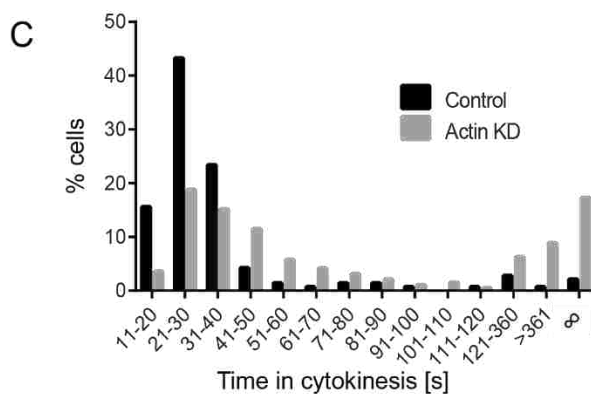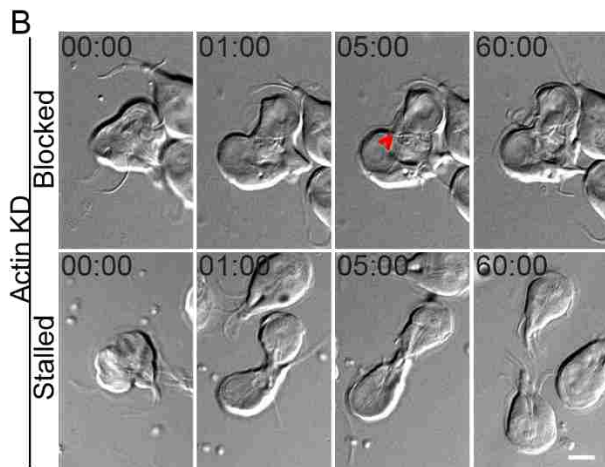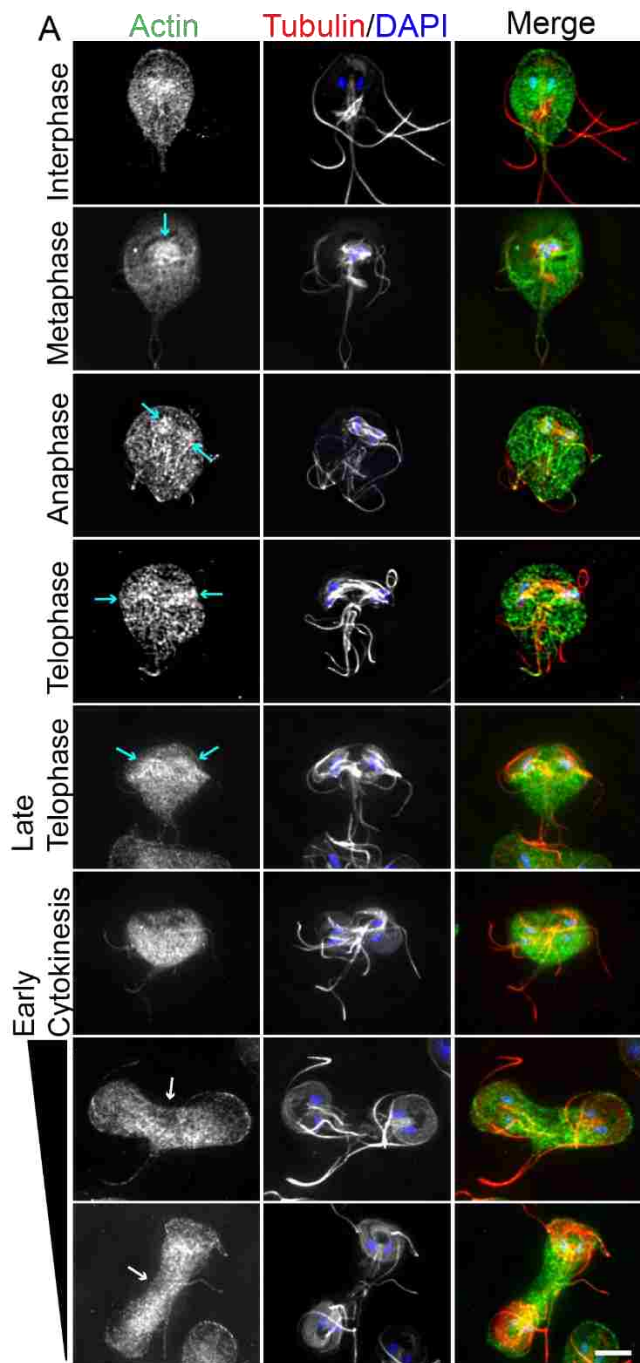
Fig. 3. Actin is required for abscission. (**A**) Immunofluorescence localization of Actin (green), tubulin (red), and DNA (blue), throughout the cell cycle. Actin accumulated around spindles and developing daughter ventral discs (cyan arrows). During cytokinesis, actin is found at relatively lower levels at the leading edge of the cleavage furrow (white arrows, analysis in Fig S5). (**B**) Live cell imaging of actin knockdown reveals blocked and stalled cell phenotypes. Block of cytokinesis resulted from a flagella crossing the cleavage furrow path (red arrowhead, see Movie 5). The stalled cell completes cytokinesis after approximately 60 minutes (see Movie 6). Time-stamp, mm:ss and scale bars=5 μm. (**C**) Histogram of time to complete cytokinesis. Actin knockdown cells (n=191) take longer to divide than cells treated with the morpholino control (n =141). Data acquired from at least three independent experiments. (**D**) Functional box plot of bootstrapped LOESS curves for actin KD cells (green, n=12) taking 6-15 minutes to divide compared with typical control cells (blue, n=20) shows a delay in abscission.
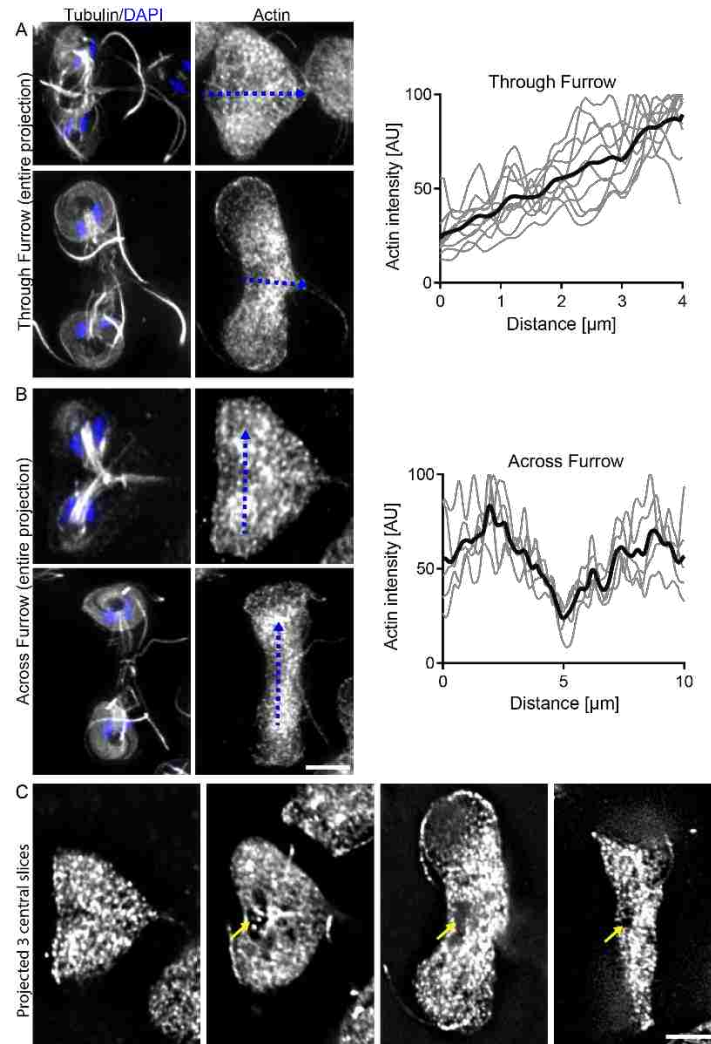
Fig. S5 Actin is cleared ahead of the advancing furrow. (**A**) Average projections of cells early and midway through cytokinesis with plot of actin intensities along the furrow of ten cells, black line is mean. Note low levels in the first 1 µm of the furrow. (**B**) Average projections of cells early and late in cytokinesis with plot of actin levels across the furrow of five cells, black line represents the mean. Note that in contrast to cells with a contractile ring, actin levels dip precisely at the midpoint of the cell. (**C**) Projected images of three central optical sections for cells at progressive stages of cytokinesis. Note that actin is cleared just ahead of the advancing furrow (yellow arrows). Scale bars=5 µm.
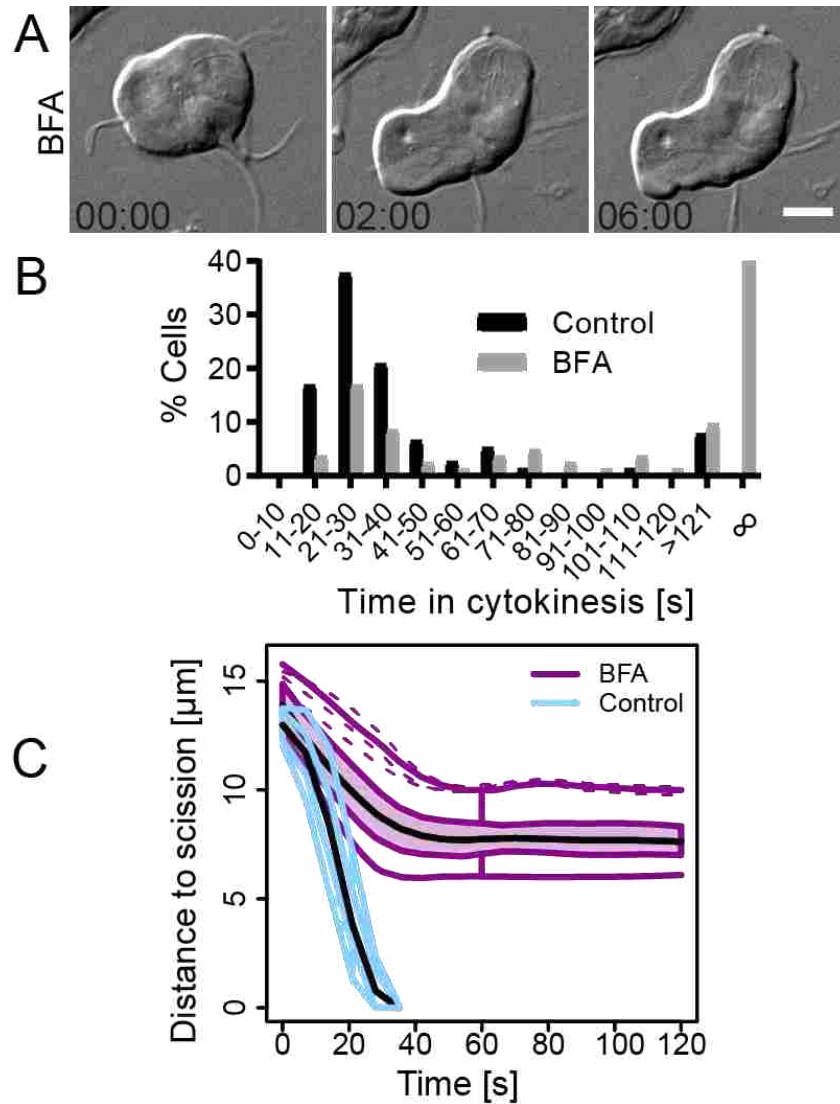
Fig. 4. Membrane partitioning is essential for cytokinesis. (**A**) Time-lapse images of a representative Brefeldin A (BFA) treated cell attempting cytokinesis. Note that furrow ingression consistently stops shortly after the start of cytokinesis (See Movie 5). Scale bar=5 μm (**B**) Histogram of cytokinesis timing for BFA-treated (25 μM, n=83) and control cells (0.35% DMSO, n=106). Data for BFA acquired from three independent movies, data for DMSO control from 2 independent movies. (**C**) Functional box plot of bootstrapped LOESS curves for furrow ingression measurements of BFA-treated (pink, n=12) and control cells (blue, n=12).
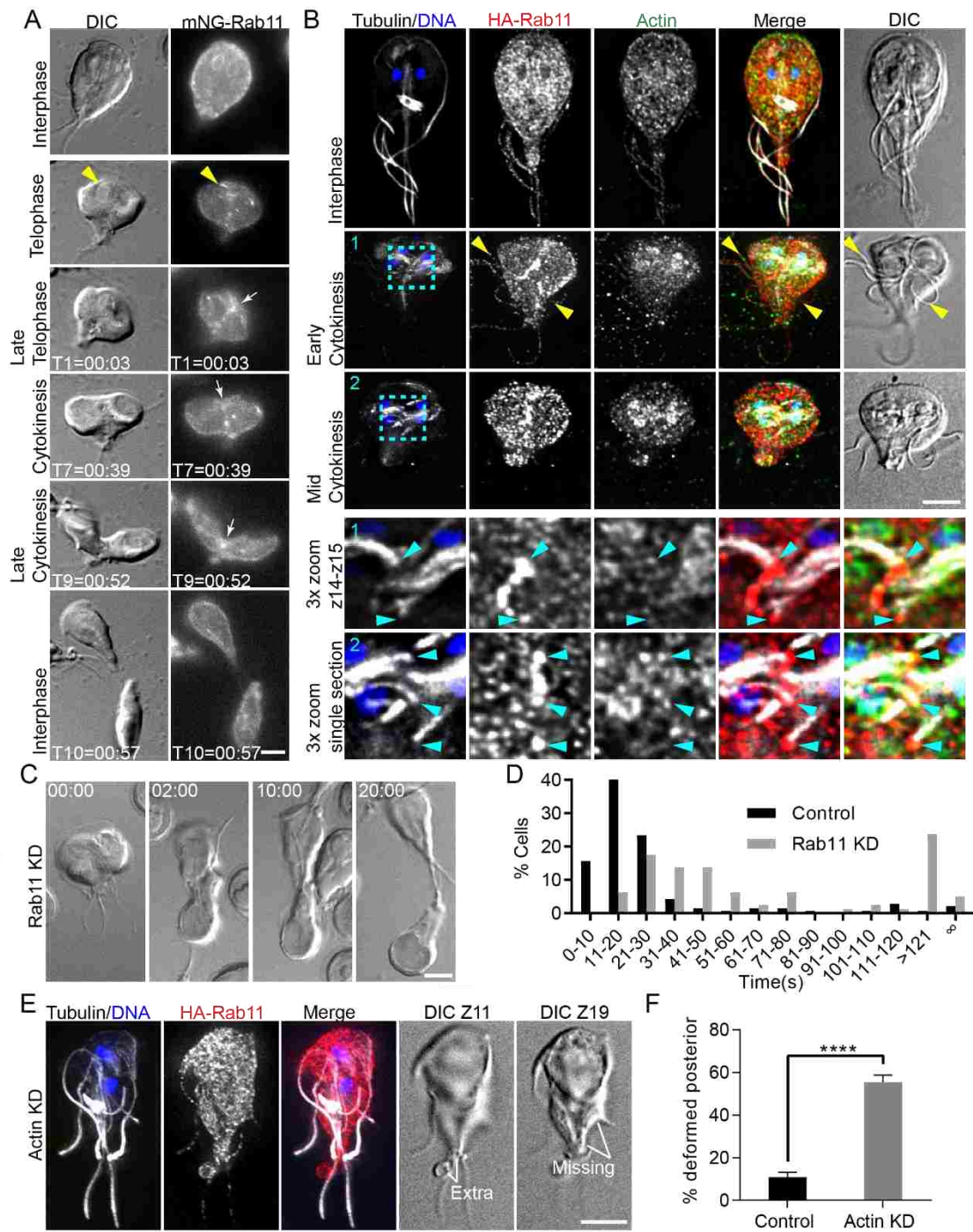
Figure 5

Fig. 5. Rab11 traffics to the furrow on flagella and is required for abscission. (**A**) mNG-Rab11 localization through the cell cycle. In late telophase Rab11 is recruited to intracytoplasmic axonemes (yellow arrowhead) and immediately before anterior-posterior furrow ingression Rab11 delineates the furrow (white arrow). mNG-Rab11 remained in the cleavage furrow and at the leading edge of the advancing furrow during cytokinesis (white arrow). Time-stamp, mm:ss. (**B**) Immunofluorescence localization of tubulin (grayscale), actin (green), HA-Rab11 (red) and DNA (blue). HA-Rab11 localized to the ER in interphase cells. During late telophase Rab11 loaded onto flagella (yellow arrowheads). Just ahead of anterior to posterior furrow progression HA-Rab11 accumulated in the furrow. Enlarged images correspond to cyan boxes with two or one optical section that show Rab11 and actin accumulating at the ends of the nascent flagella pointed out with blue arrowheads. (**C**) Rab11 antisense morpholino treated cells are delayed in abscission and frequently have abnormal furrow positioning. (**D**) Histogram of division timing for Rab11 KD (n=80) and morpholino control (n=141). (**E**) Example of an actin knockdown cell with abnormal posterior morphology and a membrane accumulation. (**F**) Quantification of this phenotype for actin depleted (n=602) and morpholino control cells (n=613). Scale bars=5 μm

A

Tubulin/DAPI | HA-Rab11 | Actin | Merge | DIC

Cytokinesis

Zoom

Coloc Actin/Rab

B

DIC | Actin | Tet::HA-Rab11^{DN} | Merge/DAPI

Cytokinesis

C

DIC | Actin | Tet::HA-Rab11^{CA} | Merge/DAPI

Cytokinesis

D

% in cytokinesis

HA-Rab11 | Tet::HA-Rab11 | Tet::HA-Rab11^{CA} | Tet::HA-Rab11^{DN}

E

kD   Ctrl   Rab11 KD

43 ——— Actin

35

HA-Rab11^{MS}

~70% reduction
24hrs after KD

Figure S6

58
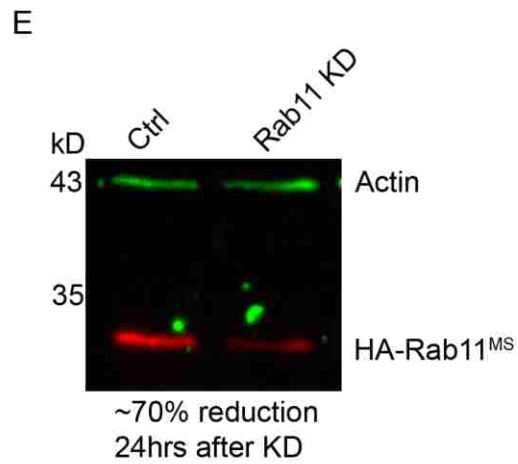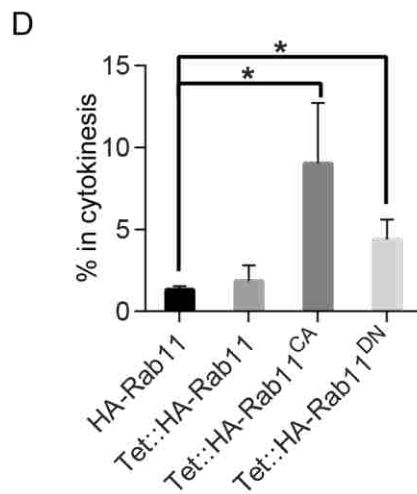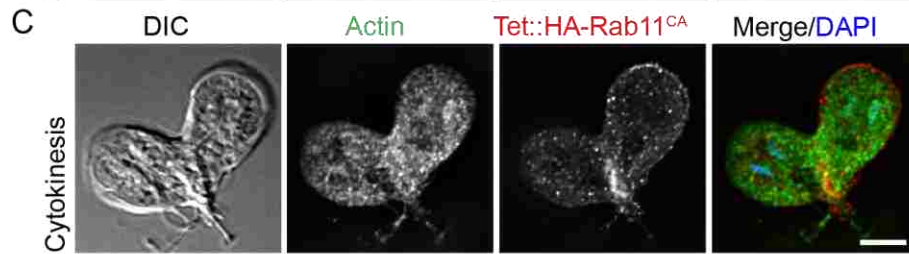
Fig S6 Rab11 traffics on intracytoplasmic axonemes and dominant mutants block cytokinesis. (**A**) Another example of Rab11 and actin being enriched at the ends of nascent flagella. This cell is from an experiment where the culture was partially synchronized using the microtubule inhibitor albendozole. This treatment presumably caused the observed flagella misorientation. However, this orientation allows the nascent posterolateral flagella to be more easily observed and demonstrates that Rab11 and actin tracked the position of the flagella tips. Boxed region is magnified, regions of Actin and Rab11 co-localization are shown in green with tubulin in magenta. (**B**)Fixed pTet::HA-Rab11^{DN} (dominant negative) expressing cells accumulated HA-Rab11^{DN} between arrested daughter cells. (**C**) pTet::HA-Rab11^{CA} (constitutively active) expressing cells accumulated HA-Rab11^{CA} between daughter cells and failed in cytokinesis. Scale bars=5 μm. Note the ab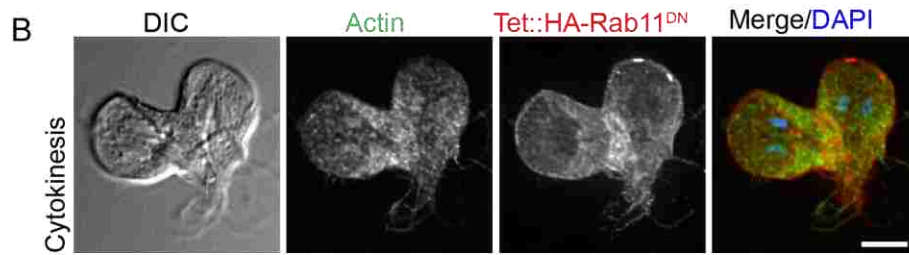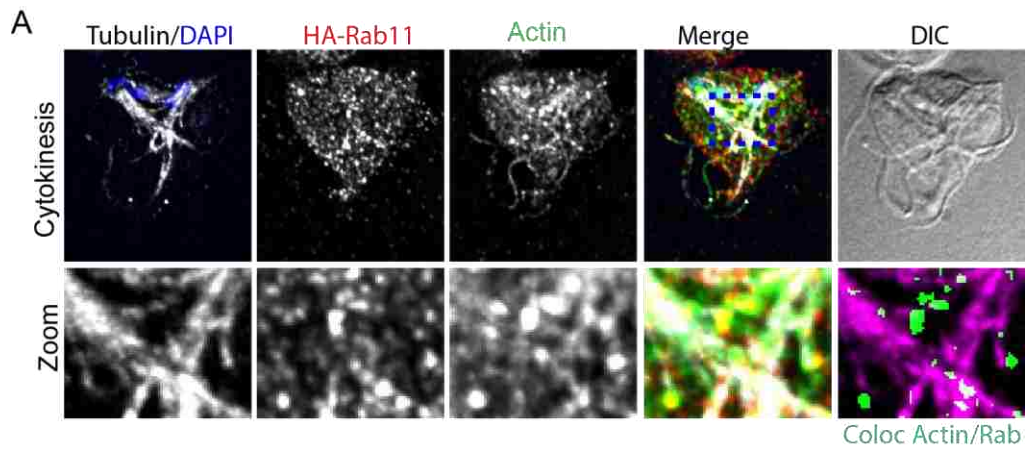normal placement of the cleavage furrow in (B) and (C). (**D**) Quantification of cells in the process of cytokinesis (active or arrested) for the indicated Rab11 mutant fixed 24 hours after Tet induced expression. At least 1,400 cells from three independent experiments were counted for each condition. *P<0.05. (E) Western blot showing that the Rab11 antisense translation blocking morpholino effectively depletes Rab11.
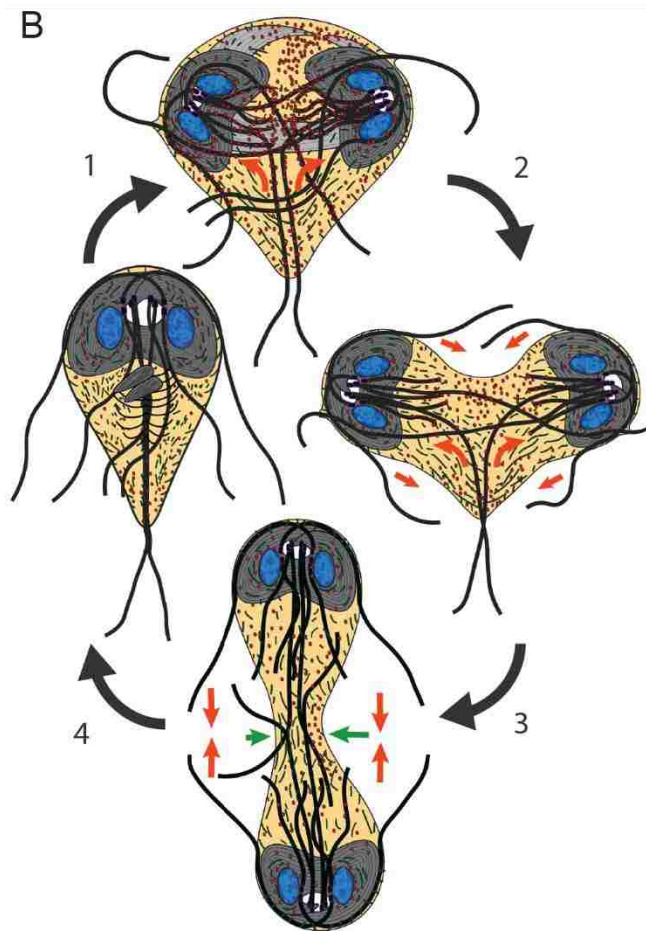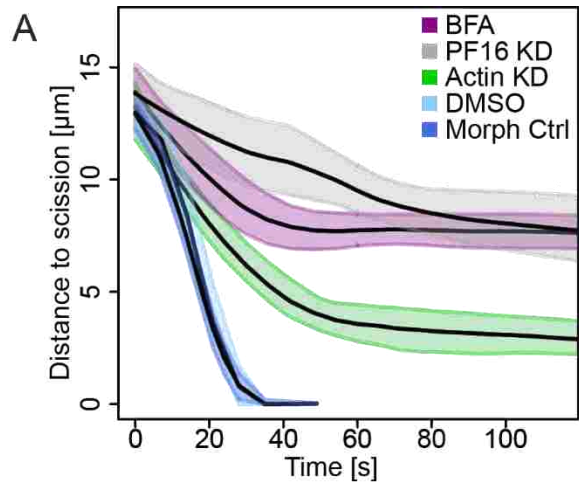
Fig. 6. Model for cytokinesis in *Giardia*. (**A**) Comparison of experimental perturbations and their corresponding control treatments. Note the distance to scission at which each perturbed cellular system slowed or arrested division. The stall point is interpreted as the point at which the pathway contributes to furrow progression. (**B**) Model for myosin independent cytokinesis. The ventral discs in grey, actin in green, Rab11 in red, and forces driving daughter cell separation are indicated by orange arrows. 1.) Mitosis is initiated, actin positions the microtubule cytoskeleton. 2.) Rab11 loads onto the intracytoplasmic axonemes and is guided into the furrow by the nascent axonemes. Ventral disc opening permits furrow progression, the intracytoplasmic caudal flagella push daughter discs in opposite directions to initiate a furrow. 3.) Caudal axonemes continue pushing discs apart, differential cortical actin and Laplace pressure (green arrows) direct furrow advancement. 4.) Flagella propulsion generates cortical tension between daughter cells and actin and Rab11 coordinate membrane remodeling for abscission.

Chapter 3

The ventrolateral flange a lamellipodia-like structure in *Giardia*

William R. Hardin[1], Renyu Li[1], Andrew Shelton[1], Aaron Halpern[2], Germain C. M. Alas[1], Pavla Tumova[3], Richard Johnson[3], Michael MacCoss[3], Joshua Vaughan[2], Alexander R. Paredez[1*]

[1]Department of Biology, University of Washington, Seattle, United States; [2]Department of Chemistry, University of Washington, Seattle, United States, [3]Department of Tropical Medicine, 1st Faculty of Medicine, Charlies University in Prague and Faculty Hospital Bulovka, Czech Republic, Department of Genome Sciences, University of Washington, Seattle, United States[3]

Abstract: Cell morphology is largely controlled by the cytoskeleton. The actin-cytoskeleton modifies cell morphology by generating the forces necessary to change cell shape for processes including, cell migration, endocytosis, and cytokinesis. Only through the regulation of actin-binding proteins (ABPs) are cells able to execute these dynamic events. The evolutionarily basal intestinal parasite *Giardia lamblia* lacks all canonical ABPs. However, despite the lack of canonical ABPs, *Giardia* actin is required for conserved cellular functions, including maintaining cell shape. In an effort to identify ABPs, PHI blast was used to search for WH2 domain containing proteins. This search led to the discovery of Flangin, a protein that interacts with actin and is enriched in a lamellipodia-like structure known as the ventrolateral flange (VLF). Subsequently, Rac, the single Rho family GTPase in *Giardia* was found to localize to the VLF. Live-cell imaging revealed the VLF is static during interphase, but grows during mitosis and is immediately reassembled upon daughter cell reattachment. Knockdown (KD) studies of Flangin, actin, and Rac result in the VLF being either thinner than control cells or fully collapsed. Taken together Flangin, actin, and Rac are the first proteins identified in the VLF and each is critical for its assembly. Actin and Rac were also shown to serve parallel roles in the lamellipodia. With the dynamics of the VLF established and an initial group of proteins

identified to the VLF, there is an opportunity to explore the function of this understudied structure.

Importance: The ventrolateral flange (VLF), is an enigmatic lamellipodia-like structure found at the host-parasite interface in *Giardia lamblia*. It was previously hypothesized that the VLF aids in attachment through membrane adhesion. Yet proteins responsible for building the VLF have remained unidentified and the attachment hypothesis is still poorly understood. Here we identify a novel actin binding protein (ABP) that localizes to the VLF implicating actin in VLF formation. We show that actin and Flangin are both required for flange formation. Subsequent to identifying actin as an essential component to VLF assembly, GlRac was also found to serve a critical role in regulating VLF assembly. This work is the first to identify components in the VLF and begins to unravel the molecular underpinnings of this dynamic and often overlooked structure.

Introduction:

The cytoskeleton is responsible for the mechanical properties and shapes of cells. The actin cytoskeleton is essential to maintaining cell shape and forms the central organizing scaffold for the cell. Thus, changes in cell structure are often driven by or at least concomitant with changes in actin assembly [1]. Assembly of actin filaments from their monomeric subunits and regulation by actin-binding proteins (ABPs), is necessary to change the shape of cells and produce cellular protrusions [2]. Despite the central importance the actin cytoskeleton contributes to cell shape across the eukaryotic phylogenic tree, most of our understanding comes from studies performed on model systems. *Giardia lamblia* is a common waterborne pathogen

63

that infects 280 million people each year [3]. In addition to being a major parasite, *Giardia* belongs to possibly the earliest diverging eukaryotic lineage and possesses a lamellipodia-like structure called the ventrolateral flange (VLF) [4-7]. The VLF is a protrusion that appears as a thin flexible skirt-like structure encircling interphase cells. The VLF remains an enigmatic structure and a single study attempts to probe VLF function. These findings are based exclusively on scanning electron microscope (SEM) data, and suggest the VLF aids in attachment through membrane adhesion [8]. The VLF has been challenging to study and often overlooked. There are currently no known proteins that localize to the VLF, it is not well preserved during standard giardial fixation process, and the majority of *Giardia* biology is interpreted from analyzing fixed samples, making it difficult to understand VLF dynamics. As a result, the molecular mechanism coordinating VLF dynamics and the timing of these events remain unexplored. Given many pathways in *Giardia* have fewer components than in well-studied model eukaryotes, investigating the VLF may potentially define both the minimal requirements for function and the portions of cellular mechanisms constrained throughout evolution [5].

Although morphologically similar there are major differences between the VLF and lamellipodia. The lamellipodia is used for cell motility, but *Giardia* does not undergo amoeboid motility [9-11]. Furthermore, the underlying cytoskeleton in the VLF is one of the most divergent of all eukaryotes. *Giardia* lacks all canonical ABPs (actin-binding proteins) thought to be common to all eukaryotes to perform critical functions. Our previous work has shown that despite the lack of canonical ABPs, *Giardia* actin is required for conserved cellular functions, including maintaining cell shape [12]. Given *Giardia*'s elaborate actin cytoskeleton and ability to perform similar functions to actin in other eukaryotes, it suggests the presence of unique

cytoskeletal regulators. We previously indicated that GlRac in *Giardia*, the sole Rho family

GTPase, and 14-3-3, are the only demonstrated regulators of the actin cytoskeleton [12, 13].

Similar to a requirement for actin in cell shape, depletion of GlRac disrupts cellular

morphogenesis [12]. Given the conserved roles actin and GlRac serve in maintaining cell shape,

there is likely a set of unidentified actin-interacting proteins that connect GlRac signaling to

regulation of cytoskeletal dynamics.

The VLF represents an opportunity to explore how a lamellipodia-like structure is

assembled in the absence of canonical ABPs. Through a bioinformatics search we identified

Flangin, a putative ABP that localizes to the VLF. This is the first protein identified that

contributes toward VLF formation and opens the prospect of exploring the role of actin in VLF

formation. We also used live-cell imaging to probe VLF and Flangin dynamics. During the

course of this study we found that GlRac, the single Rho GTPase in *Giardia* is a critical

upstream regulator for VLF assembly. Taken together this study elucidated components that

underpin and control VLF dynamics and establishes an initial molecular understanding of this

enigmatic structure.

Results:

***Giardia* possesses a lamellipodia-like structure that contains actin and Flangin**. Given that

Giardia does not contain canonical ABPs, it has been historically difficult to investigate and

understand how actin dynamics, such as cell shape, are regulated in *Giardia*. In order to identify

putative actin-binding protein(s), we performed a bioinformatics search of the *Giardia* genome

for putative WH2 domain containing proteins. The WH2 domain is a conserved short helical

domain found in actin binding proteins of diverse function [14, 15]. For example, three actin

nucleators that contain WH2-domain(s) are found in metazoans (Spire, Cordon-Bleu, and Leiomodin), and three bacterial counterparts that mimic them (VopF, VopL, and TARP), have also been identified [16-21]. Additionally, *Listeria monocytogenes* maintains ActA, a nucleation-promoting factor with a WH2 domain [22]. *Listeria* requires both ActA and a co-opting of the host Arp2/3 complex for effective nucleation [23]. This small domain is not found with simple homology searching and thus could have been missed by the *Giardia* genome project and is an ideal candidate for identifying non-canonical ABP(s) [14]. Using a PHI blast search and various PHI patterns (see materials and methods), 200 proteins were identified that contain one or more putative WH2 domain(s) (data not shown). This search resulted in the identification of Flangin (Figure S1A). Subsequent to identifying Flangin, with its three WH2 domains, a putative Bro1 domain was identified on the N-terminus (Figure S1B). The Bro1 domain is conserved and found in the protein Alix, in mammalian fibroblasts. The Bro1 domain in Alix binds to F-actin and is also a regulator of EscrtIII [24]. After pulling-down Flangin, we probed for and found actin (Figure 1A). These results are consistent with Flangin actin as a non-canonical ABP, which may help shed-light on *Giardial* actin dynamics.

Using expansion microscopy, Flangin was found to localize in the VLF (ventrolateral flange) (Figure 1B). Flangin marks the VLF and the thin flexible morphology agrees with previous scanning electron microscopy (SEM) studies [8]. To investigate VLF and Flangin dynamics over the cell-cycle, Flangin-mNG live imaging was performed. During mitosis the VLF increases in width, but during cytokinesis, it is disassembled (Figure 1C and Movie 1). Over the course of cytokinesis, Flangin-mNG relocalizes from the VLF into the cell-body. Upon daughter cell reattachment the VLF is absent, but is immediately reconstructed, growth begins in the anterior and continues along the cell-body with the posterior VLF being the last to complete

growth in 2min 23sec. As the daughter cells rebuild the VLF, Flangin moves from the cell-body

to relocalize in the VLF. To confirm the VLF changes size over the cell cycle in WT cells, we

used SEM and verified the VLF dynamics as described above (Figure 1D).

     Given the VLF morphological and growth similarities to the lamellipodia, we questioned

whether actin localized to the structure during the cell-cycle when the VLF grows. With the

inability to fluorescently tag actin or use common actin reporters, these studies were limited to

fixed cells. To observe the VLF, we allow cells to attach to coverglass before fixation to insure

the VLF is fully displayed. Prior studies likely overlooked VLF proteins because it was not fully

extended prior to fixing. Actin filamentous structures, and Flangin, were found throughout the

VLF during interphase and the cell-cycle (Figure 1E). Surprisingly, during cytokinesis when the

VLF was dismantled, there was increased co-localization between these proteins in the cell-body.

Flangin and actin are necessary for VLF assembly. Given the Flangin dynamics during the

cell-cycle and actin localization to the VLF during growth periods, we questioned whether they

had a role in VLF assembly. To probe the role of actin, we used morpholoino treatment to

deplete actin. Quantitative western blotting revealed 60% depletion at the population level, 24

hours after morpholoino treatment (Figure S2A). Actin-depleted cells resulted in either a

collapsed or thin VLF phenotype. The collapsed VLF was present, but did not extend beyond

the cell body and the thin VLF was significantly smaller compared to control cells (Figure 2A

and 2B). It is possible the two phenotypes result from differences in cell-to-cell morpholoino

penetrance across the cell population. Flangin-depleted cells appeared to have thin VLF when

compared to the control (Figure 2A and 2B). Flangin-depleted cells complete cytokinesis faster

than control cells (Figure S3). This may result from more quickly dissembling the VLF in

Flangin KD cells. From investigating Flangin KD cells undergoing mitosis, we found that actin localizes beyond the leading edge of Flangin (Figure 2C). These findings suggest actin is sufficient to expand the VLF membrane during VLF growth. These results indicate actin and Flangin are both important for VLF growth. However, Flangin is likely a structural component that is positioned in the VLF in a directionally controlled manner as actin expands the VLF membrane.

Flangin is a structural component in the VLF. VLF size is for the most part static during interphase. The VLF could maintain a fixed length through balance of catastrophe and assembly of structural protein(s) or through the use of a static scaffold. To probe these possibilities fluorescence recovery after photobleaching (FRAP) was performed on Flangin-mNG. The Flangin-mNG in the VLF showed minimal recovery after being photobleached. We conclude that Flangin-mNG is a stable structural protein during interphase (Figure 3A and 3B). The cell-body and posterlateral grooves exhibited similar recovery rates (data not shown).

GlRac is a conserved signaling component in the ventrolateral flange. The VLF morphology as well as the role of actin in VLF formation has striking parallels to lamellipodia. Rho family GTPases play a central role in regulating lamellipodia formation, therefore we questioned whether GlRac, *Giardia*'s sole Rho family of GTPases might also regulate VLF formation. An N-terminally HA-Tagged GlRac localized to the VLF (Figure 4A). Next, we questioned whether GlRac was required for VLF formation. GlRac was depleted with morpholinos and actin along with flangin were used as markers for the flange (Figure 4B). VLF organization was extremely perturbed in GlRac KD cells, instead of an even membrane lamella around the periphery of

Giardia, we observed sporadic protrusions that gave the VLF a serrated appearance. Actin and Flangin were found to accumulate in the patchy VLF protrusions. The GlRac KD cells also resulted in a significant decrease in the anterior VLF width and a greater number of serrated cells compared to the control (Figure 4C and 4D). Given these results, actin and Flangin appear to be downstream of GlRac signaling.

Dissecting the function of the VLF. With VLF dynamics explored and multiple proteins identified in the structure, we next questioned its function. The VLF remains an enigmatic structure. Currently, a single SEM based study using microfabricated surfaces to probe the role of the VLF found a role for the VLF in cell attachment [8]. With molecular VLF components identified, we probed whether Flangin, actin, and/or GlRac were necessary for attachment. Each of these proteins was depleted with morpholinos and then attachment efficiencies were measured (Figure 5). Fewer GlRac and actin KD cells maintained attachment compared to the control whereas Flangin KD did not disrupt attachment under these unchallenged conditions. The reduced attachment in GlRac and actin depleted cells may result from pleiotropic response(s). As we have observed newly dividing cells without VLFs attach immediately after cytokinesis, it appears that the VLF may not be required to establish attachment but our assay simply measured whether cells were attached to the culture tube or free swimming. Perhaps future studies could challenge attachment with shear or centripetal force [9] This is a placeholder, we will do these experiments before publication.

Given that Flangin is a predominant component of the VLF, we sought to identify interacting proteins that might inform on the function of the VLF. To identify proteins, we used affinity chromatography, which included Flangin-TwinStrep, coupled with mass spectroscopy

[13, 25-27]. Table S1 lists 100 proteins that had Flangin/control ratios greater than 1 and were statistically significant compared to the control. Bioinformatics analysis was utilized to place these hits into seven categories (Table S1). Some hits were identified that may shed light on the function of Flangin and the VLF. For example, three of *Giardia*'s seven Rab proteins were identified: Rab2a, Rab1a, and Rab2b. These identified Rabs are hypothesized to serve important roles in exocytosis and, perhaps, suggest Flangin is involved with membrane trafficking at the VLF host-parasite interface [28, 29]. Intriguingly, the largest family of Flangin-interacting proteins were the variant surface proteins (VSPs) (Table S1 A). *Giardia* contains approximately 270 VSPs and displays them on their cell surface to avoid the host immune system [30]. Although little is understood about the cellular role of VSPs and their trafficking, prior studies appear to show concentration of VSPs at the VLF. Given Flangin and VSPs possibly co localize at the VLF, it is feasible Flangin helps coordinate VSP trafficking and/or aids in displaying VSPs on the VLF cell surface. The list of Flangin-binding proteins indicate the VLF may be a hub of previously unappreciated biological function such as trafficking and display of immune evading VSPs.

Discussion:
VLF and Flangin dynamics. We set-out to determine whether *Giardia* had WH2 containing protein(s) and if so, what their function might be. Through a bioinformatics approach the WH2 containing non-canonical ABP Flangin was identified and found to be a marker for the VLF (Figure S1 and Figure 1B). Using a modified giardial fixation protocol, that preserves the VLF, our previously developed live imaging technique, and genetics, we identified the first proteins that localize and contribute to VLF formation. Subsequent to localizing Flangin in the VLF, actin, and GlRac were also identified (Figure 1D and 1E). The Flangin localization pattern and

SEM studies support the VLF similarity to the lamellipodia due to its thin flexible morphology. There are also lamellipodia-like protrusions along portions of the VLF, indicative of lamellipodia structures found in model systems (Figure 1B). The function of these protrusions remains unclear.

After finding Flangin marks the VLF, the dynamics during cell division were explored. Although the VLF does not change in size during interphase, it grows wider during mitosis, is consumed during cytokinesis, and re-forms after cell division (Figure 1C, D, and E). It is possible the VLF grows during mitosis to maintain attachment during a time of vulnerability. The ventral disk is the main structure used for cell attachment, however, at the end of mitosis the parental disk is dissembled leaving cells temporarily susceptible to being swept down the intestine-track by peristaltic flow. Perhaps the VLF grows in size to increase host-parasite contact in order to prevent being swept away when the main adhesive structure is absent. This possible role in attachment is supported by a previous study that found the VLF could establish connections to microfabricated pillars which prevented normal ventral disc function [8].

Flangin and actin are essential for VLF assembly. Given the VLF dynamics and morphological similarities with the lamellipodia, its not surprising actin localizes to the VLF and biochemically interacts with Flangin (Figure 1A and D). Actin and Flangin appear to be involved with coordinating VLF growth dynamics. The collapsed and thin VLF resulting from actin and Flangin depletion are consistent with these findings. Given the variability in cell-to-cell morpholino penetrance, this helps explain the variable thin and collapsed VLF phenotypes seen in actin depleted cells. Cells with a collapsed VLF likely reflect a stronger phenotype and more clearly highlight the critical role actin plays in driving VLF growth (Figure 3A and B). We

propose actin is necessary for VLF plasma membrane expansion, whereas, Flangin is a structural protein assembled to support the VLF. Simultaneous to actin pushing against the VLF plasma membrane, Flangin is positioned to support the VLF. Flangin depleted cells that are undergoing mitosis support this idea. In these cells, actin localizes beyond the leading edge of Flangin, suggesting actin is sufficient to drive VLF plasma membrane expansion (Figure 3C). The VLF is unique in its ability to maintain persistence during interphase given that lack of canonical ABPs. Recent findings in fibroblasts found that tropomyosin, together with coronin 1B and Arp2/3, are responsible for enhancing the persistence of lamellipodial protrusions [10]. Given tropomyosin is absent in *Giardia*, perhaps Flangin serves as a structural protein involved with maintaining VLF persistence during interphase.

Flangin the VLF disassembly and cytokinesis. In trophozoites, the VLF is only disassembled during cytokinesis and Flangin relocalizes to the cell-body during this process. Furthermore, the FRAP data indicates Flangin is a structurally stable protein during interphase and Flangin-$_{1\text{-}300}$-mNG stabilizes the VLF (Figure 2A and C). Taken together these data indicate Flangin and the VLF may physically impede cleavage furrow advancement and their disassembly may be a critical cytokinetic requirement. Given that *Giardia* undergoes one of the fastest rates of cytokinesis among all eukaryotes and membrane trafficking is required to complete cytokinesis [31], it is possible the VLF is consumed during cytokinesis because it serves as a membrane reservoir to complete the process. A membrane reservoir would help support the rate of cytokinesis. The use of a reservoir to support specific events during cell-division has already been observed in *Giardia*. For example, the median body serves as a tubulin reservoir for both

spindles and daughter ventral disks [31]. Although the VLF dynamics do not contribute to amoeboid motility, *Giardia* appears to have evolved novel uses for an analogous structure.

GlRac signaling is critical for VLF assembly. Precedent exists for Rho family GTPase controlling the lamellipodia through coordination of the cytoskeleton [32]. Like other lamella, we found that GlRac, the only Rho family GTPase found in *Giardia*, localizes to the VLF (Figure 4A). Subsequent to this localization, GlRac depletion studies resulted in thin and serrated VLF (Figure 4B, C, and D). These findings suggest GlRac is an essential upstream signaling component of VLF assembly. We presume the patchy phenotype results from regions of accumulated GlRac. It is tempting to speculate that GlRac works to coordinate the cytoskeleton during VLF maturation. For example, GlRac could trigger actin-based polymerization promoting actin based VLF growth. A general role in coordinating the cytoskeleton would be in line with Rho GTPase function in other eukaryotes [33]. Considering that GlRac is the evolutionary founding member of the Rho family GTPase and that *Giardia* belongs to a potentially early-branching group of eukaryotes, our results suggest that the ancestral Rac homolog was capable of regulating multiple processes.

The multiple role(s) of the VLF. To date the only suggested role for the VLF was derived from SEM data stating a role in adhesive activity [8]. Our findings indicate the VLF aids in attachment, but only when GlRac and actin are depleted (Figure 5). These attachment phenotypes may result from pleoptriopic responses, given that GlRac and actin are involved with numerous cellular processes. The Flangin KD cells failed to show attachment defects in our study, but this may be a result of not testing for the quality of attachment. Attachment quality

could be interrogated by exposing Flangin KD cells to incrementally increasing centripetal and/or shear force. It's possible the VLF serves as a "gasket" surrounding cells to help improve hydrodynamic flow and aid in attachment. In Flangin depleted cells, perhaps a less prominent VLF will lead to cells less likely to withstand force that challenges attachment.

In addition to attachment, we hypothesized that the VLF may serve other functions in the cell. Proteomic analysis of Flangin-binding proteins was performed to help elucidate this question. Variant surface proteins were found as the largest family of interacting proteins (Table 1). Very little is understood regarding VSPs and antigenic variation in *Giardia*. A single VSP is displayed on the cell surface at a time, but the cellular mechanism involved with trafficking the VSP to the surface remains poorly understood [34]. Given that during every cell cycle the VLF is disassembled and re-built, re-building of the VLF would be an opportune time to direct trafficking of VSPs to the cell surface (Figure 1D and 1E). Flangin could be tested for a role in VSP trafficking by determining whether an epitope tagged VSP localizes to the VLF in Flangin KD cells. If the VLF is adhesive, VSPs are candidate adhesion molecules as they coat the entire cell surface. FRAP could be used to probe whether Flangin might serve as a scaffold for holding VSP in place. It would be possible to determine whether VSPs are stable and similar to Flangin during interphase (Figure 3). If Flangin is involved with VSP trafficking to the VLF, we suspect very little VSP turnover in interphase cells. Overall, we propose the VLF functions as both an adhesive structure and a membrane reservoir.

Material and Methods.

Strain and culture conditions. *Giardia* strain WB Clone 6 (ATCC 50803) was cultured as in [35]

74

Morpholino knockdown. Knockdown experiments were performed as described in [36] using

the actin morpholino oligonucleotide 5' GCAGGGTTGTCGTCTGTCA- TTTAC 3', Flangin

(ORF 7031) morpholino oligonucleotide 5'CGAGAGCGCAAGGATTCTGATGCAT 3', Rac

morpholino oligonucleotide 5' TATCCTCATTTCCTGTACTAGTCAT 3', and a control

morpholino oligonucleotide 5' CCTCTTACCTCAGTTA CAATTTATA 3', sourced from Gene

Tools.

Vector Construction.

All constructs used in this study were made using standard techniques, see Dataset S1 for

sequences and workflow. Construction of the HA-GlRac is described in reference [37].

Expansion microscopy.

Performed as described in [38].

Immunoprecipitation and Western blotting.

Blotting and actin biochemical interaction were performed as in [13].

Scanning electron microscopy.

Performed as described in [39].

Fluorescent live imaging.

In an effort to increase the mitotic index, cells were treated with 0.25µM Albendazole ~4hrs

before being imaged. Cells were chilled with ice for 20 minutes to detach from the culture tube

and then placed into an Attofluor cell chamber (Molecular Probes) and incubated in a GasPak EZ

anaerobic pouch (BD) for 1-2 hrs at 37° C. Cells were then washed four times with SB5050

(0.1% K2HP04, 0.06% KH2P04, 1% glucose, 0.2% NaCl, 0.2% cysteine-HCI monohydrate,

0.02% ascorbic acid, 0.0228% ferric ammonium citrate, 0.05% bovine bile and 5% bovine

serum, pH 7.1; see Dataset S1 for variants tested). Drug-free cells were overlaid with a mixture

of 0.7-1% ultra-low gelling agarose (Sigma A2576) melted in HBS (137mM NaCl, 5mM KCl, 0.91mM Na_2HpO_4-heptahydrate, 5.55mM Glucose, 20mM HEPES, and pH7) and diluted into SB5050, left at room temperature for 10 min to solidify the agarose. Imaging was performed under 2.5% O_2, 5% CO_2, and 37° C (Oko Lab Boldline CO_2/O_2). Time-lapse imaging was performed on a DeltaVision Elite microscope (GE, Issaquah, WA) equipped with DIC optics, using a 100x1.4 NA or 60x1.42 NA objective, and sCMOS 5.4 PCle Air-cooled camera (PCO-TECH Inc).

Immunofluorescence microscopy.

Fixed imaging was modified from [37] using starve and release cells (3.5 hours) to increase mitotic index [35]. Cells were allowed to attach to coverslips before being fixed. Images were acquired on the above mentioned microscope.

Fluorescence Recovery after Photobleaching.

Fluorescence recovery after photobleaching (FRAP) was performed on Flangin-mNG in the VLF to measure the movement and turnover. Cells were chilled with ice for 20 minutes to detach from the culture tube and then placed into an Attofluor cell chamber (Molecular Probes) and incubated in a O_2/CO_2 incubator (Panasonic) for 1-2 hrs at 37° C. Cells were overlaid with a mixture of 0.7-1% ultra-low gelling agarose (Sigma A2576) melted in HBS (137mM NaCl, 5mM KCl, 0.91mM Na_2HpO_4-heptahydrate, 5.55mM Glucose, 20mM HEPES, and pH7), and then left at room temperature for 10 min to solid ify the agarose. All experiments were conducted using a FRAP-enabled DeltaVision Spectris, 488 nm solid-state laser, 100% laser power, 50 mW laser, and 25 ms stationary pulse. The first image was acquired approximately 2 ms after the bleach event. The first min, images were acquired every 10 sec for 1 min, for the following 2 min every 20 sec, then at 50sec intervals over the following 6 min, after which

images were acquired every 100 sec for the remainder of the experiment. Normalized mNG fluorescence recovery was calculated by subtracting the background noise from the ROI intensity measurement; the background-subtracted intensity measurement was then divided by a fluorescent control ROI intensity measurement to normalize for photobleaching due to imaging.

Statistical analysis.

Statistically significant differences between KD and control groups were obtained using GraphPad Prism 7.02 software and unpaired t test with Welch's correction.

Quantitating cell attachment.

Cells were depleted for either Flangin, actin, or GlRac (see above for KD protocol), allowed to re attach, and 21 hrs after the KD they were iced and placed into 13mL culture tubes. 24 hrs after the KD the number of unattached and attached cells were counted by diluting to 20,000 cells/mL and a Coulter counter (MoxiZ) was used. Three independent replicates of each cell line and control were analyzed.

Flangin affinity chromatography.

Performed as described in [39].

Mass spectroscopy.

Performed as described in [4040]

References
1. Ono, S., *A plague of actin disassembly.* J Biol Chem, 2017. **292**(19): p. 8101-8102.
2. Pollard, T.D. and J.A. Cooper, *Actin, a central player in cell shape and movement.* Science, 2009. **326**(5957): p. 1208-12.
3. Baldursson, S. and P. Karanis, *Waterborne transmission of protozoan parasites: review of worldwide outbreaks - an update 2004-2010.* Water Res, 2011. **45**(20): p. 6603-14.
4. Ciccarelli, F.D., et al., *Toward automatic reconstruction of a highly resolved tree of life.* Science, 2006. **311**(5765): p. 1283-7.
5. Morrison, H.G., et al., *Genomic minimalism in the early diverging intestinal parasite Giardia lamblia.* Science, 2007. **317**(5846): p. 1921-6.
6. Hampl, V., et al., *Phylogenomic analyses support the monophyly of Excavata and resolve relationships among eukaryotic "supergroups".* Proc Natl Acad Sci U S A, 2009. **106**(10): p. 3859-64.
7. Sousa, M.C., et al., *Adherence of Giardia lamblia trophozoites to Int-407 human intestinal cells.* Clin Diagn Lab Immunol, 2001. **8**(2): p. 258-65.
8. Erlandsen, S.L., A.P. Russo, and J.N. Turner, *Evidence for adhesive activity of the ventrolateral flange in Giardia lamblia.* J Eukaryot Microbiol, 2004. **51**(1): p. 73-80.
9. Fletcher, D.A. and R.D. Mullins, *Cell mechanics and the cytoskeleton.* Nature, 2010. **463**(7280): p. 485-92.
10. Brayford, S., et al., *Tropomyosin Promotes Lamellipodial Persistence by Collaborating with Arp2/3 at the Leading Edge.* Curr Biol, 2016. **26**(10): p. 1312-8.
11. Fritz-Laylin, L.K., et al., *The genome of Naegleria gruberi illuminates early eukaryotic versatility.* Cell, 2010. **140**(5): p. 631-42.
12. Paredez, A.R., et al., *An actin cytoskeleton with evolutionarily conserved functions in the absence of canonical actin-binding proteins.* Proc Natl Acad Sci U S A, 2011. **108**(15): p. 6151-6.
13. Paredez, A.R., et al., *Identification of obscure yet conserved actin associated proteins in Giardia lamblia.* Eukaryot Cell, 2014. **13**(6): p. 776-84.
14. Edwards, J., *Are beta-thymosins WH2 domains?* FEBS Lett, 2004. **573**(1-3): p. 231-2; author reply 233.
15. Qualmann, B. and M.M. Kessels, *New players in actin polymerization--WH2-domain-containing actin nucleators.* Trends Cell Biol, 2009. **19**(6): p. 276-85.
16. Quinlan, M.E., et al., *Drosophila Spire is an actin nucleation factor.* Nature, 2005. **433**(7024): p. 382-8.
17. Ahuja, R., et al., *Cordon-bleu is an actin nucleation factor and controls neuronal morphology.* Cell, 2007. **131**(2): p. 337-50.
18. Chereau, D., et al., *Leiomodin is an actin filament nucleator in muscle cells.* Science, 2008. **320**(5873): p. 239-43.
19. Tam, V.C., et al., *A type III secretion system in Vibrio cholerae translocates a formin/spire hybrid-like actin nucleator to promote intestinal colonization.* Cell Host Microbe, 2007. **1**(2): p. 95-107.
20. Liverman, A.D., et al., *Arp2/3-independent assembly of actin by Vibrio type III effector VopL.* Proc Natl Acad Sci U S A, 2007. **104**(43): p. 17117-22.
21. Jewett, T.J., et al., *Chlamydial TARP is a bacterial nucleator of actin.* Proc Natl Acad Sci U S A, 2006. **103**(42): p. 15599-604.

22.   Boujemaa-Paterski, R., et al., *Listeria protein ActA mimics WASp family proteins: it activates filament barbed end branching by Arp2/3 complex.* Biochemistry, 2001. **40**(38): p. 11390-404.

23.   Welch, M.D., et al., *Interaction of human Arp2/3 complex and the Listeria monocytogenes ActA protein in actin filament nucleation.* Science, 1998. **281**(5373): p. 105-8.

24.   Pan, S., et al., *Involvement of the conserved adaptor protein Alix in actin cytoskeleton assembly.* J Biol Chem, 2006. **281**(45): p. 34640-50.

25.   Schmidt, T.G., et al., *Development of the Twin-Strep-tag(R) and its application for purification of recombinant proteins from cell culture supernatants.* Protein Expr Purif, 2013. **92**(1): p. 54-61.

26.   Witte, C.P., et al., *Rapid one-step protein purification from plant material using the eight-amino acid StrepII epitope.* Plant Mol Biol, 2004. **55**(1): p. 135-47.

27.   Junttila, M.R., et al., *Single-step Strep-tag purification for the isolation and identification of protein complexes from mammalian cells.* Proteomics, 2005. **5**(5): p. 1199-203.

28.   Langford, T.D., et al., *Giardia lamblia: identification and characterization of Rab and GDI proteins in a genome survey of the ER to Golgi endomembrane system.* Exp Parasitol, 2002. **101**(1): p. 13-24.

29.   Marti, M., et al., *An ancestral secretory apparatus in the protozoan parasite Giardia intestinalis.* J Biol Chem, 2003. **278**(27): p. 24837-48.

30.   Adam, R.D., et al., *The Giardia lamblia vsp gene repertoire: characteristics, genomic organization, and evolution.* BMC Genomics, 2010. **11**: p. 424.

31.   Hardin, W.R., et al., *Myosin-independent cytokinesis in Giardia utilizes flagella to coordinate force generation and direct membrane trafficking.* PNAS, 2017. **(In Press)**.

32.   Wu, Y.I., et al., *Spatiotemporal control of small GTPases with light using the LOV domain.* Methods Enzymol, 2011. **497**: p. 393-407.

33.   Eden, S., et al., *Mechanism of regulation of WAVE1-induced actin nucleation by Rac1 and Nck.* Nature, 2002. **418**(6899): p. 790-3.

34.   Pimenta, P.F., P.P. da Silva, and T. Nash, *Variant surface antigens of Giardia lamblia are associated with the presence of a thick cell coat: thin section and label fracture immunocytochemistry survey.* Infect Immun, 1991. **59**(11): p. 3989-96.

35.   Sagolla, M.S., et al., *Three-dimensional analysis of mitosis and cytokinesis in the binucleate parasite Giardia intestinalis.* J Cell Sci, 2006. **119**(Pt 23): p. 4889-900.

36.   Carpenter, M.L. and W.Z. Cande, *Using morpholinos for gene knockdown in Giardia intestinalis.* Eukaryot Cell, 2009. **8**(6): p. 916-9.

37.   Krtkova, J., et al., *Rac Regulates Giardia lamblia Encystation by Coordinating Cyst Wall Protein Trafficking and Secretion.* MBio, 2016. **7**(4).

38.   Chozinski, T.J., et al., *Expansion microscopy with conventional antibodies and fluorescent proteins.* Nat Methods, 2016. **13**(6): p. 485-8.

39.   Tumova, P., J. Kulda, and E. Nohynkova, *Cell division of Giardia intestinalis: Assembly and disassembly of the adhesive disc, and the cytokinesis.* Cell Motility and the Cytoskeleton, 2007. **64**(4): p. 288-298.

40.   Wisniewski, J.R., et al., *Universal sample preparation method for proteome analysis.* Nat Methods, 2009. **6**(5): p. 359-62.

Figure S1

A. PHI pattern   L-[LMFK]-X(1,3)-I-X(3,9)-L-[KNRH]-[KRHQSQPN]-[VILATSG]
   Query sequnce   DM SCAR AAF53042

   AA   WH2 domains
   362   LKVIDLEGKLAELKRLRDAHEEEIRQLKIEL
   490   LKARDIEIERLRSLCEVFFEQSYQQSLKAA
   854   LKQSIASQETAFTCLRSTVEEKDKETANLRM

B.   Flangin
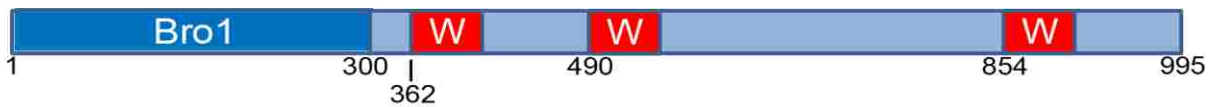
FIG S1 Bioinformatic search for the WH2 domain containing proteins identified Flangin. (A) Flangin (ORF 7031) was identified using a PHI pattern modeled after WH2 domains and the query sequence DM SCAR AAF53042. (B) Flangin has a putative N-terminus Bro1 domain and three putative WH2 domains. Flangin is 995 kDa.

Figure 1

A.

IP –HA

AUK-HA   Flangin-HA

Blot

Actin

–Ctrl

B.

Flangin-HA

C.

	DIC	Flangin-mNG	

Mitosis

-00:25sec

Cytokinesis

00:25

Interphase

00:50

Interphase

06:15

E.

Actin/DAPI   Flangin/DAPI   Merge

Interphase

Anaphase

Telophase

Cytokinesis

D.

Interphase   Mitosis   Mitosis   Cytokinesis
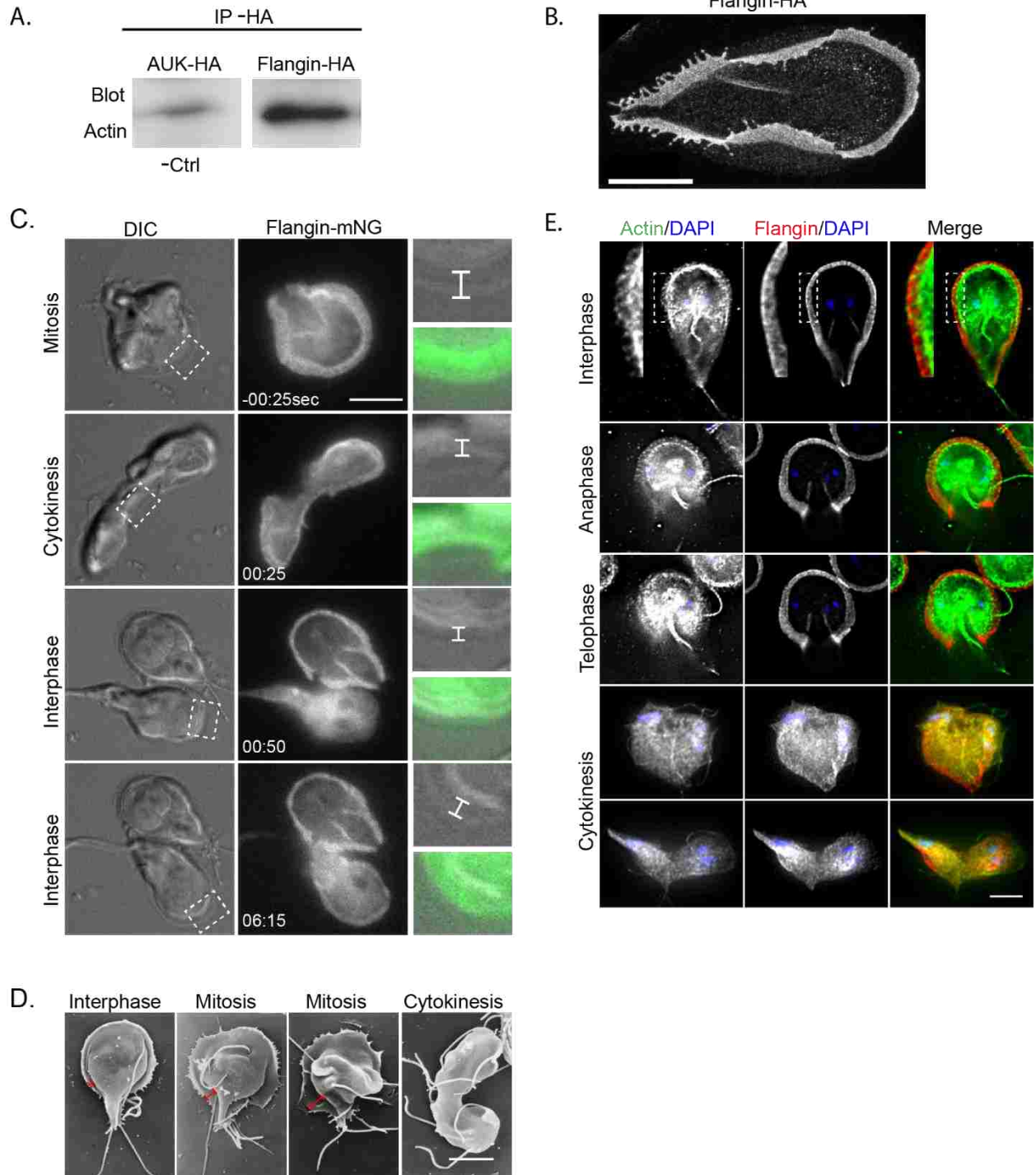
FIG 1 *Giardia* possesses a lamellipodia-like structure that contains actin and Flangin. (A) Immunoprecipitation from *Giardia* extracts of C-terminally HA-Tagged Flangin, followed by anti-actin Western blotting demonstrates Flangin interacts with actin. (B) Confocal fluorescence image of expanded *Giardia* cell with maximum intensity projection. Fixed cell expressing Flangin-HA and immunostaining against HA using conventional 488nm antibody. Scale bar 5 μm. (C) Live cell imaging and characterization of Flangin-mNG over the cell cycle. During mitosis, Flangin-mNG localizes to the VLF. Upon cytokinesis, the VLF is disassembled concomitant to Flangin-mNG relocalizing to the cell body. Newly attached daughter cells have small VLF and rebuilds simultaneous to Flangin-mNG relocalizing to the VLF. The insets shows measurement bar indicating VLF dynamics and Flangin-mNG localization during the cell cycle and in a newly attached daughter cell. (D) Scanning electron microscopy shows VLF growth during mitosis and no VLF during cytokinesis (red dimension bar). (E) Immunofluorescence localization of actin (green), Flangin-HA (red), and DNA (blue), throughout the cell cycle. Actin and Flangin accumulate to the VLF during interphaes and mitotic VLF growth. The insets show enrichment of actin and Flangin in the VLF. During cytokinesis, the cell body is yellow; possibly indicating increased actin and Flangin localization. Scale bar 5 μm. DIC, differential interference contrast images. Scale bar 5 μm.

Figure S2

A.

kD	Ctrl	Flangin KD	
95			Flangin-HA
43			Actin

~60% reduction
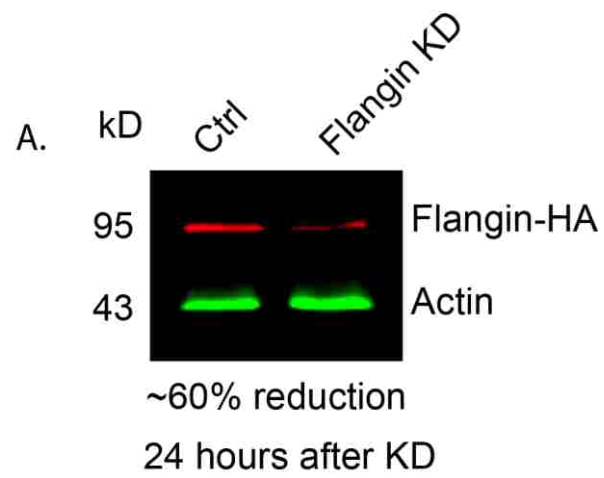
24 hours after KD

FIG S2 (A) Western blot showing 60% reduction in Flangin 24 hours after morpholino treatment.

Figure 2
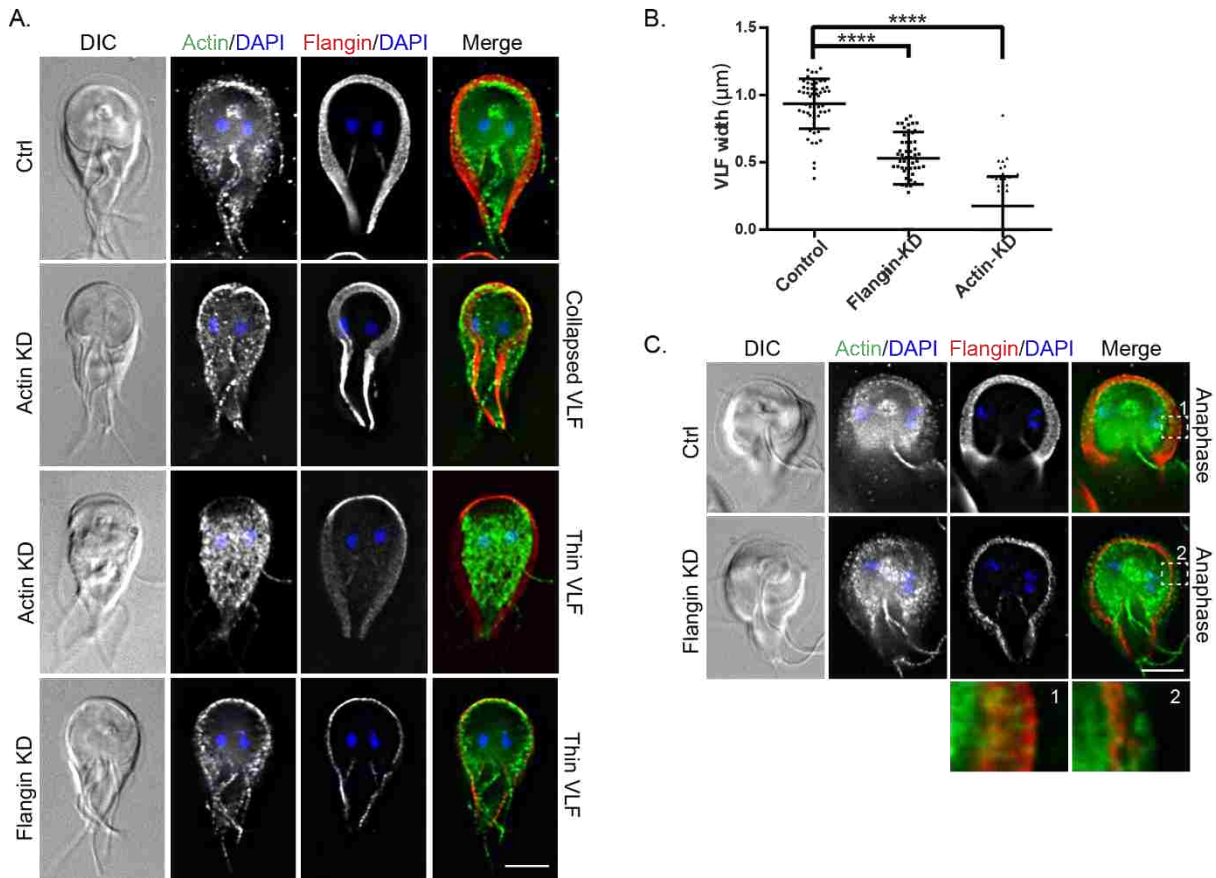
FIG 2 Flangin and actin are necessary for VLF assembly. (A) Trophozoites were stained for actin (green), Flangin-HA (red), and DNA (blue). For actin KD cells the VLF was either fully collapsed, the VLF stayed within the boundaries of the cell body, or more thin than control cells. Flangin-HA KD cells had thin VLF's. (B) Quantification of VLF width when measured at cell anterior from independent experiments; control (n=57), Flangin-HA (n=54), and actin (n=51). Statistical significance was evaluated for Flangin-KD and Actin-KD respectively, t test. ****, P<0.0001 and P<0.0001. (C) Mitotic cells were stained for actin (green), Flangin-HA (red), and DNA (blue). The insets show actin beyond the leading edge of Flangin-HA in Flangin-HA KD cells during VLF dynamics. DIC, differential interference contrast images. Scale bar 5 μm.

Figure S3

A.
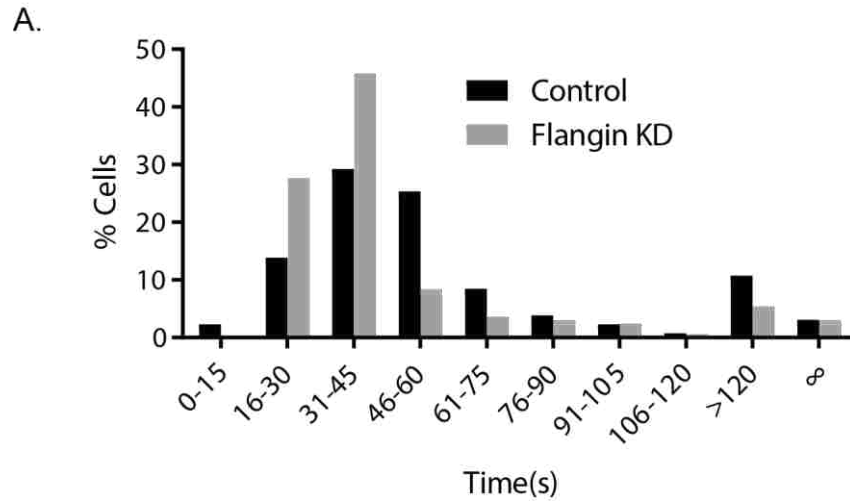
FIG S3 Cytokinesis timing of control and Flangin KD cells. (A) A normalized bar chart showing the timing of cytokinesis for control (black) and Flangin KD cells (gray). Cytokinesis median time: control 49sec and Flangin KD 35sec.

Figure 3

A.

B.
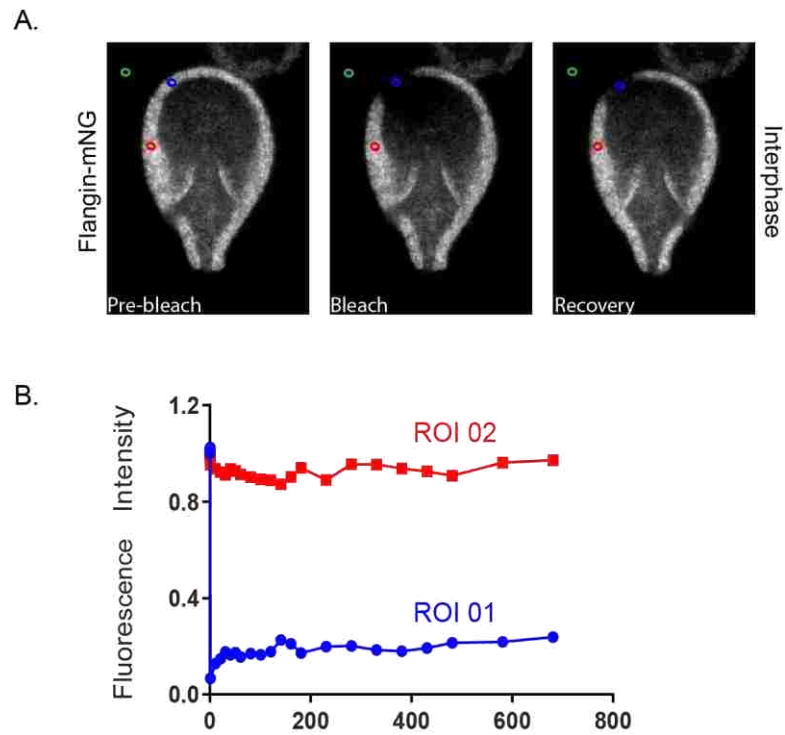
FIG 3 Flangin is a structural protein that is removed from the VLF for the completion of cytokinesis. (A) Fluorescence Recovery after Photobleaching (FRAP) was performed on the VLF of Flangin-mNG cells, Blue circle bleached ROI 01, Red circle non-bleached ROI 02, and Green circle background ROI 03. (B) ROI 01 showed minimal post-bleaching recovery after 12min compared to ROI 02.

Figure 4
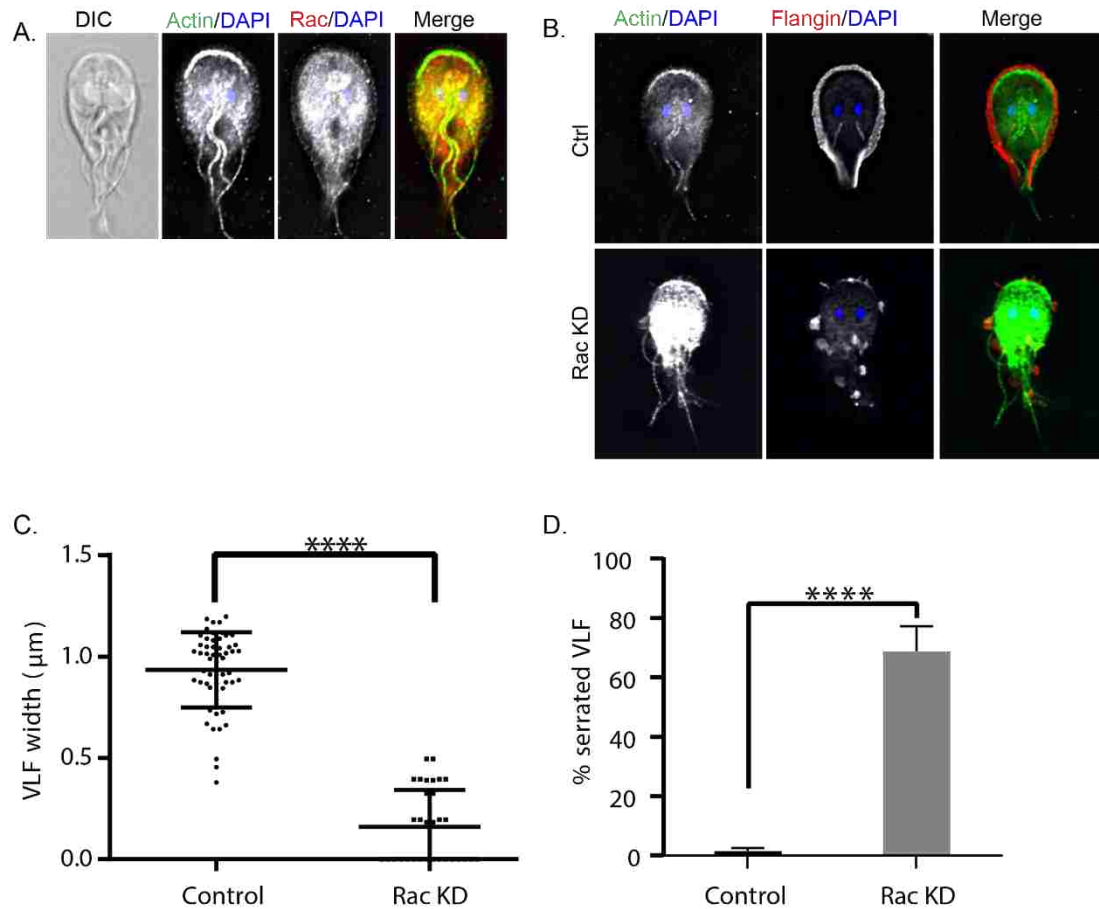
FIG 4 Rac is a signaling component for VLF assembly. (A) Immunofluorescence localization of actin (green), HA-Rac (red), and DNA (blue). Actin and Rac localize to the VLF. (B) Rac KD cells resulted in serrated VLF's compared to control cells. Actin and Flangin localize to the sparsely populated VLF regions. (C) Quantification of VLF width measured at cell anterior from independent experiments; control (n=57) and Rac KD (n=32). Statistical significance was evaluated by using t-test. ****, P<0.0001. (D) Quantification of serrated cells. Cells with three or more serrations were counted and serration was defined as a gap/opening along the VLF; control (n=596) and Rac KD (n=618). Statistical significance was evaluated by using t-test. ****, P< 0.0001. Scale bar 5 μm.

Figure 5

A.
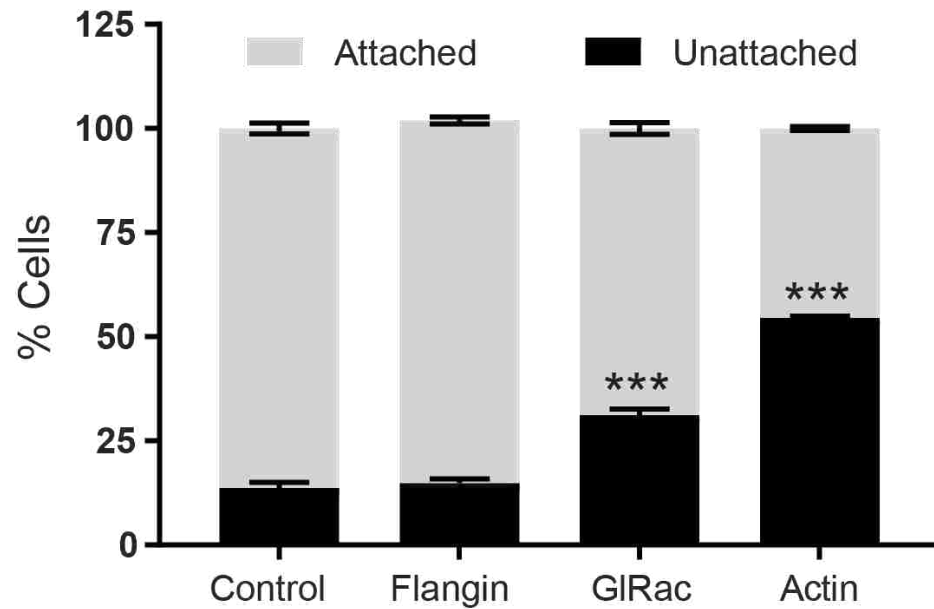
FIG 5 Quantitating the role of Flangin, GlRac, and actin in cell attachment. (A) Each protein was depleted and attached and unattached cells were counted. Three technical replicates for unattached cells were conducted. Mean ± SEM n=3, control 13.73 ± 0.7799, Flangin 14.81 ± 0.622, GlRac 31.23 ± 0.8322, and actin 54.48 ± 0.2525. GlRac and actin showed a statistical significance compared in the number of unattached cells compared to the control, t-test ***, P< 0.0001 and ***, P< 0.0001, respectively.

Table S1

S1 A

VARIANT SURFACE PROTEIN (VSP)							
ORF	Name/Description	MW	#Peptides	ttest	wt_av	Flangin_av	Flagin/wt
14586	VSP with INR	75531.14	75	0.0	0.075	75	1000.0
6372	High cystein>	56010.97	8	0.0	0.008	8.33333	1000.0
137606	VSP	89006.19	56	0.0	0.667	55.6667	83.5
137618	VSP	88660.58	208	0.0	3	208.333	69.4
111933	VSP	75401.49	43	0.0	0.667	42.6667	64.0
112801	VSP	76442.87	77	0.0	1.333	77	57.8
113797	VSP with INR	72540.78	68	0.0	1.333	68	51.0
113439	VSP with INR	73891.24	25	0.0	0.667	25.3333	38.0
113450	VSP with INR	74848.48	73	0.0	2	73.3333	36.7
137617	VSP	75502.96	47	0.0	1.333	47	35.3
101074	VSP with INR	76763.95	130	0.0	5	130	26.0
137612	VSP	89600.18	27	0.0	1.333	27	20.3
115797	VSP with INR	70226.63	10	0.0	0.667	9.66667	14.5
113093	VSP	66729.4	8	0.0	0.667	8.33333	12.5
11521	VSP	64144.38	11	0.0	1.333	11	8.3
137721	VSP	42880.07	9	0.0	1.333	8.66667	6.5
13194	VSP AS8	63070.23	10	0.0	1.667	9.66667	5.8
116477	VSP	76114.58	16	0.0	3	15.6667	5.2
137761	VSP	16868.42	7	0.0	1.667	6.66667	4.0

S1 B

AXONEMAL/CYTOSKELETON							
ORF	Name/Description	MW	#Peptides	ttest	wt_av	Flangin_av	Flangin/wt
111950	Dynein heavy chain	570319.1	9	0.007	0	9	1000
33660	Spindle pole protein, putative	236334.11	13	2E-05	0.013	13	1000
13475	Axoneme-associated protein	35010.74	376	7E-06	26.33	375.667	14.3
14895	Spindle pole protein, putative	33147.97	8	0.0167	1.333	7.66667	5.8
17153	Alpha-11 giardin	33935.73	291	2E-05	58.67	291	5
16745	Axoneme-associated protein	33320.21	361	7E-05	72	361.333	5
15097	Alpha-14 giardin	35632.37	20	0.004	6.333	20.3333	3.2
14551	Alpha-6 giardin	33889.83	17	0.0129	5.333	17	3.2
112846	Kinesin-3	32972.85	17	0.0325	7.667	17	2.2
7796	Alpha-2 giardin	33657.15	56	0.001	26	55.6667	2.1
11683	Alpha-3 giardin	30876.82	16	0.0122	8	15.6667	2
17230	Gamma giardin	174782.88	42	0.0037	21.67	42	1.9
4410	SALP-1	29827.66	30	0.0005	61	109.333	1.8
11654	Alpha-1 giardin	10447.97	109	0.0005	61	109.333	1.8
103373	Alpha-7.1 giardin	103966.99	70	0.0017	39.67	69.6667	1.8
114119	Alpha-7.2 giardin	190521.06	83	0.0014	47.67	83	1.7
114787	Alpha-7.3 giardin	254968.69	89	0.0041	51.33	89	1.7

86676	Delta giardin	72163.13	41	0.0169	25	40.6667	1.6
4812	Beta-giardin	186026.16	126	0.025	26.67	39	1.5
137716	Axoneme-associated protein	133025.75	481	0.0135	380	481	1.3
9848	Dynein light chain	150345.36	17	0.0257	13	17	1.3

S1 C

TRAFFICKING							
ORF	**Name/Description**	**MW**	**#Peptides**	**ttest**	**wt_av**	**Flangin_av**	**Flangin/wt**
114674	Hypothetical protein*	73023.92	29	0.0	0.029	28.6667	1000.0
15499	Hypothetical protein*	48834.44	9	0.0	0.009	8.66667	1000.0
9489	V-SNARE	26142.53	6	0.0	1.333	6.33333	4.8
15567	Rab2a	23748.72	22	0.0	7.667	22.3333	2.9
9558	Rab1a	23107.17	13	0.0	4.667	13	2.8
16636	Rab2b	24594.77	12	0.0	7	12.3333	1.8
102108	Clathrin heavy chain	206953.97	39	0.0	26.67	39	1.5
23833	Vacuolar protein sorting 35	87504.34	22	0.0175	15.33	22.3333	1.5

S1 D

SIGNALING							
ORF	**Name/Description**	**MW**	**#Peptides**	**ttest**	**wt_av**	**Flangin_av**	**Flangin/wt**
17299	Kinase, NEK-like	130505.52	6	0.0	0.006	5.66667	1000.0
102034	Kinase, NEK-frag	108209.21	21	0.0	0.021	21	1000.0
11390	Kinase, NEK	85184.27	59	0.0	7.667	59	7.7
15215	Phosphatase	35321.23	9	0.0	1.333	9	6.8
15410	Thr protein kinase	31698.17	89	0.0	15	89.3333	6.0
15409	Kinase, NEK	57009.88	284	0.0	68.67	283.667	4.1
15411	Kinase, NEK-frag	78005.9	47	0.0	22	47	2.1
10698	Phosphorylase B kinase gamma	85288.82	13	0.0265	6	12.6667	2.1
8826	Glucokinase	37713.01	17	0.0	12.33	17.3333	1.4

S1 E

METABOLIC							
ORF	**Name/Description**	**MW**	**#Peptides**	**ttest**	**wt_av**	**Flangin_av**	**Flangin/wt**
93551	Metalloprotease, insulinase family	128508.26	38	0.0	4	38	9.5
17327	Xaa-Pro dipeptidase	49672.49	91	0.0	23.67	91	3.8
10623	Phosphoenolpyruvate carboxykinase	73844.74	23	0.0	6	23	3.8
21118	Long chain fatty acid CoA ligase 5	84578.72	34	0.0	14.33	34	2.4
16779	Cathepsin B precursor	32760.97	15	0.0	7	14.6667	2.1
11118	Enolase	48219.97	94	0.0	45.67	94.3333	2.1
15832	Aminoacyl-histidine dipeptidase	56680.88	51	0.0	25.33	51	2.0
113892	Long chain fatty acid CoA ligase, putative	84547.69	36	0.0	18	35.6667	2.0
33769	NADH oxidase lateral	53336.28	104	0.0	54	103.667	1.9

	transfer candidate						
113021	Acetyl-CoA carboxylase/pyruvate	148195.03	19	0.0112	10.33	19	1.8
9719	NADH oxidase	47004.07	31	0.0	17	31	1.8
93358	Alcohol dehydrogenase	97133.87	119	0.0	86.67	118.667	1.4

S1 F

UNKNOWN/GIARDIA SPECIFIC							
ORF	**Name/Description**	**MW**	**#Peptides**	**ttest**	**wt_av**	**Flangin_av**	**Flangin/wt**
15329	Protein 21.1	145192.06	8	0.0	0.008	8.33333	1000.0
14434	Protein 21.1	49682.83	10	0.0	0.01	9.66667	1000.0
11720	Hypothetical protein	48468.17	25	0.0	0.025	25	1000.0
95192	Protein 21.1	124350.49	7	0.0	0.007	7.33333	1000.0
96732	Hypothetical protein	383733.1	7	0.0	0.007	6.66667	1000.0
5879	Protein 21.1	139428.14	21	0.0	0.021	21	1000.0
8448	Unspecified protein	12499.03	7	0.0	0.007	6.66667	1000.0
16353	Hypothetical protein	83652.78	14	0.0	1.667	14	8.4
24842	Protein 21.1	201475.94	8	0.0	1.667	8	4.8
32999	Hypothetical protein	51467.44	84	0.0	17.67	84.3333	4.8
93294	Hypothetical protein	138987.55	40	0.0003	10	40.3333	4.0
114777	Hypothetical protein	72714.83	14	0.0	4.667	14.3333	3.1
41212	Hypothetical protein	149291.94	154	0.0	50.67	153.667	3.0
6464	Hypothetical protein	141567.55	26	0.0	9.667	26.3333	2.7
17551	Protein 21.1	118713.62	16	0.0	8	15.6667	2.0
17342	Hypothetical protein	72495.6	9	0.0	4.667	9	1.9
102023	Protein 21.1	91915.64	13	0.0	7.667	13.3333	1.7
94463	Hypothetical protein	53389.68	24	0.0	18.67	24.3333	1.3
17249	Coiled-coil protein	115967.61	288	0.0	28	288.333	10.3
113677	Coiled-coil protein	38584.18	378	0.0	52.67	377.667	7.2
15591	Coiled-coil protein	120516.45	75	0.0	13.67	74.6667	5.5
10167	Coiled-coil protein	42910.44	127	0.0	45	127.333	2.8
9515	Coiled-coil protein	43021.63	32	0.0	12	32	2.7

S1 G

MISC.							
ORF	**Name/Description**	**MW**	**#Peptides**	**ttest**	**wt_av**	**Flangin_av**	**Flangin/wt**
92246	Cation-transporting ATPase	151938.12	8	0.0	0.008	7.66667	1000.0
5867	Cysteinyl-tRNA synthetase	72993.44	7	0.0	0.007	6.66667	1000.0
86681	Glutaminyl-tRNA synthetase	80130.54	17	0.0	6.667	17.3333	2.6
10521	Arginyl-tRNA synthetase	70294.97	30	0.0	13.67	29.6667	2.2
8855	P115, putative	104090.21	10	0.0	6	10.3333	1.7
5795	Leucine-rich repeat protein	85450.23	14	0.0	8.667	14.3333	1.7
9413	Protein disulfide isomerase PDI2	50408.15	47	0.0	34.67	47.3333	1.4
14670	Protein disulfide isomerase PDI3	12668.78	14	0.0	11	14	1.3

>VSP potential

*Clathrin Yeast-Two Hybrid Hit

Dataset S1

Vector Construction	
Plasmid	Sequence
pKS-Flangin-3HA-NEO (GL50803_7031)	F- 5' ggcgcgccCAAAGCAATCTACCGGCAGC 3'
	R- 5' TGTTGGATGCCGATCTACCGaccggt 3'
pKS_Flangin-mNG_PAC	F- 5' ggaccggtATGGTGAGCAAGGGCGAGGA 3'
	R- 5' CATGGACGAGCTGTACAAGTAAgcggccgcgg 3'
pNlop4_Flangin-$_{1-300}$-N11-mNG_NEO	F- 5' CGCCAATGCTCTTCAATTGcttaagGGATCCGGAGGCGGTTCAGGCGGAGG 3'
	R- 5' cggaaagaattcctaggatccttacttgtacagctcgtcca 3'
TS tag made for pKS_Flangin-TS_PAC	F- 5' CCGACCGGTGGGAGCGGTGGATCGGG 3'
	R- 5' ACTGCGGCCGCTTCACCGCCAGAACC 3'

Vector Construction	
Plasmid	Notes
pKS-Flangin-3HA-NEO (GL50803_7031)	Flangin was amplified from WBC6 genomic DNA
	The restriction enzymes AscI and AgeI were used to linearize the pKS-3HA_Neo vector. Traditional ligation was used to insert Flangin into the linerized pKS-3HA_Neo vector.
pKS_Flangin-mNG_PAC	mNG amplifed from mNG template (Allele Biotechnology) using primers
	The restriction enzymes AgeI and NotI were used to linearize the pKS-Flangin-mCherry_PAC vector. Traditional ligation was used to insert mNG into the linerized pKS_Flangin_PAC vector.
pNlop4_Flangin-$_{1-300}$-N11-mNG_NEO	N11-mNG amplifed from pKs_N11-mNG_NEO
	The restriction enzymes AflII and BamHI were used to linearize the pNlop4_Flangin-$_{1-300}$-3HA_NEO vector. Gibson cloning was used to ligate the N11-mNG and linerized pNlop4_Flangin-$_{1-300}$-NEO vector.
pKS_Flangin-TS_PAC	TS tag was amplifed, pKS_Flangin-_PAC was linerized with Age1 and Not1, and then both were ligated.

Dataset S1 Workflow for vector construction.